

**ANALYSIS AND OPTIMIZATION OF PORTAL AXLE UNIT USING
FINITE ELEMENT MODELLING AND SIMULATION**

By

OOI JONG BOON

A thesis submitted to the Department of Mechanical and Material Engineering,
Faculty of Engineering Science,
Universiti Tunku Abdul Rahman,
in partial fulfilment of the requirements for the degree of
Master of Engineering Science
January 2013

This thesis is wholly dedicated to
my beloved mother Chooi Mei Ngan, my sister Ooi Guek Cheng,
and my grandmother Tang Ah Nghoh
for their love and support.

ABSTRACT

ANALYSIS AND OPTIMIZATION OF PORTAL AXLE UNIT USING FINITE ELEMENT MODELLING AND SIMULATION

Ooi Jong Boon

Portal axle is a gearbox designed to increase the ground clearance of the vehicle for off-road driving conditions. The higher ground clearance depends on the arrangement of gear train of the portal axle. The gear train and shafts are the most critical part in the portal axle as they transmit and withstand very high loads. They should be designed to withstand overloading and lightweight for greater durability and performance of the portal axle. Stress and vibration analysis of the gear train and shafts are necessary in evaluating the design for gear train and shaft. The method to determine the gear stress analytically has been developed extensively by the American Gear Manufacturers Association (AGMA), and experimental techniques in investigating the vibration behaviour of spur gears were well documented. However, the AGMA method is limited to a tooth gear analysis and many assumptions need to be taken into account. The setup of experiment for investigating the vibration behaviour of the gear train in the portal axle can be expensive and difficult due to the complexity of the gear parts to be tested upon.

In this thesis, the characteristics of the gear train of the portal axle was investigated by analysing the gear contact stresses, bending stresses, and the vibration behaviour of the gears by using finite element analysis (FEA) software ANSYS. The actual motion behaviour of the gear train can be studied comprehensively through the FEA modelling and simulation. Three gear train designs for the portal axle were proposed and modelled to distinguish the stress and vibration characteristics between them. The effect of the gear teeth in single and double contact and the non-ideal loading conditions of the gear trains were also investigated by increasing the gear angular positions.

This thesis was also dedicated to improving the torsional strength of the output shaft of the portal axle. A three-dimensional (3D) hollow shaft with rib was proposed and developed using FEA. The L25 Taguchi orthogonal array (OA) was applied to determine the optimum set of parameters for the proposed shaft. The strength and weight of the optimised model were compared with the benchmarking output shaft. The optimized model has improved torsional strength when compared to the benchmarking shaft and the hollow shaft. Both FEA and the Taguchi optimization method were proven effective in evaluating and improving the strength of the gear train and shaft of the portal axle. Therefore, they can be used as a novel approach for gear train and shaft design evaluation which is needed in the small workshop scale industries.

ACKNOWLEDGEMENT

First and foremost, I would like to express my sincere appreciation and deepest gratitude to my supervisor, Dr. Wang Xin for her guidance, invaluable advice, understanding and considerations on my works. I was able to gain a lot of experiences, skills and knowledge from her. I wish to sincerely express my gratitude to my co-supervisor, Dr. Lim Ying Pio who had provided me continuous guidance, directions and advice when I was conducting my works.

I also wish to indicate special gratitude and deepest thankfulness to Ir. Qua Hock Chye, Dr. Tan Ching Seong, Dr. Wong Kok Cheong, and Dr. Ho Jee-Hou for their invaluable technical guidance and advice throughout the course of this research.

In addition, I acknowledge the faculty and the staff of the Department of Mechanical Engineering in Universiti Tunku Abdul Rahman and Tunku Abdul Rahman College, who have provided me with the most cooperative assistance to my research work.

Last but not least, a big appreciation is also dedicated to my beloved family and friends who have given me encouragement and morale support throughout the duration of my study.

APPROVAL SHEET

This thesis entitled “**ANALYSIS AND OPTIMIZATION OF PORTAL AXLE UNIT USING FINITE ELEMENT MODELLING AND SIMULATION**” was prepared by OOI JONG BOON and submitted as partial fulfilment of the requirements for the degree of Master of Engineering Science at Universiti Tunku Abdul Rahman.

Approved by:

(Dr. WANG XIN)

Date:

Supervisor

Department of Mechatronics and Biomedical Engineering

Faculty of Engineering Science

Universiti Tunku Abdul Rahman

(Dr. LIM YING PIO)

Date:

Co-Supervisor

Department of Mechanical and Material Engineering

Faculty of Engineering Science

Universiti Tunku Abdul Rahman

FACULTY OF ENGINEERING AND SCIENCE
UNIVERSITI TUNKU ABDUL RAHMAN

Date: 29 January 2013

SUBMISSION OF THESIS

It is hereby certified that **OOI JONG BOON** (ID No: **09UEM09189**) has completed this thesis entitled “**ANALYSIS AND OPTIMIZATION OF PORTAL AXLE UNIT USING FINITE ELEMENT MODELLING AND SIMULATION**” under the supervision of Dr. WANG XIN (Supervisor) from the Department of Mechatronics and Biomedical Engineering, Faculty of Engineering and Science, and Dr. LIM YING PIO (Co-Supervisor) from the Department of Mechanical and Material Engineering, Faculty of Engineering and Science.

I understand that the University will upload softcopy of my thesis in pdf format into UTAR Institutional Repository, which may be made accessible to UTAR community and public.

Yours truly,

(OOI JONG BOON)

DECLARATION

I hereby declare that the dissertation is based on my original work except for quotations and citations which have been duly acknowledged. I also declare that it has not been previously or concurrently submitted for any other degree at UTAR or other institutions.

(OOI JONG BOON)

Date _____

TABLE OF CONTENTS

	Page
ABSTRACT	ii
ACKNOWLEDGEMENT	iv
APPROVAL SHEET	v
SUBMISSION OF THESIS	vi
DECLARATION	vii
TABLE OF CONTENTS	viii
LIST OF TABLES	xii
LIST OF FIGURES	xiii
LIST OF ABBREVIATIONS	xvii
LIST OF NOTATIONS	xviii
CHAPTERS	
1.0 INTRODUCTION	1
1.1 Research Background	1
1.2 Research Objective	6
1.3 Thesis Overview	7
2.0 LITERATURE REVIEW	9
2.1 Gear bending stress analysis	9
2.2 Gear contact stress analysis	12
2.3 Vibration analysis of the gear train	14
2.4 Gear misalignment and its effect	16
2.5 Torsion analysis of the shaft	17

2.6	Taguchi method for shaft optimization	18
3.0	STRESS ANALYSIS OF THE GEAR TRAIN UNDER NON-IDEAL LOADING	20
3.1	Finite element analysis	20
3.1.1	Modelling of the gear train	21
3.1.2	Gear bending stress	22
3.1.3	Gear contact stress	25
3.2	Gear Experiment	28
3.3	Analytical method	31
3.3.1	Lewis equation and AGMA standard for gear bending stress	31
3.3.2	Hertzian equation and AGMA standard for gear contact stress	35
3.4	Validation of the FEA model	38
3.4.1	Gear bending stress comparison	38
3.4.2	Gear contact stress comparison	39
3.5	Model of the three gear train designs	40
3.6	Effect of non-ideal loading to the gear stresses	44
3.6.1	Effect of the out of plane misalignment	46
3.6.2	Effect of the tilt angle misalignment	48
3.6.3	Effect of the axial separation misalignment	50
3.7	Conclusion	52
4.0	VIBRATION ANALYSIS OF THE GEAR TRAIN UNDER NON-IDEAL LOADING	54
4.1	Introduction	54
4.2	Validation of the FEA model	54

4.2.1	Gear vibration experiment	55
4.2.2	Gear vibration analysis by using FEA	57
4.2.3	Comparison between FEA and experiment	60
4.3	Effect of non-ideal loading to the gear train vibration	61
4.3.1	Modal analysis of the gear train without idler gear	62
4.3.2	Modal analysis of the gear train with one idler gear	65
4.3.3	Modal analysis of the gear train with two idler gears	68
4.3.4	Forced frequency response of the gear train without idler gear	70
4.3.5	Forced frequency response of the gear train with one idler gear	73
4.3.6	Forced frequency response of the gear train with two idler gears	75
4.4	Conclusion	77
5.0	PARAMETRIC OPTIMIZATION OF THE HOLLOW SHAFT WITH RIB	79
5.1	Introduction	79
5.2	Validation of FEA hollow shaft model	80
5.2.1	Torsional stress evaluation by using FEA	80
5.2.2	Torsional stress evaluation by using Distortion Energy Theory	83
5.2.3	Torsional stress evaluation by using experiment	84
5.2.4	Results comparison	87
5.3	Model of the hollow shaft with rib	88
5.4	Parametric analysis of the hollow shaft with rib	89
5.4.1	Effect of the hollow shaft thickness	89

5.4.2	Effect of the rib thickness	90
5.4.3	Effect of the depth of spokes	91
5.4.4	Effect of the rib fillet radius	92
5.4.5	Effect of the number of spokes	93
5.5	Parametric optimization of the hollow shaft with rib	94
5.5.1	L25 Taguchi Orthogonal Array	94
5.5.2	Strength and weight comparison of the optimized shaft	97
5.6	Conclusion	99
6.0	CONCLUSIONS AND FUTURE WORK	100
6.1	Conclusions	100
6.2	Contributions	101
6.3	Future Work	102
	REFERENCES	103
	APPENDICES	109

LIST OF TABLES

Table	Page
3.1 Material properties and design parameters of the test gears.	22
3.2 Design parameters of the input gear, idler gear, and output gear.	40
3.3 The effect of the three different misalignments to the bending stress and contact stress at the output gear of the three gear train design.	53
4.1 Design parameters of the two mating spur gears.	55
4.2 First ten mode shapes of gear train without idler gear (IN and OT indicate the input gear and output gear respectively).	64
4.3 First ten mode shapes of gear train with one idler gear (IN, ID and OT indicate the input gear, idler gear and output gear respectively).	67
4.4 First ten mode shapes of the gear train with two idler gears (IN, ID1, ID2, and OT indicate the input gear, idler gear 1, idler gear 2, and output gear respectively).	69
4.5 The effect of the three different misalignments to the overall amplitude of the three gear train designs in free and forced vibration.	78
5.1 Dimensions and material properties of the hollow shaft with rib.	89
5.2 Factorial design of the shaft model with five factors and five levels.	95
5.3 L25 Taguchi Orthogonal Array design factors of the shaft model.	95
5.4 Analysis of Variance of the five parameters.	96
5.5 Diagnostic analysis of the L25 Taguchi OA design factor.	97
5.6 Comparison of shaft models based on strength and weight reduction.	98

LIST OF FIGURES

Figure		Page
1.1	Difference between normal and portal axle unit.	1
1.2	Portal axle gear train with two idler gears.	2
3.1	FEA general steps for obtaining the gear bending and contact stress.	21
3.2	Optimum mesh element size by stress convergence method.	23
3.3	Mesh model of the gear train.	23
3.4	Load and constraints of the gear train model.	24
3.5	Point probe of tooth root bending stress at a) Gauge A, b) Gauge B, and c) Gauge C of the output gear.	25
3.6	Refined mesh elements of 2 mm by 40 mm at the contacting gear teeth surface of the output gear.	26
3.7	Contact and target elements between the gear teeth in contact.	27
3.8	Detailed view of gear tooth contact stress distribution of the output gear.	28
3.9	Strain gauges at respective position measured at a distance from tooth tip and left tooth.	29
3.10	Strain gauges mounted on the tooth surface of the output gear.	30
3.11	Strain measurement system instrumentation for measuring the output gear bending stress.	31
3.12	Lewis cantilever beam diagram.	32
3.13	Loads and length dimensions used for determining the tooth bending stress.	33
3.14	Load at HPSTC in determining the gear tooth bending stress.	34
3.15	Hertzian model of the two cylinders in contact.	35
3.16	Two involute teeth in contact.	36
3.17	Comparison between the FEA, experiment and analytical bending stress at the output gear.	38

3.18	Comparison between the FEA and analytical contact stress at the output gear.	39
3.19	Detailed view of the three gear train designs.	41
3.20	Angular intervals of the gear pair contact of the gear train.	42
3.21	Gear train with one idler gear in single tooth contact at 0°, 4° and 8° angular positions.	43
3.22	Gear train with one idler gear in load sharing at 10°, 14° and 18° angular positions.	43
3.23	Details of three types of misalignment of the gear train.	45
3.24	Effect of out of plane misalignment to the bending stress of the output gear of the three gear train designs.	46
3.25	Effect of out of plane misalignment to the contact stress of the output gear of the three gear train designs.	47
3.26	Effect of tilt angle misalignment to the bending stress of the output gear of the three gear train designs.	49
3.27	Effect of tilt angle misalignment to the contact stress of the output gear of the three gear train designs.	50
3.28	Effect of axial separation misalignment to the bending stress of the output gear of the three gear train designs.	51
3.29	Effect of axial separation misalignment to the contact stress of the output gear of the three gear train designs.	52
4.1	Design parameters of a) Gear A and b) Gear B.	55
4.2	Experiment apparatus for gear vibration testing.	56
4.3	Mounting positions of the dynamic strain gauges and accelerometers.	57
4.4	Surface probe at the root fillet and web center surface of Gear A.	59
4.5	Pre-stressed conditions of the two mating spur gears.	59
4.6	Comparison of the acceleration frequency response at the web center surface and tooth root of Gear A (1000 RPM).	60
4.7	Comparison of the strain response at the web center surface and tooth root of Gear B (3119 RPM).	61

4.8	The 8 th mode shape of the gear train without idler gear in a) normal loading, b) out of plane, c) tilt angle, and d) axial separation.	63
4.9	Maximum deformation of the gear train without idler gear in the first ten mode shape.	65
4.10	The 8 th mode shape of the gear train with one idler gear in a) normal loading, b) out of plane, c) tilt angle, and d) axial separation.	66
4.11	Maximum deformation of the gear train with one idler gear in the first ten mode shape.	67
4.12	The 8 th mode shape of the gear train with two idler gears in a) normal loading, b) out of plane, c) tilt angle, and d) axial separation.	68
4.13	Maximum deformation of the gear train with two idler gears in the first ten mode shape.	70
4.14	X direction deformation against frequency for the gear train without idler gear under non-ideal loading conditions.	71
4.15	Y direction deformation against frequency for the gear train without idler gear under non-ideal loading conditions.	71
4.16	Z direction deformation against frequency for the gear train without idler gear under non-ideal loading conditions.	72
4.17	X direction deformation against frequency for the gear train with one idler gear under non-ideal loading conditions.	73
4.18	Y direction deformation against frequency for the gear train with one idler gear under non-ideal loading conditions.	74
4.19	Z direction deformation against frequency for the gear train with one idler gear under non-ideal loading conditions.	74
4.20	X direction deformation against frequency for the gear train with two idler gears under non-ideal loading conditions.	75
4.21	Y direction deformation against frequency for the gear train with two idler gears under non-ideal loading conditions.	76
4.22	Z direction deformation against frequency for the gear train with two idler gears under non-ideal loading conditions.	76
5.1	Procedure for determining the optimum set of parameters of the hollow shaft with rib.	79

5.2	Boundary condition settings on the hollow shaft model.	80
5.3	Convergence of torsional stress at 3 mm mesh element size for the hollow shaft model.	81
5.4	Mesh model of the hollow shaft.	82
5.5	Maximum torsional stress of the hollow shaft model.	82
5.6	Layout diagram of the hollow shaft in 2D.	83
5.7	Bonding of the strain gauge on the polished surface of the hollow shaft.	85
5.8	Mounting of the hollow shaft on the Tinius Olsen torsion tester.	86
5.9	Strain measurement system of the torsion tester machine.	86
5.10	Torsional stress comparison between the FEA model, experimental model, and the analytical model.	87
5.11	Model of the hollow shaft with rib with five types of parameter.	88
5.12	Torsional stress versus hollow shaft thickness of the hollow shaft with rib.	90
5.13	Torsional stress versus rib thickness of the hollow shaft with rib.	91
5.14	Torsional stress versus depth of spokes of the hollow shaft with rib.	92
5.15	Torsional stress versus rib fillet radius of the hollow shaft with rib.	93
5.16	Torsional stress versus the number of spokes of the hollow shaft with rib.	94

LIST OF ABBREVIATIONS

2D	Two dimensional
3D	Three dimensional
4WD	Four wheel drive
AGMA	American Gear Manufacturers Association
AISI	American Iron and Steel Institute
ANOVA	Analysis of Variance
ANSI	American National Standards Institute
ASME	American Society of Mechanical Engineers
CAD	Computer Aided Design
CNC	Computer Numerical Control
DAQ	Data Acquisition System
DOE	Design of Experiments
FEA	Finite Element Analysis
FFT	Fast Fourier Transform
HPSTC	Highest point of single tooth contact
IGES	Initial Graphics Exchange Specification
ISO	International Organization for Standardization
NI	National Instruments
OA	Orthogonal array
PC	Personal Computer

LIST OF NOTATIONS

σ_t	Gear bending stress
W_t	Tangential load
p_d	Diametral pitch
b_w	Face width
Y	Lewis form factor
t	Tooth thickness
W_r	Radial load
K_o	Overload factor
K_v	Dynamic factor
K_H	Load distribution factor
K_S	Size factor
K_B	Rim thickness factor
m_t	Transverse module
$2a$	Band of contact between the two cylinders
W	Normal load
E_1	Modulus of Elasticity of the pinion
E_2	Modulus of Elasticity of the gear
ν_1	Poisson's ratio of the pinion
ν_2	Poisson's ratio of the gear
R_1	Radii of the involute curve at the contact point of the pinion
R_2	Radii of the involute curve at the contact point of the gear
r_{b1}	Pitch radius of the pinion
r_{b2}	Pitch radius of the gear

C_p	Plastic coefficient
d_p	Root diameter of the pinion
C_f	Surface condition factor
$[M]$	Mass matrix
$[C]$	Damping coefficient matrix
$[K]$	Stiffness matrix
$\{\delta\}$	Deformation vector of the element nodes
$\{F\}$	External load vector on the element nodes
ω	Natural frequency
$\{\delta_0\}$	Mode shape vector
σ_x	Normal stress in x direction
σ_y	Normal stress in y direction
M	Bending moment
D	External diameter of the shaft
d	Internal diameter of the shaft
τ_{xy}	Maximum shear stress
T	Torque
$\sigma_{1,2}$	Principal stresses
σ_e	von Mises stress

CHAPTER 1

INTRODUCTION

1.1 Research background

Portal axle unit is a special gearbox unit designed to increase the vehicle's ground clearance. This gearbox can also be regarded as off-road technology where the axle tube is above the center of the wheel hub. It allows driving on off-road so that the vehicle can go over high terrains and obstacles. Portal axles are normally installed on heavy duty vehicle such as four-wheel drive (4WD) and military truck. Figure 1.1 shows the difference between the vehicle with normal axle and the vehicle with portal axle.

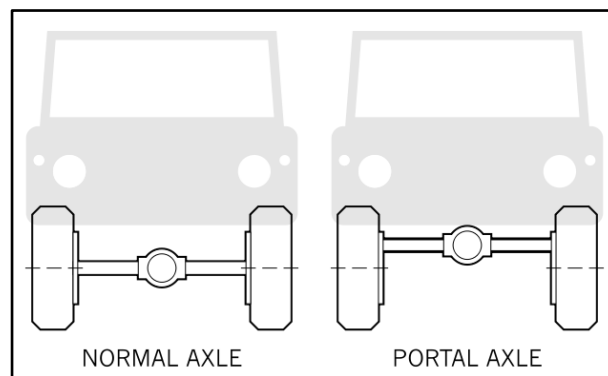


Figure 1.1: Difference between normal and portal axle unit (Tom 2007).

The portal axle gear train is designed in a single stage or a double stage to increase the vertical offset between the axle and the wheel. In the past few years, a few design concepts of the gear train were introduced for the

application of portal axle (Exaxt, 2002; The Unimog Centre.com, 2004; Axle Tech Bolt, 2009). Figure 1.2 shows an example of a portal axle gear train with two idler gears. The input gear shaft is connected to the axle whereas the output gear shaft is connected to the wheel. The gear which is meshed between the input gear and output gear is called the idler gear. The idler gear allows the input gear and output gear to rotate in one direction.

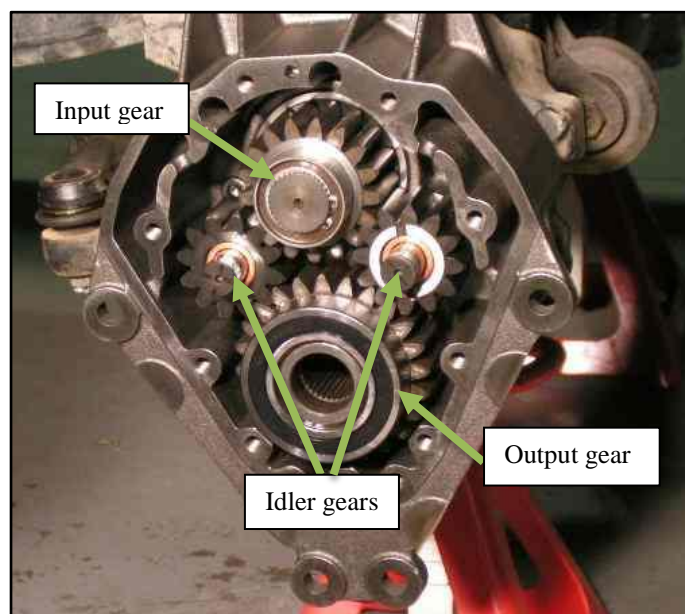


Figure 1.2: Portal axle gear train with two idler gears (Marks 4WD Adaptors 2002).

Portal axle is produced in a small scale as modification parts for vehicles to be driven off-road. The gears in portal axle are often customized in design to suit various off-road driving conditions. In practice, gear design parameters for portal axle are normally determined by referring to a number of widely accepted gear standards (THC Gears Standards 1998) such as the AGMA standards. However, the AGMA standard has some limitations for customized gear design. The AGMA standards only provided gear design

parameters that are valid for full depth involute gear tooth with certain pressure angle. The AGMA analytical gear model does not consider the radial load originated from the applied torque (Li, 2008; Hassan, 2009). In addition, the use of these gear standards requires experience in determining the gear factors. Vibration analysis and vibration monitoring of the gear train can also be assessed by these gear standards or experiment. Experiment is carried out for testing the gear's strength, vibrations and the durability of the customized gear designs. However, experiment setup is often difficult because proper setup of the gears for experiment test is required for accurate evaluation of the gear train.

Alternatively, FEA is used extensively in studying the stresses and vibrations in the gear train. With the advent of FEA and Computer Aided Design (CAD), the ability to simulate various gear design have been improved (Wei, 2004; Ooi, 2012). However, the model and the solutions in CAD and FEA must be evaluated carefully to ensure that the results are accurate. There are a number of research works done in investigating the gear tooth parameters and also validating the gear train models (Draca, 2006; Xu, 2008; Stoker, 2009). However, the gear train models were simplified and limited to the analysis of a gear tooth model in two-dimensional (2D). For a more comprehensive study on the gear train stress and vibration characteristics, a 3D gear train model should be modelled and analysed to predict the actual motion behaviour of the gear train (Bruns 2007).

In most cases, the FEA models of the gear train were analysed in ideal load positions. However, in reality, there is a slight misalignment in the gears when the gear train is operating (Stoker 2009). Small tolerances in the

fabrication of gears and small deviations in tolerances in the assemblies of gears may cause gears to fail before their specified lifetime. These deviations are present in any mechanical system. Typical tolerances can change in any three principal axis by as much as 0.02 inch. Within this small allowable tolerance, drastic changes in bending stress and contact pressure can occur. The increase in distance between the gear and pinion's axis lead to the increase in the bending stress and contact stress of the gear. Therefore, it is important to account for the misalignment in portal axle gear train.

In this research, three different gear train designs of the portal axle were modelled using Autodesk Inventor Professional 2010 software. ANSYS v12.0 software was used to investigate the gear teeth stress behaviour of the output gear in various angular positions. The gear train with no idler gear, the gear train with one idler gear and the gear train with two idler gears were modelled to investigate the gear teeth stress behaviour at the output gear. The effect of the non-ideal loading to the bending and contact stress of the output gear of the gear trains was also investigated.

Vibration analysis of the gear train is also important to ensure safe and quiet operation of the gear systems. There has been a number of research done in developing finite element models for simulating the dynamic behaviour of the gearbox systems (Li, 2008; Eritenel and Parker, 2009; Hu et al., 2011). The vibrational behaviour of the gear train models was closely dependent on the geometrical structure of the gear train, the source of load excitations and the constraints applied. In this thesis, three gear train designs were modelled by using the ANSYS software for vibration analysis. The effect of the non-ideal

loading to the vibration behaviour of the gear train designs was also investigated.

The portal axle shafts are used in transmitting power and torque from the gear train to the wheel. In the design stage, the torsional strength of the shafts must be first determined. Inaccurate evaluation of the torsional strength of the shaft may lead to complete fracture of the shaft. Although there are industry standards that can be applied in designing shafts such as the ASME and ANSI (Shigley and Mitchell 1983), experience is required in selecting proper design shaft parameters. In addition, these standards only provide design parameters for standardized shaft design and are only suitable for certain shaft applications.

Most components in the portal axle are customized for extreme operating condition where industry standards are not suitable. In designing a robust operating shaft, engineers are seeking to design shafts that are able to operate with sufficient strength but reduced weight for improved power to weight ratio. In recent years, hollow shaft is more favoured than the solid shaft because it offers increased availability and lightweight with adequate torsional strength. However, when compared between the solid shaft and hollow shaft with equal section modulus, the torsional strength of the hollow shaft is reduced by nearly half (Shigley and Mitchell 1983).

In this research, a hollow shaft with rib support at both end of the shaft was proposed for the output shaft of the portal axle. ANSYS Workbench v12.0 software was used to develop the FEA model of the output shaft. The hollow shaft thickness, rib thickness, depth of spokes, rib fillet radius, and the number of spokes are the five parameters of the rib support that were considered for the

parametric optimization of the output shaft. Firstly, the effect of each parameter to the hollow shaft torsional stress was investigated. Later, the L25 Taguchi Orthogonal Array (OA) was adopted to determine the optimum parameters for the output shaft.

1.2 Research Objective

FEA has not been used in analyzing the stress and vibrations of the gear train portal axle even though FEA has been proved for its ability to accurately predict stress and vibrations in gear trains by some authors (Wei, 2004; Draca, 2006; Xu, 2008; Ooi, 2012). There are challenges involved in modelling the gear train which include complex geometries of the gears, accurate arrangement of the gears in the gear train model, and contact surface problems (Wei 2004). In this research, the analysis of the portal axle focuses mainly on the gear train component and the output shaft component. The objectives of this thesis are:

1. to develop a 3D gear train model of the portal axle tht could accurately simulate the gear bending stress and contact stress by using FEA.
2. to investigate the gear stress and vibration behaviour of three different gear train design used in portal axle under ideal and non-ideal loading.
3. to develop a hollow shaft with rib model for the output shaft of the portal axle that can accurately simulate its torsional strength by using FEA.
4. to improve the torsional strength of the hollow shaft with rib model through parametric optimization by using Taguchi Method.

With regard to the objectives, the scopes of this research are:

1. to compare the gear bending stress and contact stress simulated by using FEA with the one obtained from experiment and analytical model.
2. to investigate the effect of non-ideal loading to the output gear bending stress and contact stress of the three gear train design.
3. to investigate the effect of non-ideal loading to the free and forced vibration of the three gear train design.
4. to compare the torsional stress of the hollow shaft model simulated by using FEA with the torsional stress obtained from the theoretical model and experiment model.
5. to determine the optimum parameters for the hollow shaft with rib model by using the L25 Taguchi OA.

1.3 Thesis Overview

This thesis consists of six chapters which describes the analysis of the gear train and output shaft of the portal axle. Chapter 1 presents a general introduction, the objectives to be achieved and lastly the layout of the thesis is briefly described. Chapter 2 covers a literature review which discusses the current approach used in evaluating the gear stress, and the vibrational behavior of the gear trains in various applications and their possible limitations. The background characteristics of the spur gears and the FEA model of the gear train developed by authors for evaluating the gear stresses, natural frequencies, mode shapes and the dynamic excitation characteristics are also

explained. The background characteristics and the current method used for the evaluation of the shaft's torsional stress are also described in this chapter.

Chapter 3 describes the stress analysis of the portal axle's gear train. Firstly, a gear train model consisting of the input gear and output gear is validated by comparison with the experiment test. Three gear train designs are developed to determine the gear bending stress and gear contact stress in different angular positions. The effect of the non-ideal loading of the output gear to the gear teeth stress of the output gear of the gear train is also investigated. In Chapter 4, vibration analysis is performed on three gear train models by using FEA. Firstly, the amplitude of deformations is investigated with respect to the first ten mode shapes of the three gear train models. Later, the forced harmonic frequency is performed on the three gear train models. The effect of non-ideal loading to the forced harmonic frequency of three gear train models is also investigated.

Chapter 5 describes the parametric optimization of a hollow shaft with rib support at both ends for the output shaft of the portal axle. Firstly, a hollow shaft model is developed by using FEA. Later, the torsional stress determined in FEA is compared with the torsional stress obtained from the experimental method and analytical method for validation. The hollow shaft with rib model is proposed and developed. Five parameters of the rib structure are considered and the effect of each parameter to the shaft torsional stress is investigated. The L25 Taguchi OA which considers five parameters and five variables is used to determine the optimum combination parameters for the hollow shaft with rib model. Chapter 6 describes the conclusions and the contributions of this thesis, and the suggestions for future work.

CHAPTER 2

LITERATURE REVIEW

2.1 Gear bending stress analysis

In the middle of the 20th century, most gear designs were based upon Lewis original bending equation (Lewis, 1893; Dolan and Broghamer, 1942). Lewis (1893) based his analysis on a cantilever beam and assumed that failure will occur at the weakest point of this beam. However, failure due to flexural stresses on bodies with changing or asymmetrical cross-sections was proved inaccurate by Dolan and Broghamer (1942). Their approach used photoelastic experiments to visualize the stress concentrations due to the fillets at the base of spur gears. By these visualization techniques they were able to predict more accurately at what stress levels gears will fail due to high bending stresses. Much earlier work was done using photoelastic experiments to design spur gears based on the stresses observed at the most critical points (Black 1936). The use of photoelastic experiment is rare due to the high cost of the equipment and it requires experience and skills to determine the gear stresses. Although this method is useful in determining static stresses in spur gears, the photoelastic trend has become more popular toward its usage in gear dynamic analysis (Shimamura and Noguchi 1965).

On the other hand, the bending stress for a standardized gear design can be estimated from numerous gear standards such as the AGMA standards and the ISO standards for gear. The AGMA standards were established in 1982

and are still widely used in gear design today. The bending stress equations found in these standards are based on the Lewis's original equation with several gear factors (Arikan 2002). The gear geometry factors found in the equations are critical in determining accurately the bending stresses for a wide variety of gears (Chong et al., 2002). These geometry factors accounted for the changing shape of the gear tooth, the point where the load is applied, as well as the fillet radius at the tip and base of the tooth.

In general, the AGMA standard is only valid for standard gear design in which the gear must have 20° of pressure angle and the gear tooth profile must be symmetrical (Kawalec et al., 2006). Thus, these gear standards are not suitable for calculating the gear stresses for gear design with customized parameters. In this situation, when it comes to designing customized gear, gear designers need to approximate the strength and durability of their gear design based on their own judgement and experience. This may lead to inaccurate evaluation of the gear strength.

Kawalec et al. (2006) have set up an experimental test on several standard gears to compare the stress results with the gear stress calculated from the AGMA standard. The authors commented on the significant difference in results but concluded that it is in an acceptable range. In the AGMA analytical tooth model, the maximum load occurs at the highest point of single tooth contact (HPSTC). It was clearly shown the position of the load at HPSTC but the direction of the load is not defined. The direction of the load strongly depends on the surface contact between gears. However, the direction of the load applied to the tooth surface is uncertain and difficult to be determined. One of the solutions to determine the correct directional load is by using FEA

to model the gears and perform simulation on the contacting gears. Thus, the gear teeth bending stress should be evaluated with respect to varying angular position of the gear tooth.

Although FEA has been around for over half a century, it was not until the increased in computing power that the real advantages of this method became apparent. In the area of gear research, the modelling of the gear tooth and simulation of the bending stress analysis using FEA is one of the significant contributions to the understanding of gear stress behaviour (Townsend and Coy 1985). The modelling of spur gears and the analysis of the stress results using the FEA has led to many insights which may not have been immediately apparent. In the FEA modelling, the first challenge to overcome is to model the geometry and dimensions of the gear correctly. Once the geometry has been modelled, the type of elements and mesh to be applied is crucial. Areas where higher stresses and deformations occur needed to be meshed more densely so that the results were accurate.

Many of the first attempts of FEA on spur gears were developed in 2D to simplify the solution. Later, the gear bending stress was analysed by applying FEA on the developed 3D spur gear models (Vijayarangan and Ganesan 1993). The advantages of this method over experimental techniques are competitive cost effectiveness and repeatable results. The accuracy of the FEA solution can be assessed by verifying that the FEA results correspond closely to experimental results. Hence, the validity of the FEA setup and technique applied can be confirmed. There are few authors who have validated their FEA models by comparing the gear stress results with the experiment results (Wei, 2004; Draca, 2006; Xu, 2008; Ooi, 2012).

The current trend of gear design is focused in designing different shaped gears to transmit higher loads without failure. The purpose of investigating the effect of the shaped gears is to precisely engineer these gears so that the maximum efficiency can be achieved and overdesign or underdesign of the gear can be avoided. By changing the shape of the gear tooth to an asymmetrical design the authors have proven a decrease in both bending stress and contact pressure (Cavdar et al. 2005). In the past, most 3D gear models developed was often a simplified model with many assumptions considered and some models are limited to analyzing the bending stress for a single involute spur gear. When the gears are operating, the gear teeth are often meshed with one or more gear teeth depending on the gear contact ratio (Wang and Howard 2005). The analysis of single gear tooth does not provide a full understanding of the actual gear meshing mechanism. Instead, a full gear bodies should be developed for a more comprehensive understanding of the gear stress analysis.

2.2 Gear contact stress analysis

The analysis of the contact pressure at the surfaces between the gear contacting teeth is also important so that one can understand how the wear resistance and the fatigue failure rate of the gear can be affected. Heinrich Hertz was the first to analyse the contact stress of the gear tooth. His theory describes the contact pressure between two deformable cylinders (Sackfield and Hills 1983). The work of Hertz (1882) was expanded by Archard (1953) who has proposed an experiment to investigate the contact pressure between

two deformable bodies. His work led to the evolution of many modern techniques and formulations that are present today for contact analysis (Archard, 1953; Flodin and Andersson, 1997). While the bending stress is dependent on the geometry and shape of the gear tooth, the contact pressure is mainly a function of the type of material in contact and the radius of curvature of the gear surface contact (Kapelevich 2000).

In recent years, there has been a number of proven research works done by authors (Kapelevich, 2000; Chen and Tsay, 2002; Kang and Choi, 2008) in investigating the contact pressure between two spur gears, helical gears and asymmetrical gearing. There are also authors (Mao, 2007; Li, 2007; Liu et al., 2010) that applied the FEA approach in their research and the results are validated and well documented. In solving contact problems using FEA, there is a vast amount of work done on the stiffness of spur gear teeth and the appropriate method used for developing a precise geometrical gear model using FEA (Arafa and Megahed 1999). In the analysis of the gear contact stress done by Wei (2004) and Draca (2006), they considered the effect of non-linearity at the beginning of contact between teeth, as well as the importance of the point of contact. The effect of the non-linearity in gear contact stress was verified by the experimental test.

Although the contact pressure problem has been solved and the accuracy of the FEA solution was validated, the model used for the evaluation of contact stress is based on the contact surface between two cylindrical bodies that are identical. This model only provides the understanding of a how contact stress is developed from the normal loading but it did not consider the friction effect due to the tangential load. One of the biggest challenges in analysing the

gear contact stress is to develop a gear tooth model that has smooth geometrical surface, precise alignment of the gear teeth to be in contact with another and solving contact problems. Properly aligned spur gears are designed to mesh with the pinion at a precise point. A slight change in the geometry or alignment of gear contact can cause a tremendous change in the contact stress.

2.3 Vibration analysis of the gear train

Vibration analysis of the gear train is also important in ensuring the gear train is operating under an acceptable level of vibrations and noise level. It can predict the resonance of the gear train excited by the dynamic input. Resonance can raise the structural stress level to cause structural failure (Berlioz and Trompette 2010). There are quite a number of contributed research works by authors (Mark, 1978; Ozguven and Houser, 1988; Lim and Singh, 1991; Choi et al., 1999) in the area of modal analysis on the gear train and gearbox, analysis of the gear train resonance, and analysis of the change of in resonance frequency upon varying excitation load.

In the past few years, there are a few works devoted to study the vibrations by using analytical method and experimental test. Ozguven and Houser (1988) presented a thorough summary of the gear dynamic models for gear train in his research work. Choi et al. (1999) investigated a single helical gear pair of the rotor dynamics helical geared system by experimental testing. It was found that this particular system experienced severe coupled torsional, lateral, and axial vibrations. Mark (1978) analyzed the vibratory excitation of gear systems of single stage and multi-stage theoretically. Lim and Singh

(1991) presented study of the vibration analysis for complete gearboxes on three cases in which a single-stage rotor system with a rigid casing and flexible mounts, a spur gear drive system with a rigid casing and flexible mounts, and a high-precision spur gear drive system with a flexible casing and rigid mounts were analysed. Perret-Liaudet and Sabot (1994) presented another study for noise analysis of the gear train experimentally. The authors studied how the high excitation of vibration in the gears, shafts, bearings and the casing can cause high level of noise within the car or truck cab.

In the application of FEA in analyzing the gear train vibrations, Errichello (1979) have surveyed a great deal of literature on the development of a variety of simulation models for both static and dynamic analysis of different types of gear trains. The FEA program was also adopted by authors (Simon, 2000; Lin et al., 2007) to help simulate the stresses on a single stage, double stage, and gearboxes to investigate the gear failure and conduct parametric studies. Draca (2006) investigated the model of double-stage helical gear reduction using finite element analysis. The author analysed modal analysis of the model using free and forced vibration response. The dimensional effects such as the shaft length, output shaft angle effect, and bearing stiffness effects were also considered in modal analysis and compared to the benchmark model.

A dynamic analysis of a multi-shaft helical gear system was performed by Kahraman et al. (2004). A simple finite element model was developed to investigate the dynamic behaviour of a spur gear rotor system. Even though there were many work contributed by authors in the research area of gear train modelling and simulation by using FEA, their investigations are limited to a

specific gear train application where the operation behaviour of the gear train can be very different.

2.4 Gear misalignment and its effect

Gear strength, gear wear, prediction of gear dynamic loads, and gear noise are always a major concern in gear train design. However, one topic that has not been discussed thoroughly is the effect of non-ideal loading conditions on the stress and vibration behaviour of the gear train. Non-ideal conditions are characterized by a change in the tolerances or specifications which define the acceptable assembly of a gear train. Some studies have been conducted on how the noise or vibration of spur gears is affected by manufacturing error (tooth surface roughness) or misalignment (Valex and Maatar, 1996; Parey and Tandon, 2003).

Another study was conducted to investigate the increase in contact pressure and bending stress when gear is misaligned in the modelled face gear drives (Barone et al. 2003). The study observed significant increases in the contact pressure, as well as reduction in the load sharing effects of the teeth. It was suggested that the additional misalignments can be included to properly provide guidelines for gear design. One recent study of spur gear misalignment and machining errors confirmed these results (Li 2007).

Another significant work was done by Stoker (2009) in investigating the effect of gear stresses and wear under non-ideal loading by using FEA. The author has successfully modelled a 3D partially modelled gears meshed with another gear to investigate the effects of these misalignments on the bending

stress and contact pressure as it relates to the amount and location of wear. Recently, there has not been any research work in the analysis of the stress and vibration behaviour of the gear train in non-ideal loading conditions in portal axle. By accurately modelling a spur gear in mesh, the stresses and vibrations of the gear train model portal axle and the effect of the non-ideal loading can be predicted using FEA.

2.5 Torsion analysis of the shaft

Evaluation of torsion in shaft has been practiced by engineers in the past few decades and it is the key of importance in the design of shafts. Extremely high torsion resulting from overloading can cause higher fatigue failure or complete shaft breakage (Xiaolei et al. 2011). The failure in shafts normally occurs at the stress concentration area found in splined joints shaft and keyway shaft which can eventually lead to the fracture of gear shaft [59]. These stress concentrations on critical areas can be reduced by redesigning the structure of the shaft (Heisler, 1999; Jianping and Guang, 2008).

In practice, engineers apply the available standards for designing shaft based on their shaft design criteria. The standards for shaft design such as the ANSI or ASME standards provide a range of shaft design criteria extracted from verified analytical solution. However, these standards are only limited to certain type of shaft design and it lack the depth of understanding of how torsion can affect the whole shaft design. Furthermore, when it comes to customizing the shaft design, these standards may not be applicable.

In the past decade, FEA was proved to be effective by authors (Li, 2001; Bayrakceken et al., 2007; Crivelli et al., 2011) in evaluating torsion in shafts and also to help them in the investigation of failure analysis of the shaft applications. Mutasher (2009) applied FEA to determine the torsional strength of the hybrid aluminium composite drive shaft and good agreement was obtained between the finite element predictions and the experimental results. Göksenli and Eryürek (2009) applied FEA to perform torsional stress analysis on the keyway shaft of an elevator. The acceptable radius of the keyway corner was considered through studying the relationship between shaft stress and radius of the keyway corner of the shaft.

2.6 Taguchi method for shaft optimization

There has been a lot of research on the analysis of shaft in various applications. However, the strength and weight are always a major concern in shafts design. Shaft designers and engineers are constantly looking into ways to redesign shaft based on a number of parameters to achieve higher strength to weight ratio. Usually, the effect of one parameter to the shaft strength is analysed separately. This type of analysis can be less effective when considering a number of parameter because one parameter may affect another. To study the trade-offs that exist between these conflicting design goals and to explore design options, one needs to formulate the optimization problem to achieve the desired objective.

Taguchi method is an effective optimization method that has been applied in various field of research. It is a statistical method developed by

Genichi Taguchi to improve the quality of manufactured goods. Recently, it was also being applied in engineering for optimizing mechanical design (Byrne and Taguchi, 1987; Box and Bisgaard, 1988; Ross, 1996). In this method, the orthogonal array (OA) is proposed depending on the factors and variables to be optimized. Kotcioglu et al. (2012) have performed experimental investigation for optimizing design parameters in a rectangular duct with Plate Fins heat exchanger by using Taguchi Method. Gunes et al. (2011) applied Taguchi method to determine the optimum values of the design parameters in a tube with equilateral triangular cross-sectioned coiled wire insert. From their research work, the effect of the design parameters was investigated by using Taguchi method. To date, Taguchi method was rarely applied in mechanical design problems such as in gear and shaft designs even though the optimization is proved effective (Byrne and Taguchi, 1987; Otto and Antonsson, 1991). Based on the above mentioned applications, Taguchi method can be used in optimizing shaft design.

CHAPTER 3

STRESS ANALYSIS OF THE GEAR TRAIN UNDER NON-IDEAL LOADING

3.1 Finite element analysis

In this section, the steps for developing the 3D gear train model and the FEA technique are described in details. Figure 3.1 shows the general procedure in determining the bending and contact stress of the gear train. In modeling of the gear train, the gears required for the gear train are modeled based on the design parameters. The material properties and gear parts assembly are also assigned in this stage. This is followed by the FEA pre-processing stage where the mesh element, the load, and constraint are set on the gear train model. In order to determine the bending stress and contact stress accurately, different mesh element settings and FEA solver are required in separate setup. In the FEA post-processing stage, the FEA solution for the gear train model is completed. The maximum von Mises stress is obtained from the contour plot of the gear train. Thus, the bending and contact stress analysis can be performed by correlating the change in applied load and gear parameters.

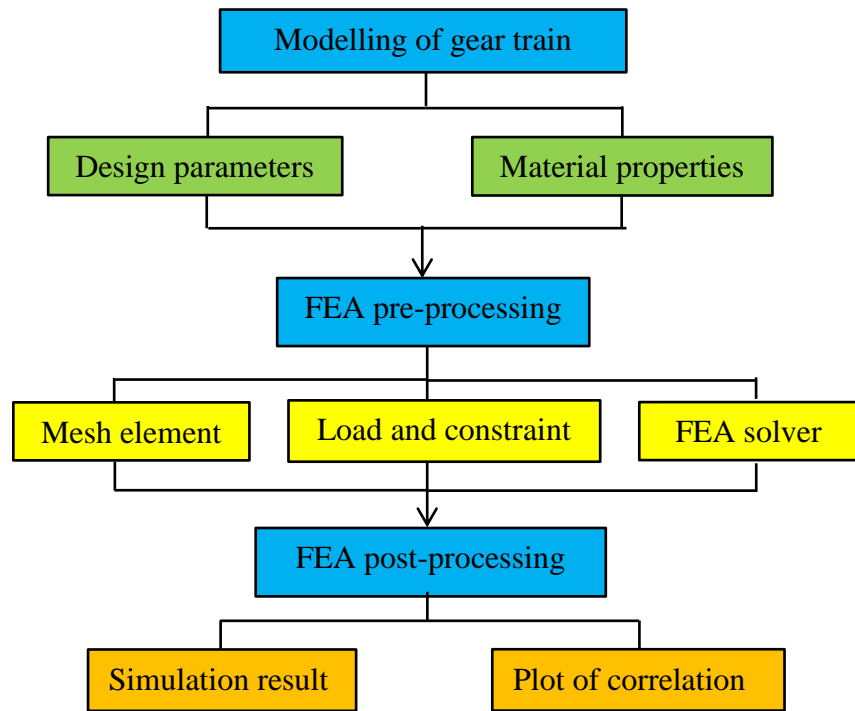


Figure 3.1: FEA general steps for obtaining the gear bending and contact stress.

3.1.1 Modeling of the gear train

A simple gear train with one input gear and one output gear are modeled by using Autodesk Inventor Professional software. The input and output gear are modeled according to Sanders (2010) experiment gear model as shown in Table 3.1. The input gear and output gear are positioned and constrained to mesh at a single tooth contact in between them. The gear contact surfaces between gears are aligned to touch tangentially by using constraint functions in Autodesk Inventor software. Later, the gear train model is converted into IGES file and imported to ANSYS software.

Table 3.1: Material properties and design parameters of the test gears.

	Input gear	Output gear
Material	9310 Steel	
Modulus of Elasticity	210 GPa	
Yield Strength	1.8 Gpa	
Ultimate Strength	2.0 Gpa	
Poisson's Ratio	0.30	
Number of teeth	34	30
Pitch diameter	144 mm	127 mm
Module	0.4233 mm	
Pressure angle	20°	
Face width	25.4 mm	
Transverse tooth thickness	6.57 mm	
Root diameter	131.75 mm	114.75 mm

3.1.2 Gear bending stress

In the FEA pre-processing, 'static structural' type is selected for the analysis by using ANSYS software. The mesh of the gear model is defined by using ANSYS mesh setting. In ANSYS mesh setting, the 'brick element' is selected for generating mesh elements on the gear train model. When the gear tooth of the output gear is subjected to tangential load, the tooth root is the weakest point. Hence, the tooth root area of the output gear is meshed with higher density mesh. The optimum mesh density is determined based on the convergence of the maximum effective stress. In order to determine the optimum mesh size for meshing the tooth root area, the convergence limit of the effective root stress is determined when the mesh element size is gradually reduced as shown in Figure 3.2. The effective stress starts to converge when the mesh refinement size element is 3 mm.

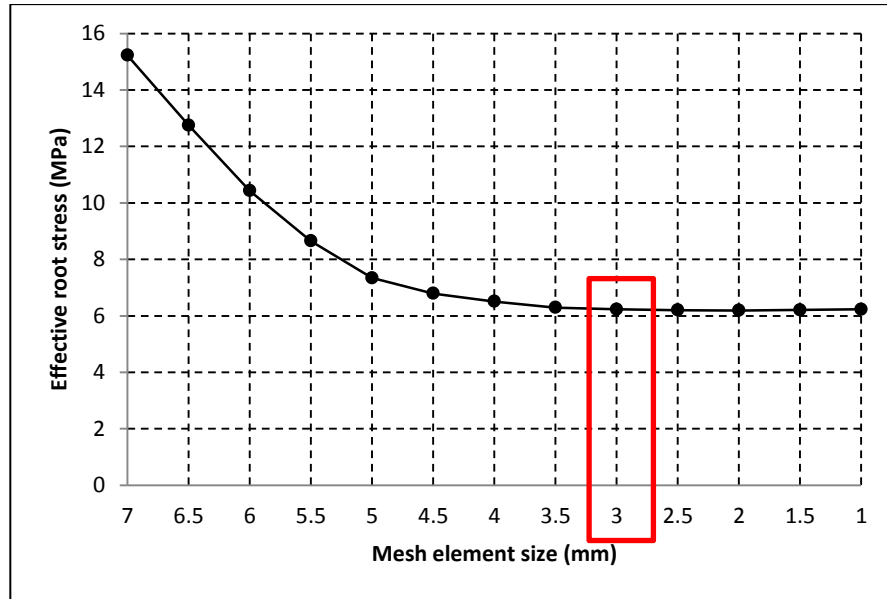


Figure 3.2: Optimum mesh element size by stress convergence method.

Figure 3.3 shows the generated mesh model of the gear train consisting of 90% hexahedron elements and 10% of tetrahedrons and prism elements. In ANSYS mesh setting, pure meshing of brick elements is not possible due to the complicated structure of the model. From the mesh model, the number of elements and nodes generated are 12381 and 40120 respectively.

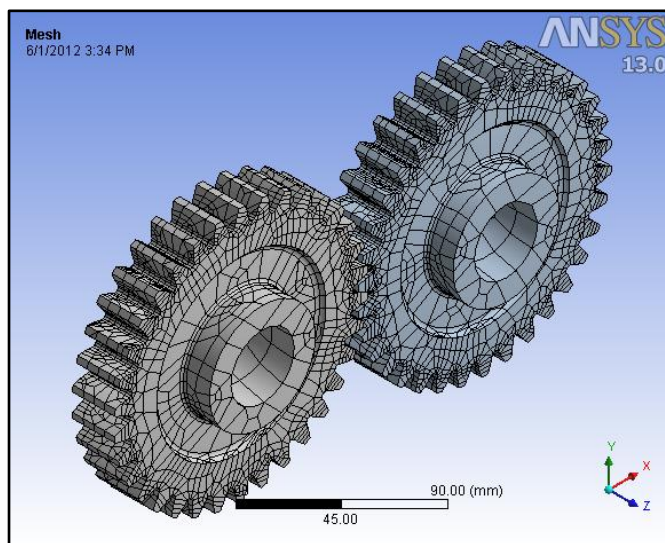


Figure 3.3: Mesh model of the gear train.

In ANSYS setup, the boundary conditions are set on the gear train. Figure 3.4 shows the load and surface constraints set in the ANSYS setup for simulating the static bending stress. Torque load of 700 Nm and tangential cylindrical support are applied on the hub surface of the input gear. In the tangential cylindrical support, the surface is rigid and restricts the input gear to rotate about its axis. The driven gear's inner surface is fixed at the hub surface to allow bending load at the gear teeth. The contact surfaces between gears are set to be rigid by selecting contact type to 'No Separation'. This contact type allows the load transfer from the torque without friction. In addition, the load can be transmitted directly to the tooth root instead to the contact surface.

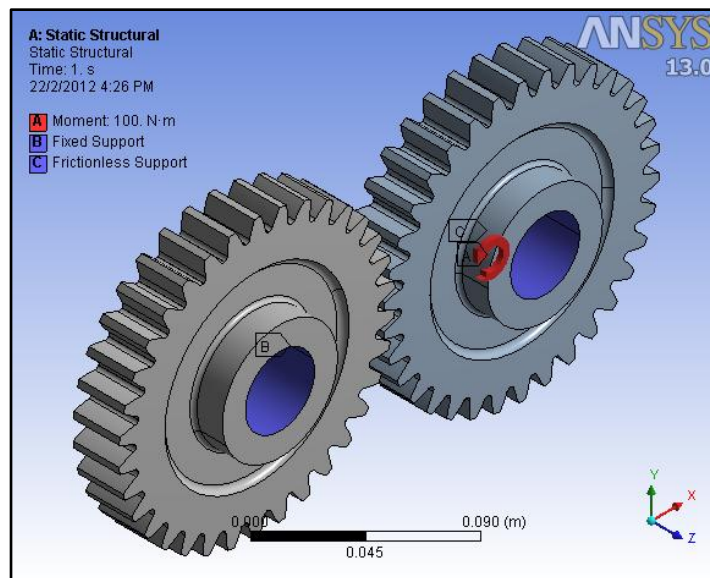


Figure 3.4: Load and constraints of the gear train model.

In the FEA post-processing, the 'von Mises stress' type result was selected in ANSYS. The bending stress is probed at three different gear tooth root locations (Gauge A, Gauge B, and Gauge C) of the output gear as shown in Figure 3.5. The results are recorded for comparison with the experiment.

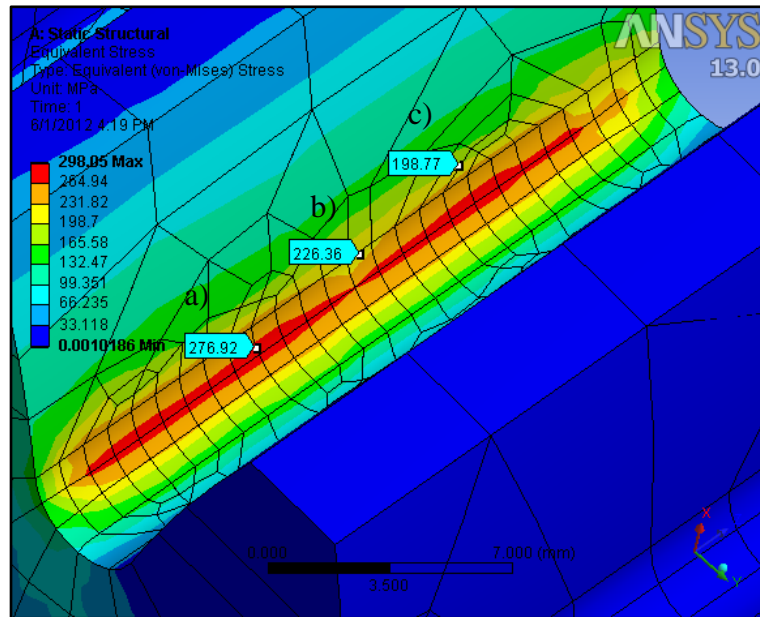


Figure 3.5: Point probe of tooth root bending stress at a) Gauge A, b) Gauge B, and c) Gauge C of the output gear.

3.1.3 Gear contact stress

In this section, the ‘static structural’ type is selected in ANSYS. In ANSYS mesh settings, ‘brick element’ is selected to construct the mesh model of the gear train and the surface mesh refinement of 3 mm is set on the area of teeth surface contact between the input gear and output gear. The area of contact at the gear teeth surface representing the 3 mm refined mesh is approximately 2 mm by 40 mm as shown in Figure 3.6. The generated mesh of the gear train model consists of 126463 nodes and 41409 elements.

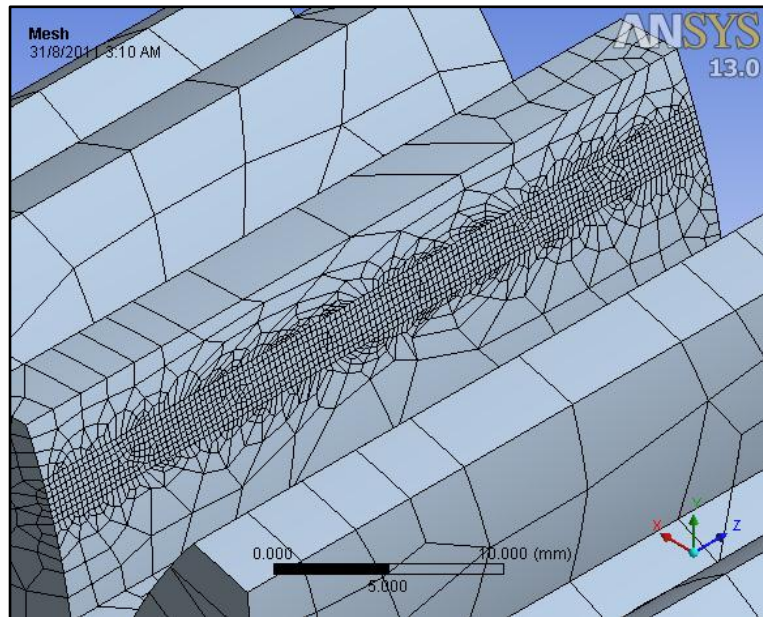


Figure 3.6: Refined mesh elements of 2 mm by 40 mm at the contacting gear teeth surface of the output gear.

In ANSYS, non-linear contact between the surface-to-surface contact elements is considered. There are three types of contact settings in ANSYS setup in which Penalty method, Lagrange multiplier, or Augmented Lagrange can be selected as a solver. The penalty method uses a spring contact to establish a relationship between two contact surfaces. The spring stiffness is called the contact stiffness. The penalty method modifies the present stiffness matrix by adding large terms to prevent too much penetration. The Lagrange method is an iterative series of penalty methods. The contact tractions (pressure and frictional stresses) are augmented during equilibrium iterations so that the final penetration is smaller than the allowable tolerance. Compared to the penalty method, the Lagrange method usually leads to better conditioning and is less sensitive to the magnitude of the contact stiffness. The Augmented Lagrange method utilizes both of these two methods to solve the contact problem. Therefore, the Augmented Lagrange method is selected as a solver

for the contact non-linearity problem and the coefficient of friction was set to 0.2 in ANSYS setup. The input gear contact surface is set to ‘Contact Element’ and the contact surface of the output gear is set to ‘Target Element’ in ANSYS setup. Figure 3.7 shows how the contact and target element are being selected in ANSYS for the gear teeth in contact.

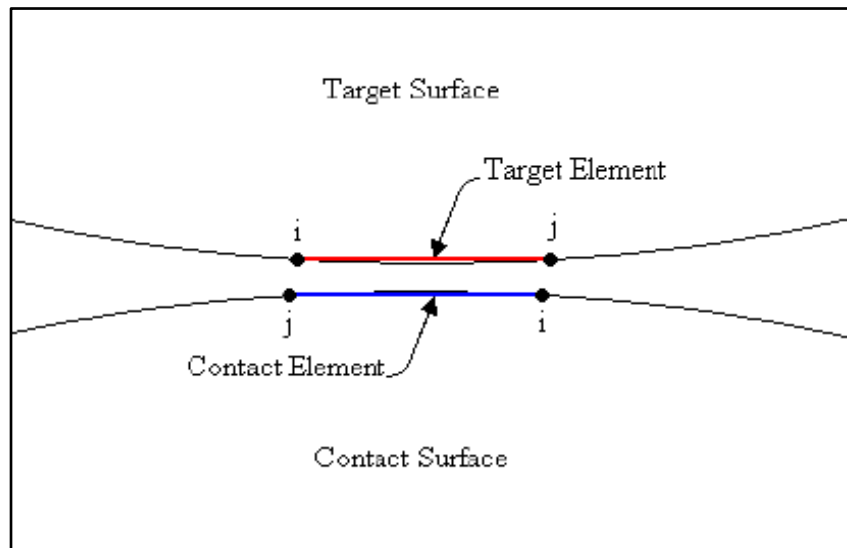


Figure 3.7: Contact and target elements between the gear teeth in contact.

The number of sub-step based on the incremental load is set to ten sub-steps. To further enhance the accuracy of the contact physically and avoiding errors, the interface treatment is set to ‘Adjust to Touch’ and the pinball region is set to ‘Auto Detection Value’ in ANSYS setup. The load and constraints set for contact stress analysis are similar to the load and constraints set for the simulation of gear bending analysis (Refer to Figure 3.4). Figure 3.8 shows a detailed contact stress distribution on the tooth surface. The contact stress distribution is quite uniform across the face width area of the gear tooth.

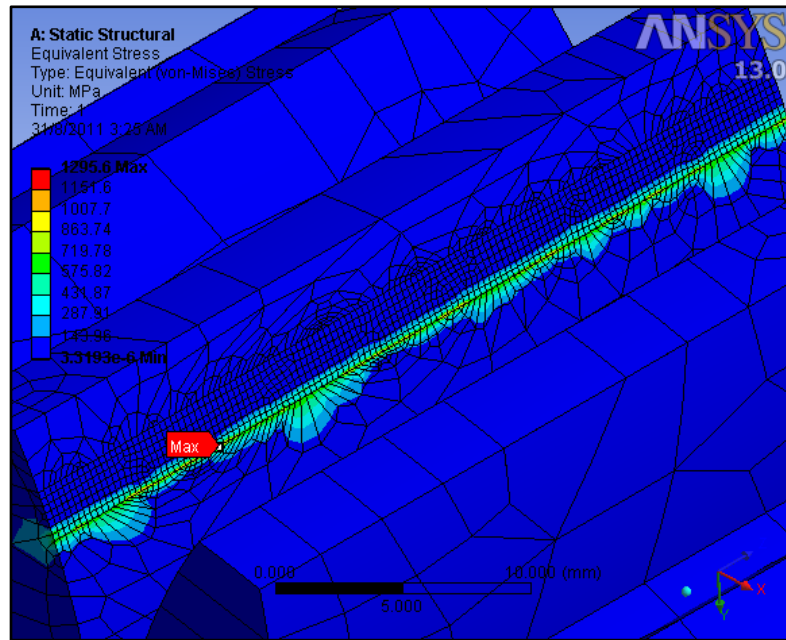


Figure 3.8: Detailed view of gear tooth contact stress distribution of the output gear.

3.2 Gear Experiment

In this section, the gear experiment setup is based on the work by Sanders (2010). Experiment test was setup on two meshing gears and the root stress was measured by installing several strain gauges at the gear root fillet area. Analyses were conducted on different gear root shape with varying pressure angle. The experimental results determined by Sanders (2010) are adopted in this research to compare and validate the gear bending stress by using ANSYS.

Vishay Micro-Measurements gauges (model number CEA-06-015UW-120) were used for the measurements. These gauges have a resistance of 120 ohms and a gauge factor of 2.05. They are flexible gauges with a cast polyimide backing and encapsulation, featuring copper-coated solder tabs, and consist of constantan alloy. The length of the active grid for each gauge was

0.38 mm. It was necessary to use gauges of this small size because the region of interest was only about 3 mm in arc length. Figure 3.9 shows the strain gauge positions in the x-direction and y-direction measured from the edge of the gear tooth at the output gear.

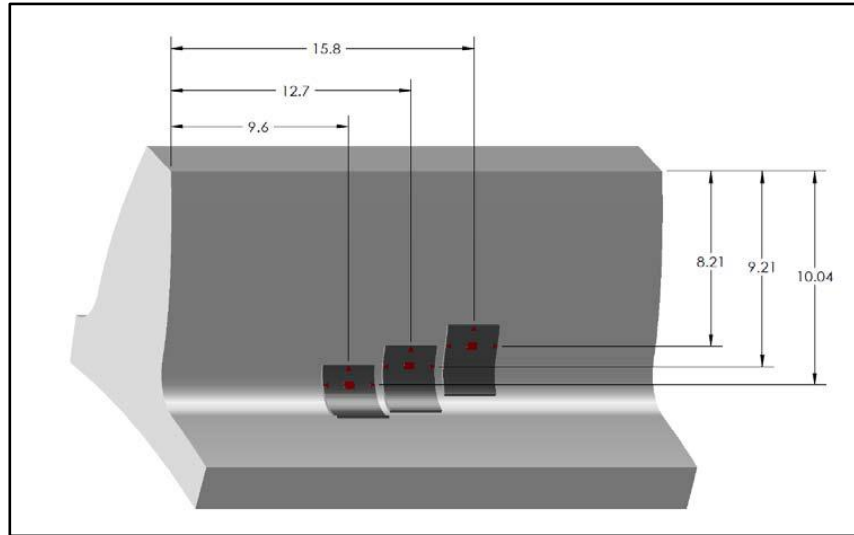


Figure 3.9: Strain gauges at respective position measured at a distance from tooth tip and left tooth (Sanders 2010).

Figure 3.10 shows the mounting of strain gauge on the tooth surface of the output gear. The actual locations of the mounted gauges were measured to confirm that the maximum deviation from the intended nominal position is well within 0.25 mm.

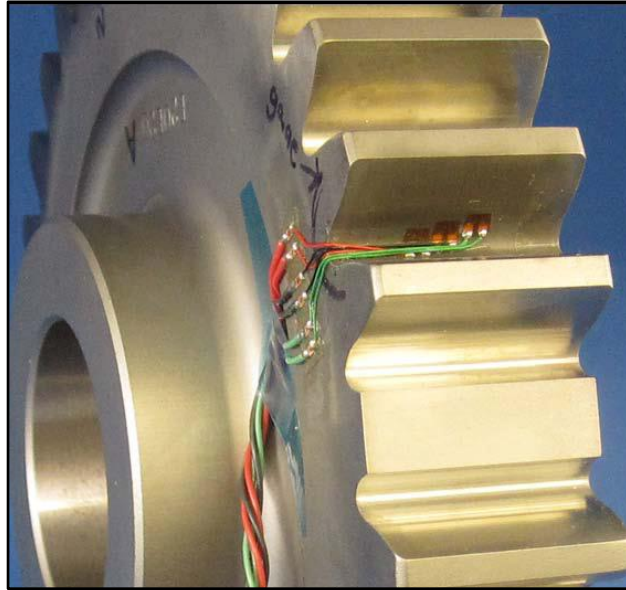


Figure 3.10: Strain gauges mounted on the tooth surface of the output gear (Sanders 2010).

The root strain signals were acquired and processed by using the instrumentation system defined in Figure 3.11. The analog signals coming from the strain gauges were fed into a National Instruments (NI) SCXI-1314 terminal block, which was plugged into the NI SCXI-1520 universal strain gauge input module. Both module 1314 and 1520 were assembled into a Wheatstone quarter-bridge configuration. The 1520 input module was connected to a NI SCXI-1000 chassis. The analog voltage signal from the chassis then travelled to a NI PCI-6052E data acquisition board in the personal computer (PC) where the analog signal was converted to a digital signal at a sampling rate of 10 kHz.

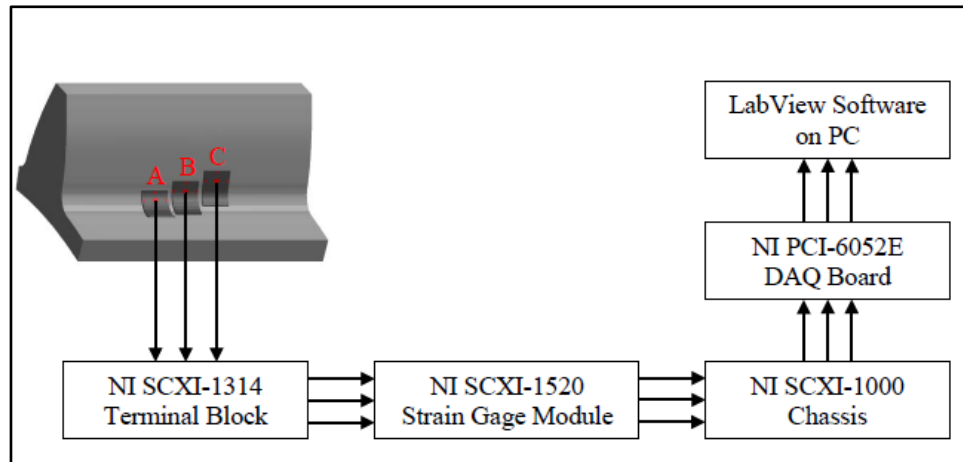


Figure 3.11: Strain measurement system instrumentation for measuring the output gear bending stress (Sanders 2010).

The digital signal was then analysed by using LabView software. The settings in LabView were set as follows: quarter-bridge configuration, 120 ohms dummy gage, “strain” output value, 2.05 gauge factor, 0 V minimum voltage, 6.25 V maximum voltage, 5 V vex voltage, sample time of “sample and hold”, and sampling rate of 10 kHz. Ten points of strain data is measured for every incremental torque of 288 Nm. The strain data files were recorded with LabView, and then imported to Microsoft Excel 2010 software for plotting the correlations.

3.3 Analytical method

3.3.1 Lewis equation and AGMA standard for gear bending stress

The Lewis equation derived by Lewis (1893) was one of the earliest methods used in determining the bending stress at the root of the gear tooth. In

this equation, the gear tooth is considered as a simple cantilever beam as shown in Figure 3.12.

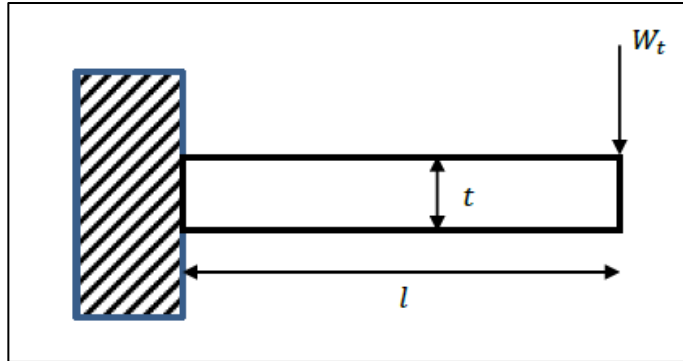


Figure 3.12: Lewis cantilever beam diagram.

The Lewis equation is stated as below,

$$\sigma_t = \frac{W_t p_d}{b_w Y} \quad (1)$$

where p_d = diametral pitch, b_w = face width, and the Lewis form factor, Y is,

$$Y = \frac{2xp_d}{3} \quad (2)$$

and x dimension can be determined from,

$$l = \frac{t^2}{4x} \quad (3)$$

With reference from the Lewis form factor diagram, for the gear with 30 teeth, full depth profile, and 20 degree pressure angle, the Lewis form factor

Y is approximately 0.35. Figure 3.13 shows the Lewis gear tooth diagram and the parameters used for determining the gear bending stress.

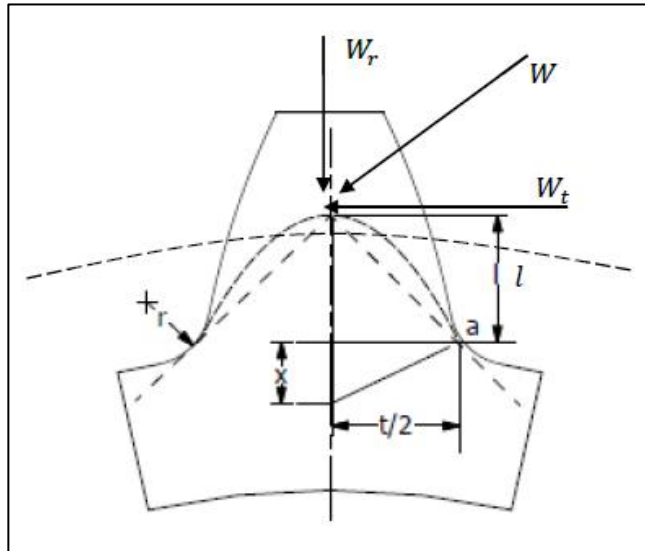


Figure 3.13: Loads and length dimensions used for determining the tooth bending stress.

The Lewis equation is based on following assumptions:

1. The effect of radial load W_r is ignored.
2. The effect of stress concentration of the root fillet is ignored.
3. The load is considered at the tip of the beam.

The AGMA bending stress is a modified version of the Lewis equation. The AGMA equation takes into account many factors for evaluating the gear bending strength compared to the Lewis equation. In the AGMA standard, the bending stress at tooth root is calculated based on the load applied at HPSTC as shown in Figure 3.14. The critical section is determined by the tangential points of a parabola inscribed into the tooth profile. This parabola represents profile of the beam with uniform strength along its axis. Thus, the position of

load also distinguishes the difference between the Lewis equation and AGMA standard. With reference from the AGMA form factor diagram, considering load applied at HPSTC for gear with number of teeth 30, the AGMA form factor Y_j is approximately 0.37.

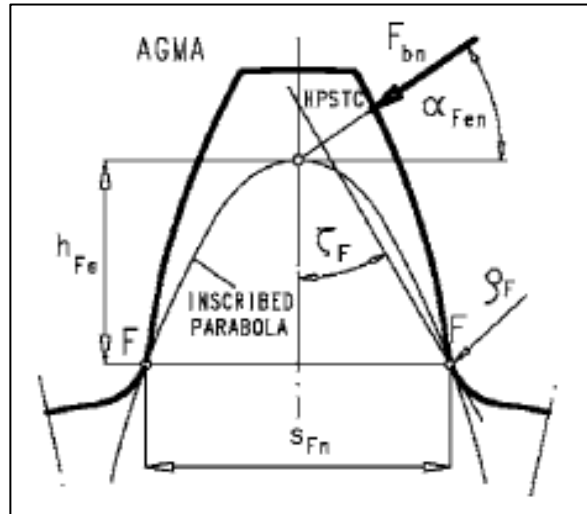


Figure 3.14: Load at HPSTC in determining the gear tooth bending stress (Kawalec et al. 2006).

The AGMA equation for calculating the gear bending stress is given as,

$$\sigma_t = W_t K_o K_v K_s \frac{K_H K_B}{b_w m_t Y_j} \quad (4)$$

where,

Y_j is the AGMA form factor

K_o is the overload factor,

K_v is the dynamic factor,

K_H is the load distribution factor,

K_s is the size factor,

K_B is the rim thickness factor,

m_t is the transverse module and,

W_t is the tangential load.

3.3.2 Hertzian equation and AGMA standard for gear contact stress

The gear contact stress can be determined analytically by using the Hertzian equation. The Hertzian contact stress of gear teeth is based on the analysis of two cylinders under a radial load. The radii of the two cylinders are the radii of curvature of the involute tooth forms of the mating teeth at the band of contact as shown in Figure 3.15.

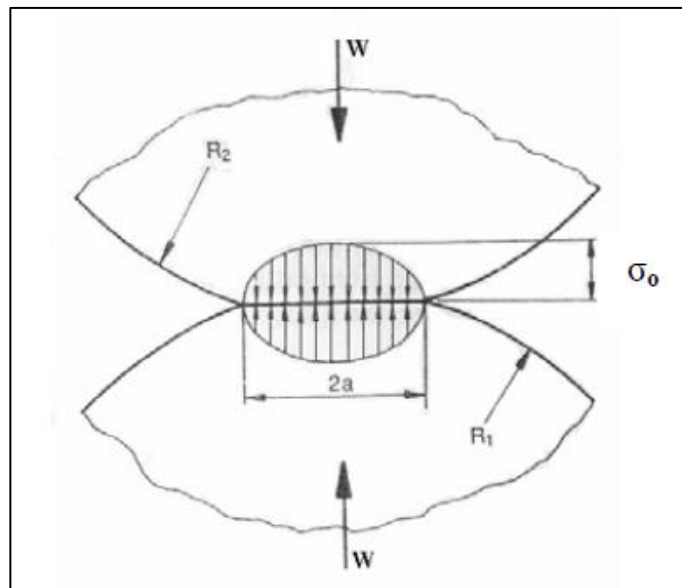


Figure 3.15: Hertzian model of the two cylinders in contact (Hassan 2009).

The band of contact between the two cylinders can be calculated as $2a$ where the deformed distance, a equals to,

$$a = 2 \sqrt{\frac{W(1 - \nu_1^2)/E_1 + (1 - \nu_2^2)/E_2}{b_w \pi (1/R_1 + 1/R_2)}} \quad (5)$$

The Hertz theory assumes an elliptic stress distribution, as shown in the Figure 3.16. The maximum stress is in the middle and given as,

$$\sigma_o = \sqrt{\frac{W(1/R_1 + 1/R_2)}{b_w \pi [(1 - \nu_1^2)/E_1 + (1 - \nu_2^2)/E_2]}} \quad (6)$$

where W is the normal load, E_1 and E_2 are the Modulus of Elasticity of pinion and gear respectively, ν_1 and ν_2 are the Poisson's ratios of pinion and gear respectively and b_w is the face width of pinion. R_1 and R_2 are the respective radii of the involute curve at the contact point.

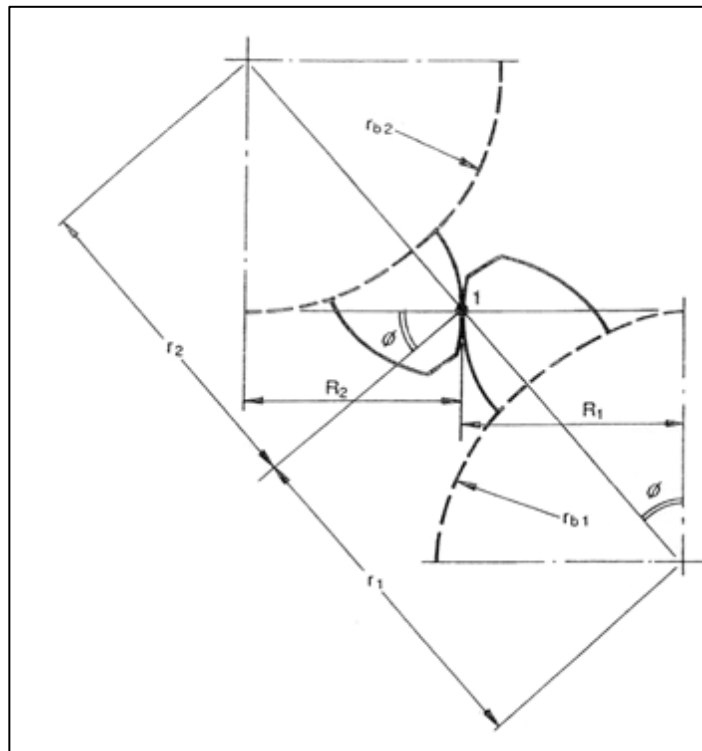


Figure 3.16: Two involute teeth in contact (Hassan 2009).

The pitch radius of the pinion and gear denoted as r_{b1} and r_{b2} respectively can be related to the gear involute radii as $R_1 = r_{b1} \sin \phi$ and $R_2 = r_{b2} \sin \phi$. Hence, the Hertz equation for contact stresses in the teeth becomes,

$$\sigma_c = \sqrt{\frac{W(1 + r_{b1}/r_{b2})}{r_{b1}b_w\pi[(1 - \nu_1^2)/E_1 + (1 - \nu_2^2)/E_2]} \sin \phi} \quad (7)$$

The assumptions considered in the Hertzian equation are pure bending of short beam, elliptic distribution of stresses at tooth contact, and friction between the gear contacting surfaces is not accounted in the stress equation. The AGMA standard for calculating the gear contact stress is also a modified version of the Hertzian equation in which several factors and coefficients to be accounted for. The AGMA contact stress equation is given as,

$$\sigma_c = C_p \sqrt{W_t K_o K_v K_s \frac{K_m C_f}{d_p b_w Y_j}} \quad (8)$$

where W_t, K_o, K_v, K_s, K_m and Y_j are the same quantities that were defined previously for the AGMA bending stress equation. C_p is the plastic coefficient and d_p is the root diameter of the pinion. The plastic coefficient can be obtained from,

$$C_p = \sqrt{\frac{1}{\pi \left(\frac{1 - \nu_1^2}{E_1} + \frac{1 - \nu_2^2}{E_2} \right)}} \quad (9)$$

3.4 Validation of the FEA model

3.4.1 Gear bending stress comparison

Figure 3.17 shows the comparison of the gear bending stress determined from FEA, experimental and analytical method. The bending stress results obtained from ANSYS are slightly lower than the experimental results with an average percentage difference of 5.16%. The bending stresses calculated by using the Lewis equation are slightly higher than the one calculated by using the AGMA bending stress equation and both results are close to the stress measurement at gauge B.

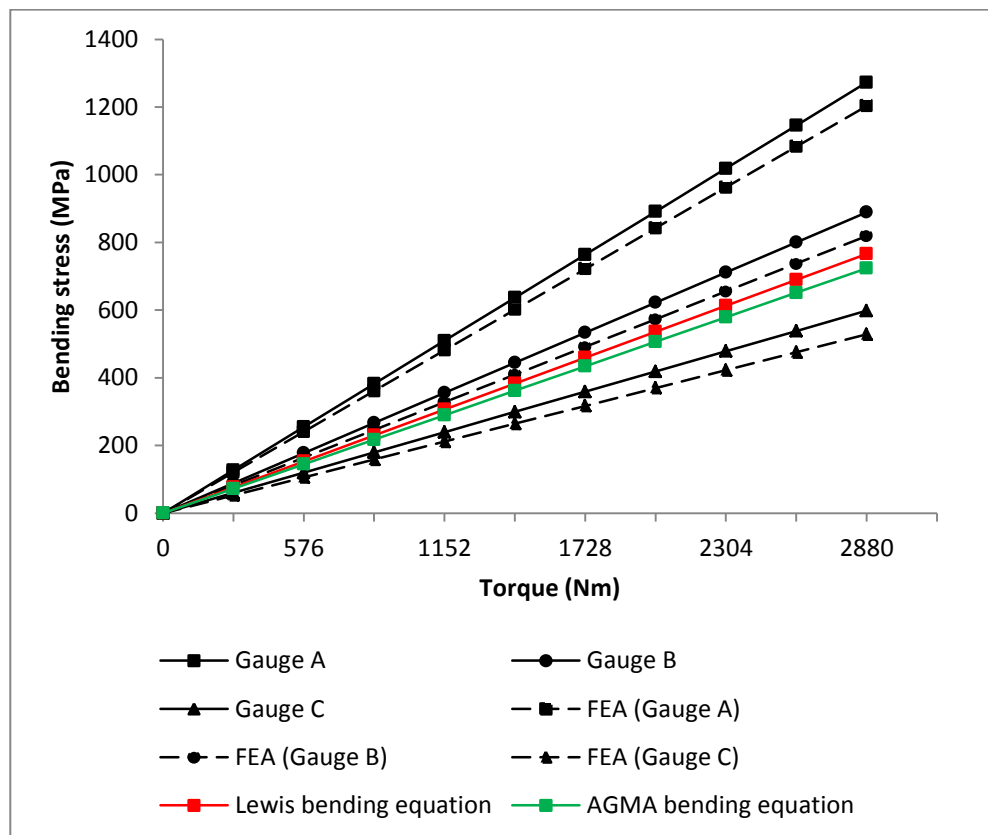


Figure 3.17: Comparison between the FEA, experiment and analytical bending stress at the output gear.

The analytical method estimates the critical stress at gauge B. The bending stress results determined using ANSYS program has close agreement with the experimental results for all the three point measurement gauges. Therefore, the gear train model developed and the procedure applied in ANSYS software are valid for determining the gear bending stress.

3.4.2 Gear contact stress comparison

The gear contact stress obtained from FEA is compared with the analytical method as shown in Figure 3.18. From the results, contact stresses determined in FEA have closer agreement to the contact stresses calculated in AGMA contact stress equation.

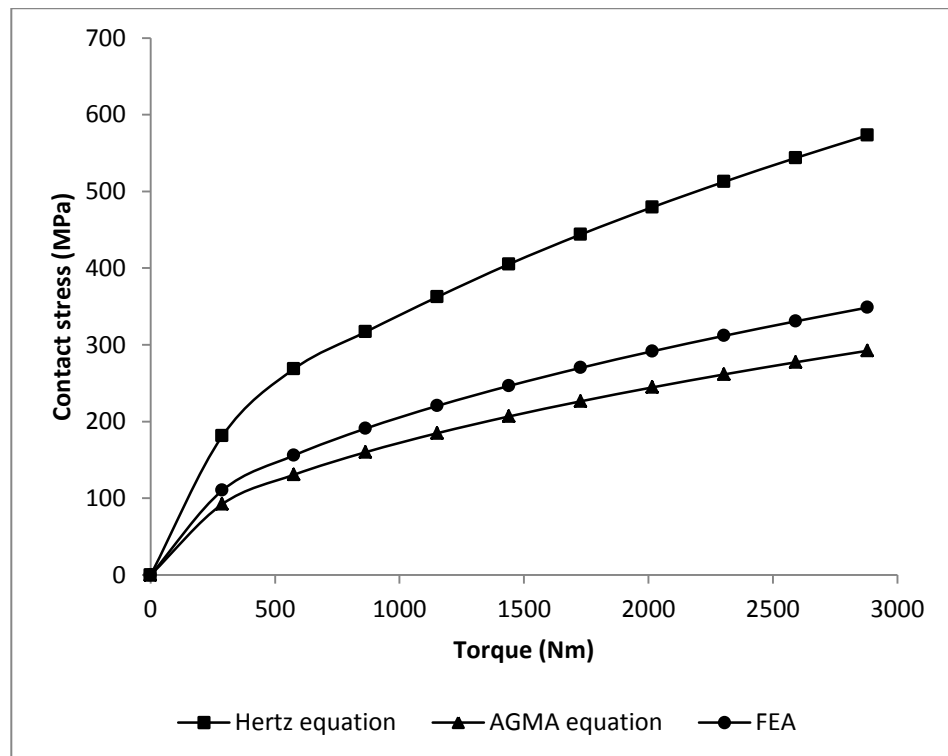


Figure 3.18: Comparison between the FEA and analytical contact stress at the output gear.

The contact stress calculated using the Hertz equation is found to be higher than the contact stress determined in FEA and AGMA equation. The average percentage difference between FEA and AGMA contact stress is 15%. The percentage difference between FEA and Hertzian contact stress is 39%.

3.5 Model of the three gear train designs

The steps for modeling three different gear train designs are described in this section. Firstly, Autodesk Inventor Professional 2010 software is used to model the 3D gear components which are the input gear, the idler gear and the output gear. The gear components are modeled according to the gear design parameters as shown in Table 3.2.

Table 3.2: Design parameters of the input gear, idler gear, and output gear.

Gear component	Input gear	Idler gear	Output gear
Gear tooth type	Standard involute, Full Depth Teeth		
Number of teeth	34	32	30
Pitch diameter	144 mm	135 mm	127 mm
Module (M)	0.4233 mm		
Face width	25.4 mm		
Pressure angle	20°		
Root fillet	2 mm		
Addendum	1.0 M		
Dedendum	1.25 M		

There are three different gear train designs considered in the interest of this research. The gear components modeled initially are arranged to form a unique gear train design. Three types of gear train arrangement are formed and illustrated in Figure 3.19. Gear train with no idler gear which is made up of one input gear and one output gear were constrained to mesh with one and another.

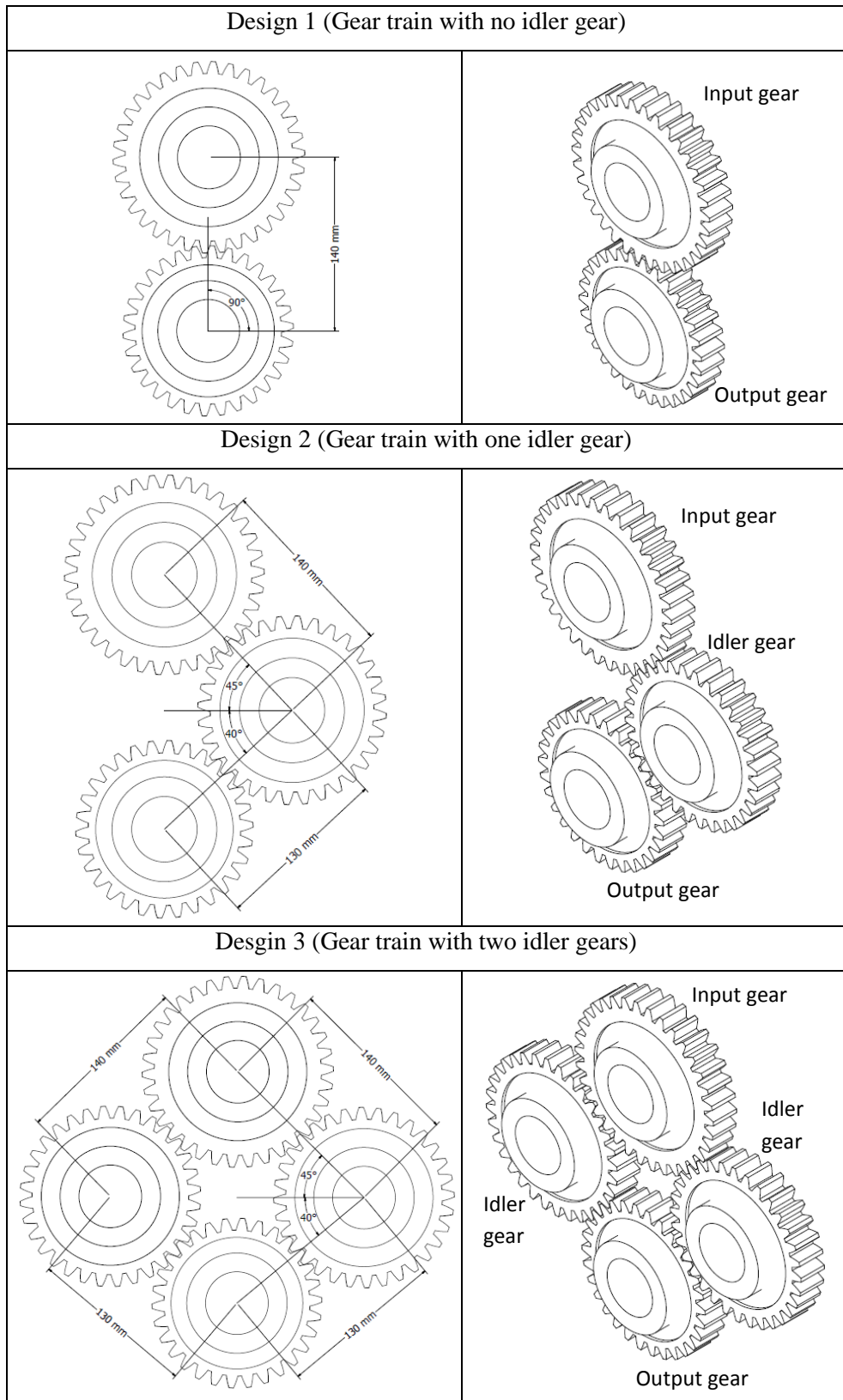


Figure 3.19: Detailed view of the three gear train designs.

The center distance between the input gear and output gear is set to 140 mm. Gear train with one idler gear is made of one input gear, one output gear and one idler gear. The idler gear is the intermediate gear which connects between the two gears. The center distance between the input gear and the idler gear is 140 mm whereas the center distance between the idler gear to output gear is 130 mm. The input gear is aligned to 45° from horizontal to mesh with the idler gear and 40° between the idler gear to output gear. Similarly, the gear train with two idler gears are arranged in the same position compared to the gear train with one idler gear but has additional idler gear attached on the other side between the input gear and output gear.

The gears in the gear train are assembled to rotate and contact with the adjacent gear in a contact ratio of 1.5. This means that in one complete cycle of a gear tooth mesh, single pair teeth contact takes place in the first half cycle and double pair teeth contact takes place during the second half cycle. Figure 3.20 illustrates the occurrences of single pair tooth contact and double pair tooth contact based on the set angular positions during one cycle of the gear tooth mesh. When the double pair teeth contact takes place, the gear teeth takes partial load in which this phenomena is called load sharing.

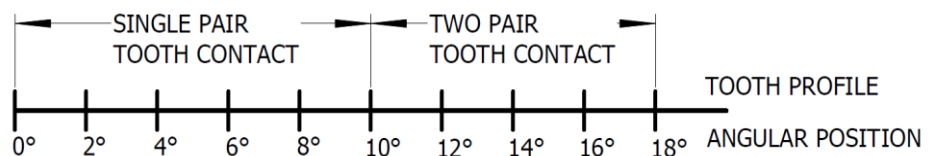


Figure 3.20: Angular intervals of the gear pair contact of the gear train.

Figure 3.21 and Figure 3.22 illustrate the technique used in Autodesk Inventor software in precisely positioning the gear train with one idler gear.

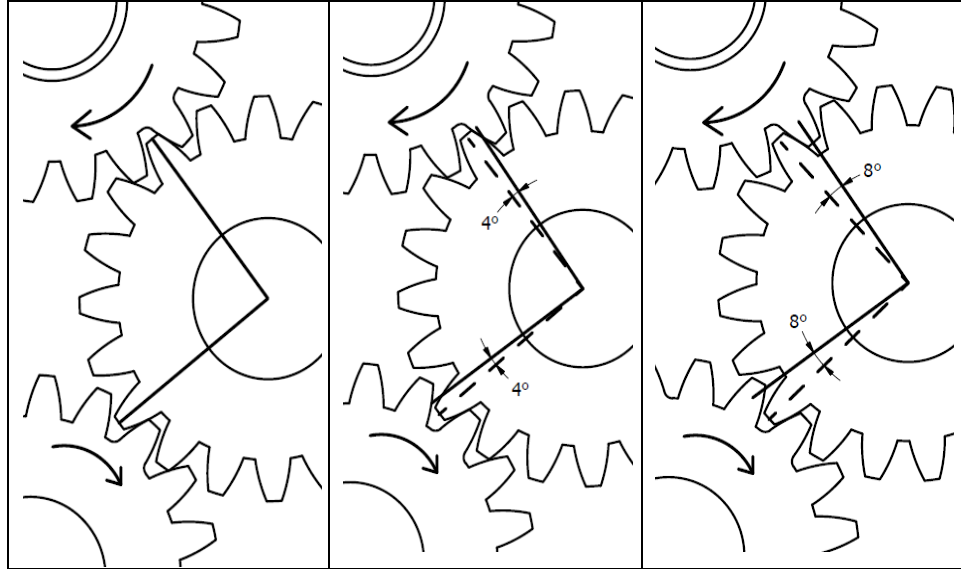


Figure 3.21: Gear train with one idler gear in single tooth contact at 0°, 4° and 8° angular positions.

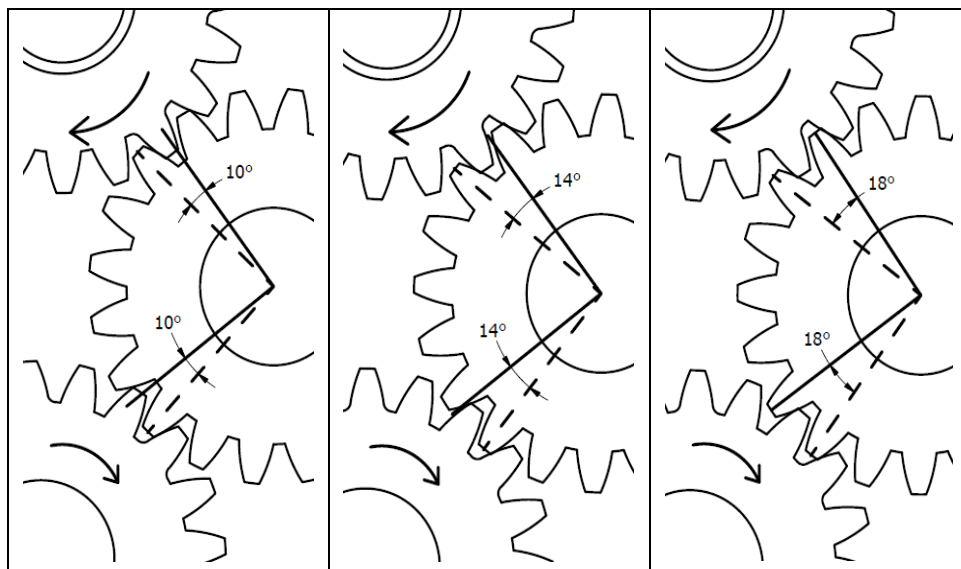


Figure 3.22: Gear train with one idler gear in load sharing at 10°, 14° and 18° angular positions.

When positioning the input gear of the gear train model, single tooth pair contact takes place when the angular position of the gears is between 0° to 10° . Subsequently, double pair teeth contact takes place when the angular position of the gears is between 10° to 20° . The same technique is applied to the other two gear train designs in positioning the gears.

3.6 Effect of non-ideal loading to the gear stresses

The output gear of the three gear train designs is misaligned to generate the non-ideal loading effect. There are three types of non-ideal loading considered for the gear trains in which the output gear will be misaligned to out of plane, tilt angle and axial separation. Figure 3.23 shows the positioning of the output gear in out of plane misalignment, tilt angle misalignment, and axial separation misalignment of the gear train with one idler gear.

In positioning the output gear to out of plane misalignment, the axis plane of the output gear is offset at 1 mm and 2 mm from the idler gear axis plane. Tilt angle misalignment at the output gear is set by changing the angle of orientation of the output gear axis plane to 1° and 2° with reference to the axis plane of the idler gear. The axial separation misalignment is the amount of offset of the center distance between the output gear and idler gear. For the gear train with one idler gear, if the axial separation is 2 mm, then the center distance between the output gear and idler gear will be increased from 130 mm to 132 mm. In setting the axial separation, the center distance between the output gear and idler gear is increased by 1 mm and 2 mm.

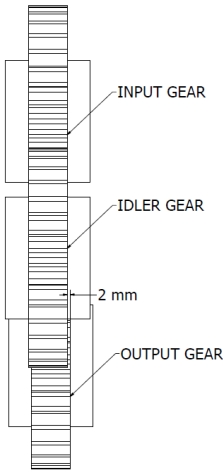
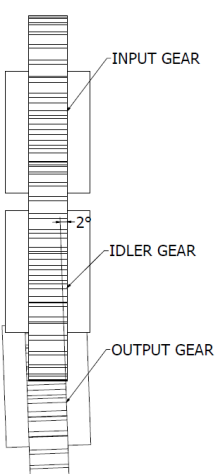
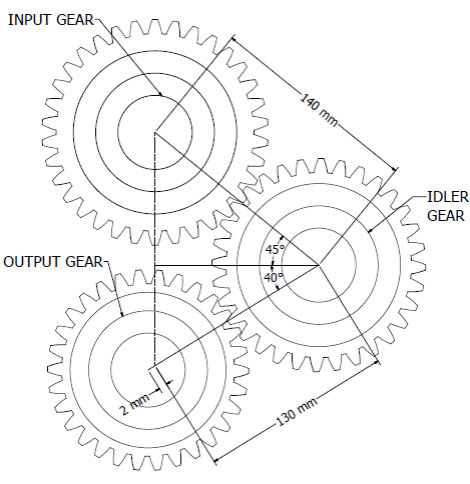
No.	Type of Misalignment	Diagram
1.	2 mm out of plane misalignment at the output gear.	 <p>The diagram shows a vertical gear train with three gears: an input gear at the top, an idler gear in the middle, and an output gear at the bottom. A horizontal dimension line indicates a 2 mm offset between the vertical axes of the idler and output gears, representing out-of-plane misalignment.</p>
2.	2° tilt angle misalignment at the output gear.	 <p>The diagram shows a vertical gear train with three gears: an input gear at the top, an idler gear in the middle, and an output gear at the bottom. A small angle of 2° is indicated between the vertical axis of the idler gear and the vertical axis of the output gear, representing tilt angle misalignment.</p>
3.	2 mm axial separation between the output gear and idler gear.	 <p>The diagram shows a gear train with three gears: an input gear at the top, an idler gear in the middle, and an output gear at the bottom. The input gear has a pitch diameter of 140 mm. The idler gear has a pitch diameter of 45 mm. The output gear has a pitch diameter of 130 mm. A horizontal dimension line indicates a 2 mm axial separation between the vertical axes of the idler and output gears.</p>

Figure 3.23: Details of three types of misalignment of the gear train.

3.6.1 Effect of the out of plane misalignment

The effect of out of plane misalignment at the output gear to the three gear train designs is analysed. Figure 3.24 shows the bending stress comparison between the three gear train designs and the effect of the out of plane misalignment at the output gear to the gear trains. In comparisons between the three gear train designs in ideal loading, the output gear of the Design 1 (gear train with no idler gear) has the highest gear tooth bending and contact stress when rotated from 0° to 18°.

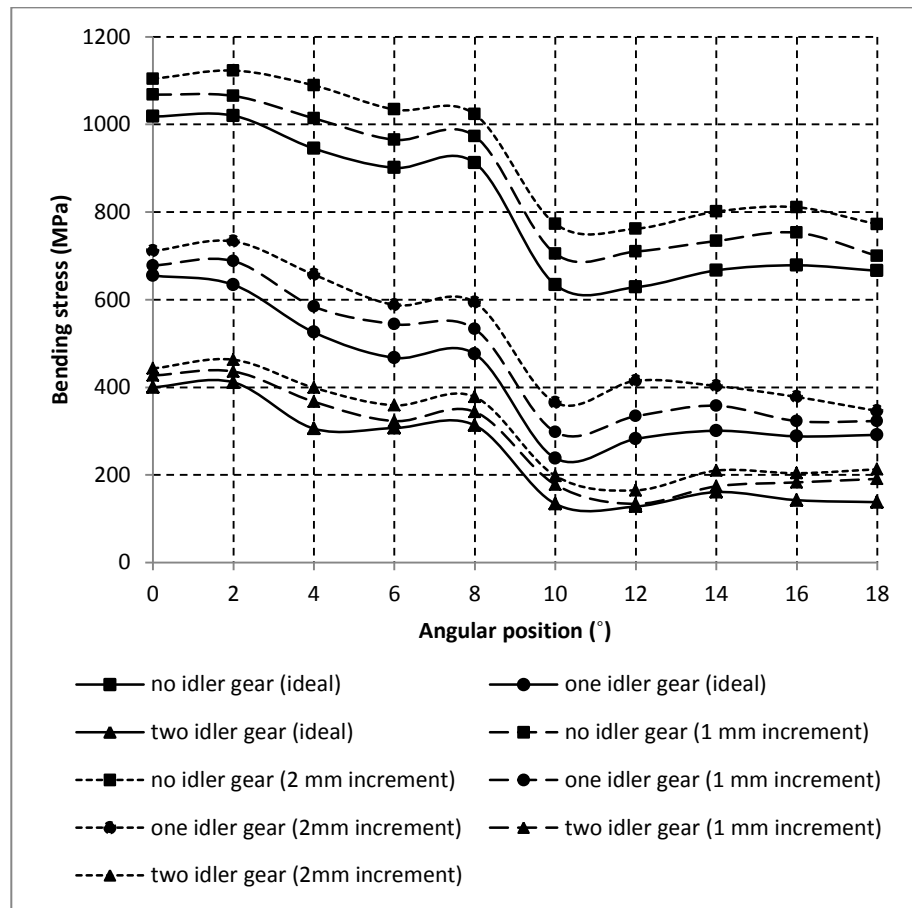


Figure 3.24: Effect of out of plane misalignment to the bending stress of the output gear of the three gear train designs.

Three gear train designs exhibit similar bending stress pattern when plotted against the increasing angular position. The out of plane misalignment causes an overall increase in bending stress of the three gear train designs. However, the bending stresses increases slightly for Design 3 (gear train with two idler gears). This shows that the Design 3 is the least affected by the out of plane misalignment.

Figure 3.25 shows the contact stress comparison between the three gear train designs and the effect of the out of plane misalignment to the gear trains. When the output gear is in out of plane misalignment, the contact stresses are critical at 4°, 8°, 14° and 18° angular positions for all gear train designs.

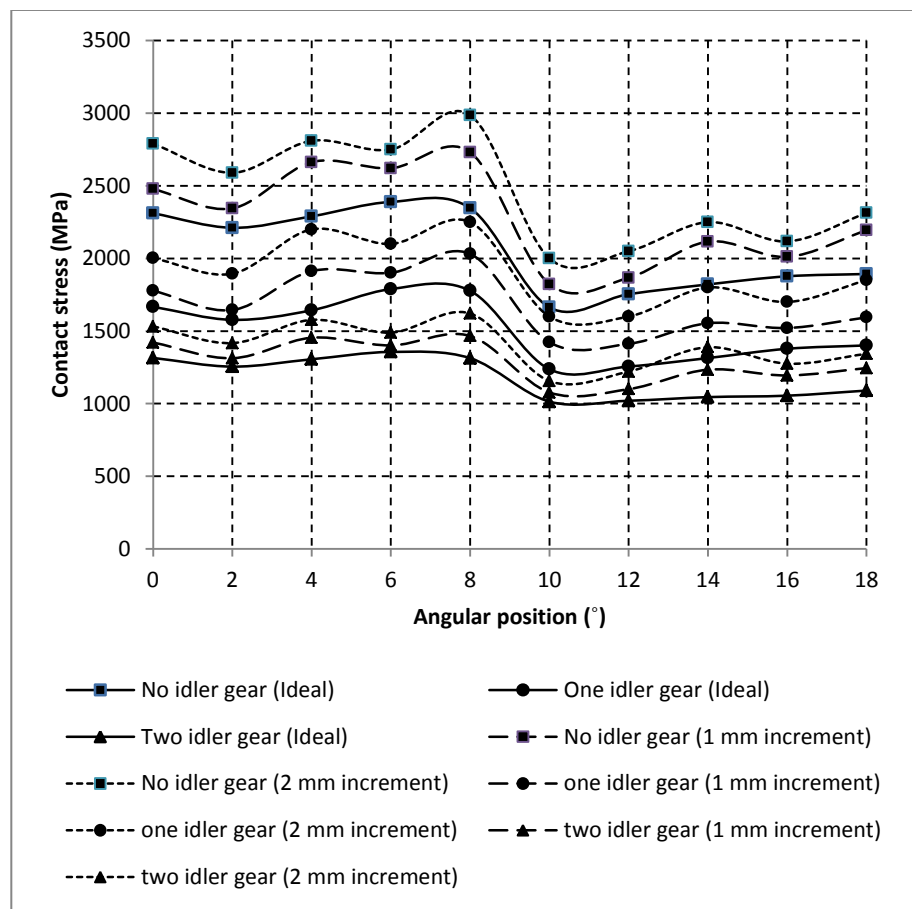


Figure 3.25: Effect of out of plane misalignment to the contact stress of the output gear of the three gear train designs.

The critical stresses formed at these angular positions are due to lower contact area surface compared to the ideal loading which has a full contact surface in gear teeth meshing. The out of plane misalignment greatly affects the contact stress at the output gear for all gear train designs. In comparison among the three gear train designs, Design 1 has overall drastic change in contact stress at the output gear when the output gear positioned to out of plane misalignment.

3.6.2 Effect of the tilt angle misalignment

The effect of tilt angle misalignment at the output gear are analysed for the three gear train designs. Figure 3.26 and Figure 3.27 show the bending stress and contact stress of the output gear in comparison of the three gear train designs and the effect of the tilt angle misalignment to the gear train designs when the output gear is tilt to 1° and 2° . In Figure 3.26, the tilt angle misalignment cause a critical bending stress at the output gear when the angular position is 8° for the all gear train designs. A drastic increase in the bending stress at this angular position is due to the twisting and bending at the gear tooth root area which occur spontaneously. In comparison between the three gear train designs, Design 1 is affected by the tilt angle misalignment the most because there is a huge increase in the bending and contact stresses when the output gear is misaligned.

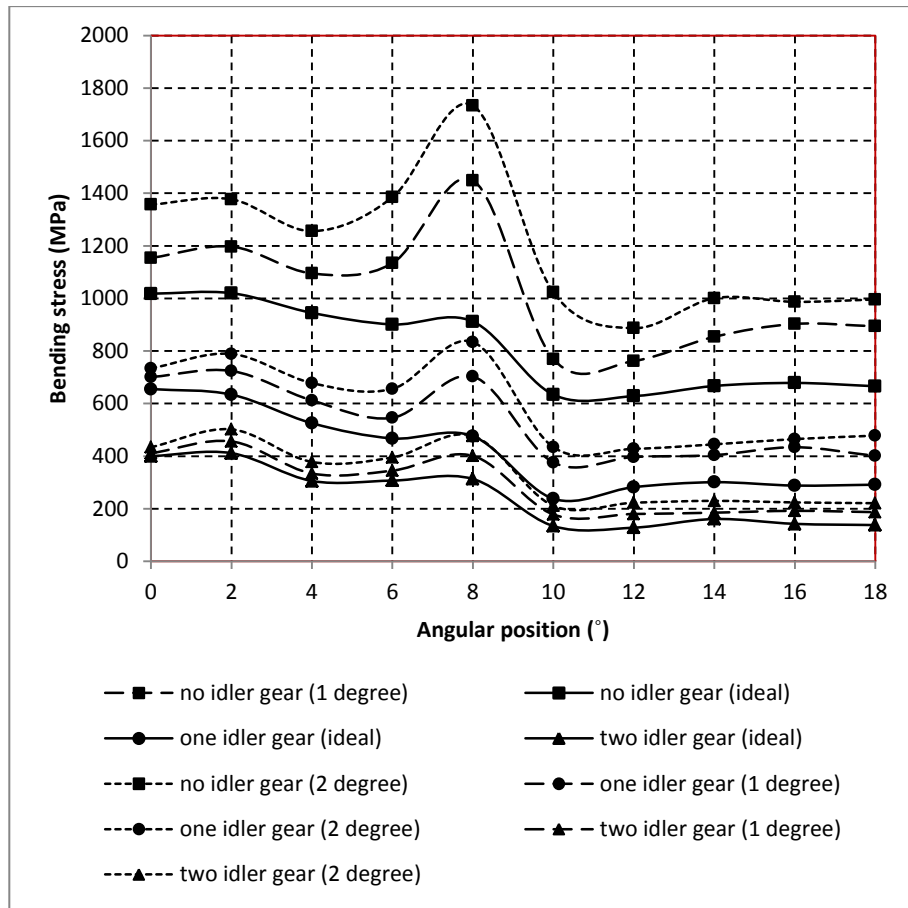


Figure 3.26: Effect of tilt angle misalignment to the bending stress of the output gear of the three gear train designs.

In comparisons of the effect of tilt angle misalignment to the contact stress at the output gear of the three gear train designs as shown in Figure 3.27, the critical contact stresses occur at 4°, 8°, and 14°. These critical contact stresses are generally caused by the small surface area of contact between the gear teeth surfaces which lead to a phenomenon called stress singularities or high stress intensities. Overall, the tilt angle misalignment at the output gear greatly influences the contact stresses of the three gear trains.

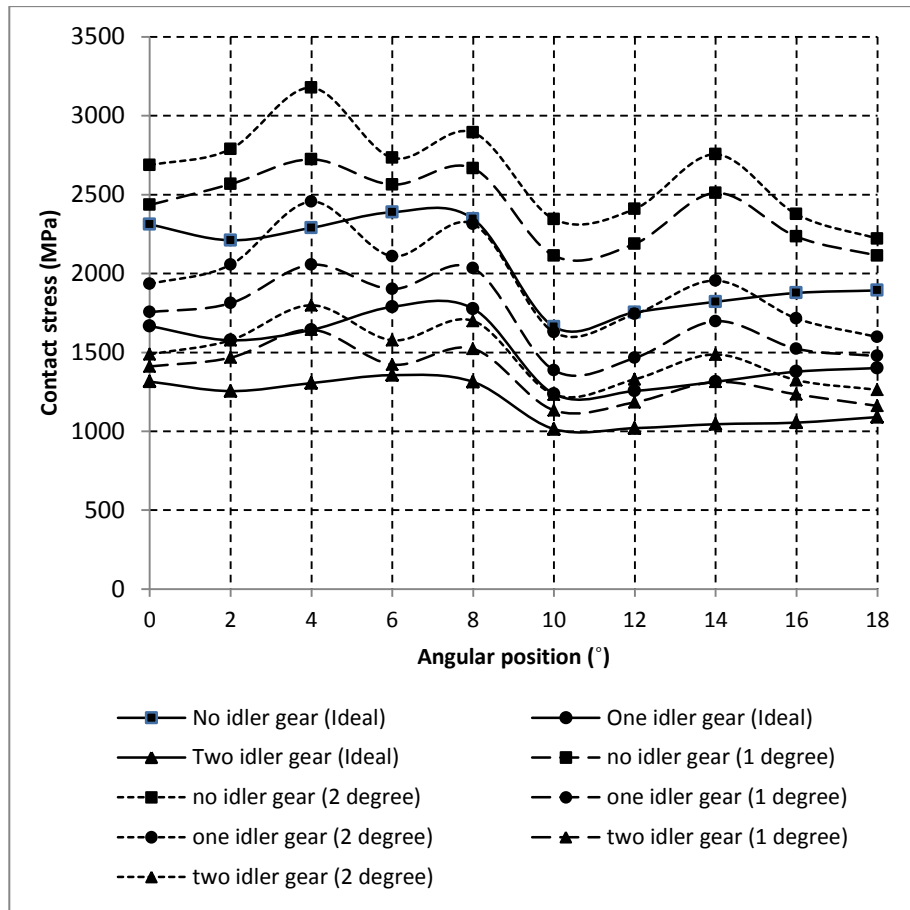


Figure 3.27: Effect of tilt angle misalignment to the contact stress of the output gear of the three gear train designs.

3.6.3 Effect of the axial separation misalignment

Figure 3.28 shows the bending stress comparison between the three gear train designs and the effect of the axial separation misalignment of the output gear to the gear trains. When the output gear is misaligned, the critical bending stresses occur at 4°, 8° and 14° for all gear train designs. In comparison between the three gear train designs, the bending stresses at the output gear for Design 1 and Design 2 are significantly affected by the axial separation misalignment. The bending stress at the output gear for Design 1 and Design 2 is increased by 25%. The high bending stresses is caused by the shifting of the

average loading position closer to the tip of the mating gear tooth and caused higher bending moment.

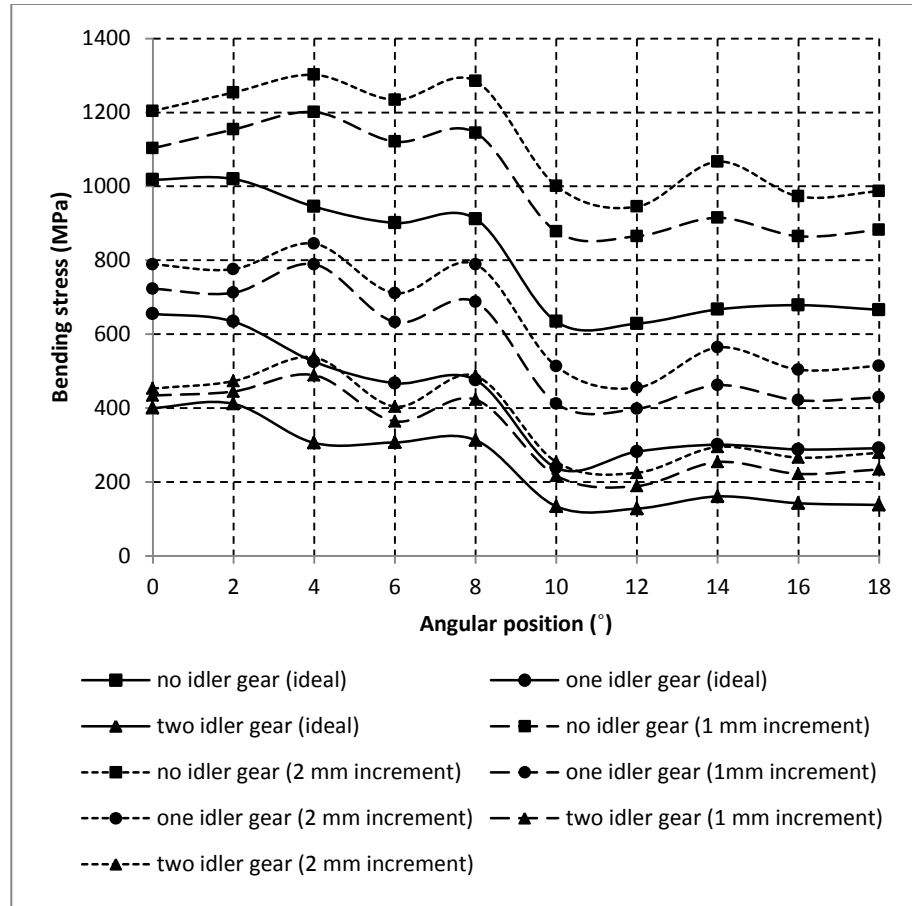


Figure 3.28: Effect of axial separation misalignment to the bending stress of the output gear of the three gear train designs.

For the contact stress comparison between the three gear train designs and the effect of the axial separation misalignment to the gear trains as shown in Figure 3.29, the critical contact stresses occur at 4°, 8°, and 14° for all gear train designs in which the critical bending stresses also fall under the same angular positions. Similar to the case of tilt angle misalignment, these critical contact stresses are caused by the small surface area of contact. In comparison between the three gear train designs, the contact stresses for Design 1 and

Design 2 are significantly affected by the axial separation misalignment. On the other hand, Design 3 is less affected by the axial separation misalignment.

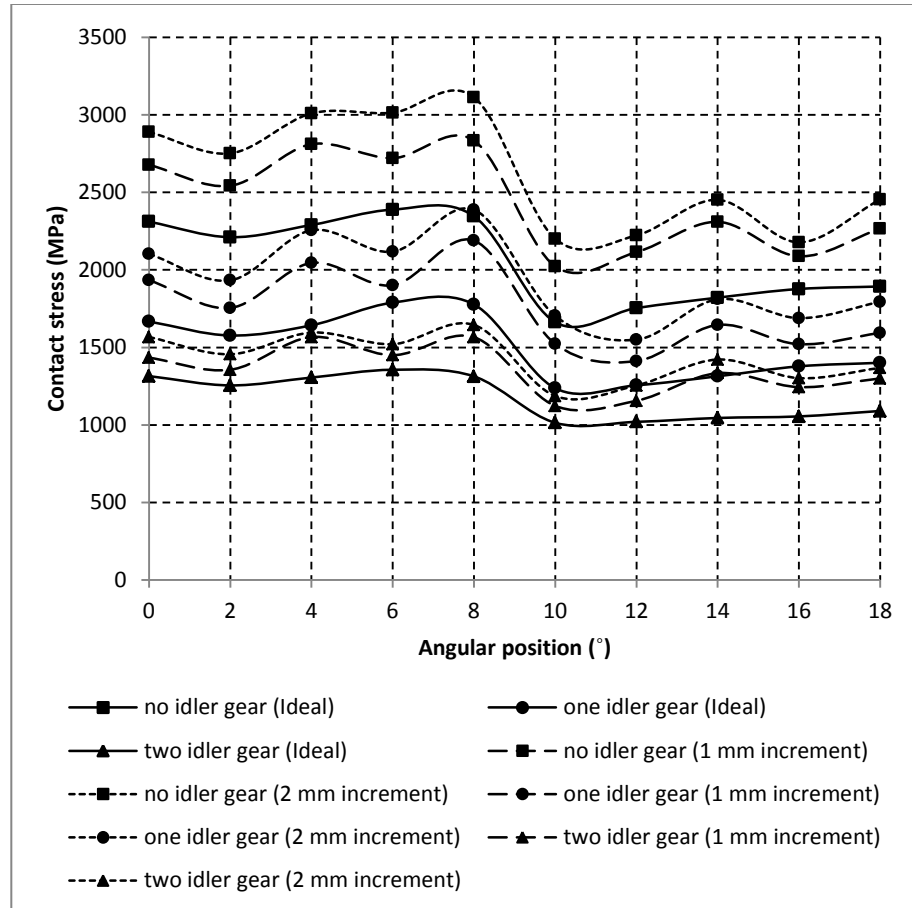


Figure 3.29: Effect of axial separation misalignment to the contact stress of the output gear of the three gear train designs.

3.7 Conclusion

The 3D models of the three different types of gear train developed by using ANSYS were able to predict the bending and contact stresses at the output gear with increasing angular position. The gear train models that are used in ANSYS were also able to predict the gear stresses at the output gear in single contact and gear load sharing. The gear train with two idler gears

exhibits the highest gear load sharing causing the bending and contact stresses at the output gear is the lowest. Table 3.3 shows a summary of the influence of the three different misalignments to the bending stress and contact stress at the output gear of the three gear train designs. The out of plane, the axial separation and the tilt angle misalignments at the output gear caused a significant increase to the bending and contact stresses of the output gear of the three gear train designs.

Table 3.3: The effect of the three different misalignments to the bending stress and contact stress at the output gear of the three gear train design.

	Non-ideal loading	Types of gear train		
		No idler gear	One idler gear	Two idler gears
Bending stress	Out of plane	Moderate	Moderate	Low
	Tilt angle	Very high	Moderate	Low
	Axial separation	Very high	High	Moderate
Contact stress	Out of plane	Moderate	Moderate	Low
	Tilt angle	Very high	High	Moderate
	Axial separation	Very high	High	Low

The difference between ideal and non-ideal cases was found to be as much as 44.45% for the bending stress and 25.15% for the contact stress. The tilt angle and axial separation misalignment contributed the most to the increase in bending and contact stress at the output gear for the gear train with no idler gear. In comparison to the three gear train designs, the gear train with two idler gears is the least affected by the three different misalignments. A tremendous increase in the bending stress and the contact stress at the output gear of the gear train would lead to gear failure sooner than expected.

CHAPTER 4

VIBRATION ANALYSIS OF THE GEAR TRAIN UNDER NON-IDEAL LOADING

4.1 Introduction

In designing the gear train of a portal axle, it is important to study its vibration behavior to ensure that the gear train is safe to operate within its operating frequency range. In this chapter, modal analysis and forced frequency response are performed on the three gear train designs of the portal axle and the effect of the non-ideal loading to the vibration behavior of the three gear train designs are investigated. Modal analysis involves the analysis of the mode shapes of the gear train upon excitation by its critical natural frequencies whereas forced frequency response involves the vibration analysis of the gear train under the load excitation. The out of plane misalignment, the tilt angle misalignment and the axial separation misalignment are non-ideal loading conditions applied to the gear train for vibration analysis.

4.2 Validation of the FEA model

Prior to performing vibration analysis on three gear train designs, FEA model of the two meshing spur gears is first validated by experimental testing. Part of results of the vibration test of the two meshing spur gear conducted by Li (2008b) are used for validating the FEA model.

4.2.1 Gear vibration experiment

The gearing parameters and dimensions of the two meshing spur gears used in the vibration test are shown in Table 4.1 and Figure 4.1 respectively. Gear A and B are the same gear parameters except dimension T1, T2 and L.

Table 4.1: Design parameters of the two mating spur gears.

	Gear A	Gear B
Gear type	Standard involute spur gear	Standard involute spur gear
Number of teeth	50	50
Module	4 mm	4 mm
Pressure angle	20°	20°
Contact ratio	1.75	1.75
Face width	40 mm	40 mm
Dimension T1	26 mm	4 mm
Dimension T2	12 mm	5 mm
Dimension L	0	11 mm
Material (JIS)	SCM 415	SCM 415

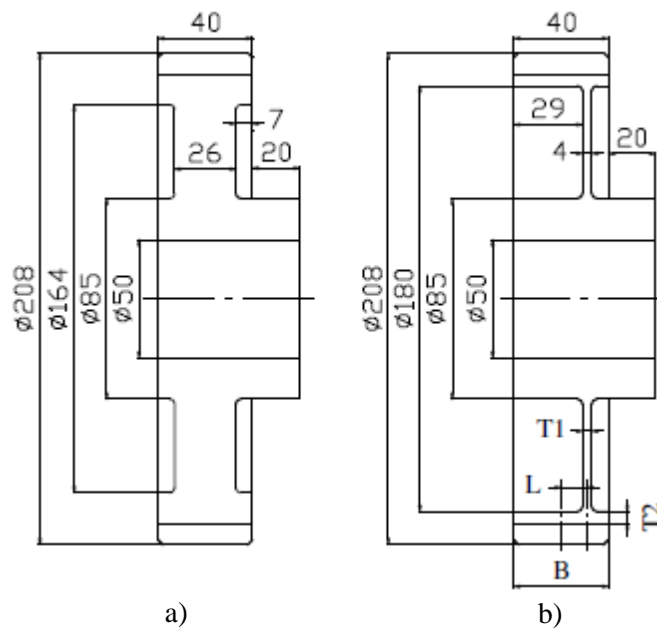


Figure 4.1: Design parameters of a) Gear A and b) Gear B (Li 2008).

A test rig with experiment apparatus was set by the author as shown in Figure 4.2. Dynamic strain gauges and accelerometers were used for vibration measurements of the meshing spur gears and positioned as shown in Figure 4.3. Two strain gauges were mounted on the tooth root fillet with adhesive loctile 638 along the tooth profile where ‘‘I’’ and ‘‘II’’ are used to express their positions. Three accelerometers are fixed on the opposite side of web surface along radial, circumferential and axial directions. Vibration measurements are conducted at speed range 500–3000 rpm when a torque 297 Nm is loaded. Dynamic strain and acceleration signals are measured by using the FFT (Fast Fourier Transform) analyzer for frequency analysis.

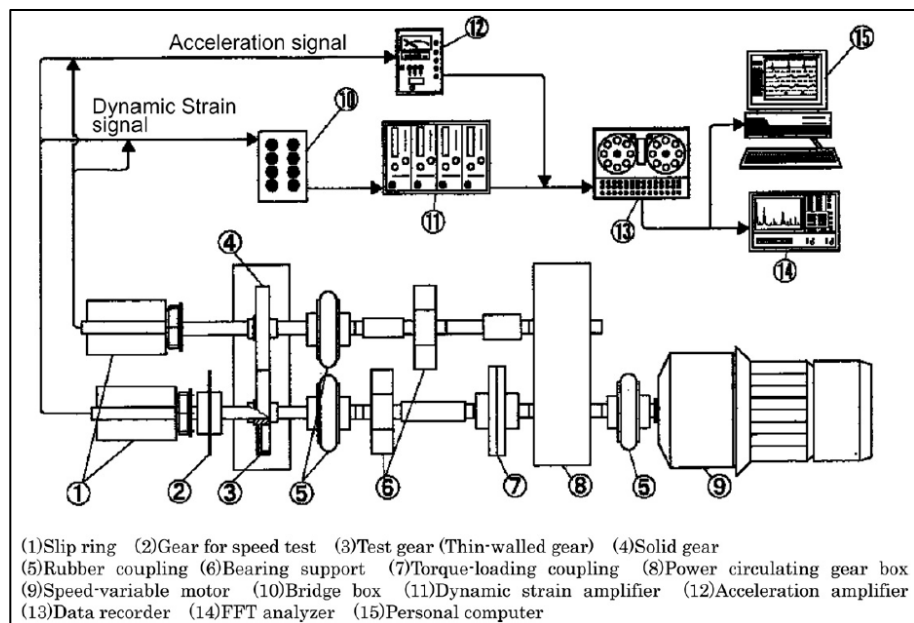


Figure 4.2: Experiment apparatus for gear vibration testing (Li 2008).

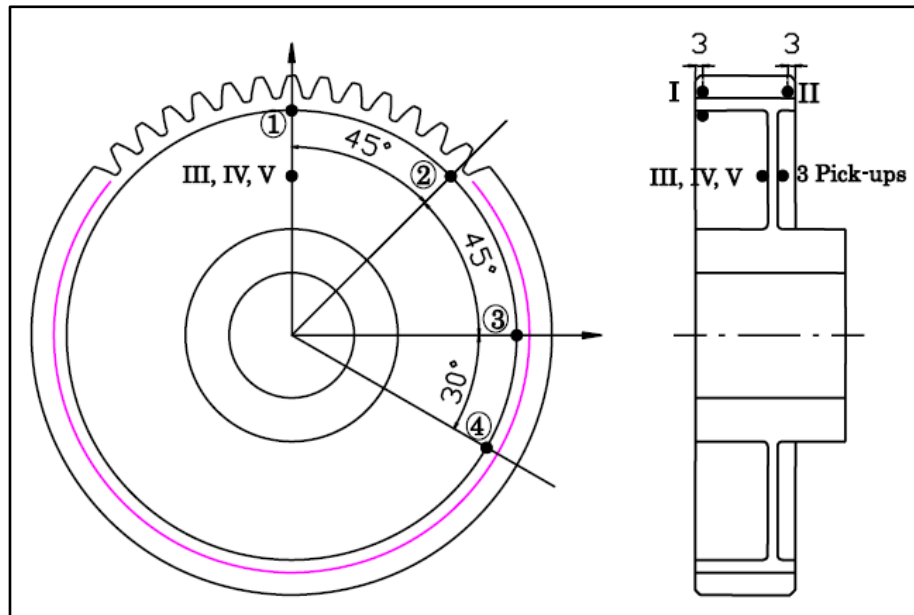


Figure 4.3: Mounting positions of the dynamic strain gauges and accelerometers (Li 2008).

4.2.2 Gear vibration analysis by using FEA

Vibration analysis of the portal axle gear train is conducted by using FEA software. It is well known that the equation of motion of structural vibration can be expressed in Equation (10) when FEA is used.

$$[M]\{\ddot{\delta}\} + [C]\{\dot{\delta}\} + [K]\{\delta\} = \{F\} \quad (10)$$

where $[M]$ is the mass matrix of the structure, $[C]$ the damping coefficient matrix of the structure, $[K]$ the stiffness matrix of the structure, $\{\delta\}$ the deformation vector of the element nodes, and $\{F\}$ is the external load vector on element nodes.

When frequency analysis of the structure is conducted, Equation (11) can be derived based on the Equation (10). In Equation (11), ω is the natural frequency of the structure and $\{\delta_0\}$ is mode shape vector of the structure.

$$(\omega^2[M] - [K])\{\delta_0\} = \{0\} \tag{11}$$

From these equations, it can be summarized that modal analysis and the search for natural frequencies of the gear train structures are independent of the damping effect and force excitation in which they are sometimes called free vibrations. On the other hand, the forced frequency response analysis requires damping ratio and force excitation input for performing this analysis.

The procedure for determining the natural frequencies of the two meshing spur gears using ANSYS software is described. Firstly, the two meshing spur gears are modeled in 3D, assembled into a compound gear, and the contact surfaces between the gears are meshed by using Autodesk Inventor software. Later, the file is saved, converted into IGES file, and imported to ANSYS software. In the ANSYS mesh settings, hexahedron element of average mesh size of 5 mm is set for meshing the gear model. In the ANSYS contact settings, the gear tooth surfaces in contact are treated to be 'Flexible' surface to allow probing strain at the root fillet. The probing surfaces for determining the strain and acceleration data are set in ANSYS as shown in Figure 4.4. The position of the probe surfaces are according to the mounting position of the strain gauges and accelerometers used in the vibration testing.

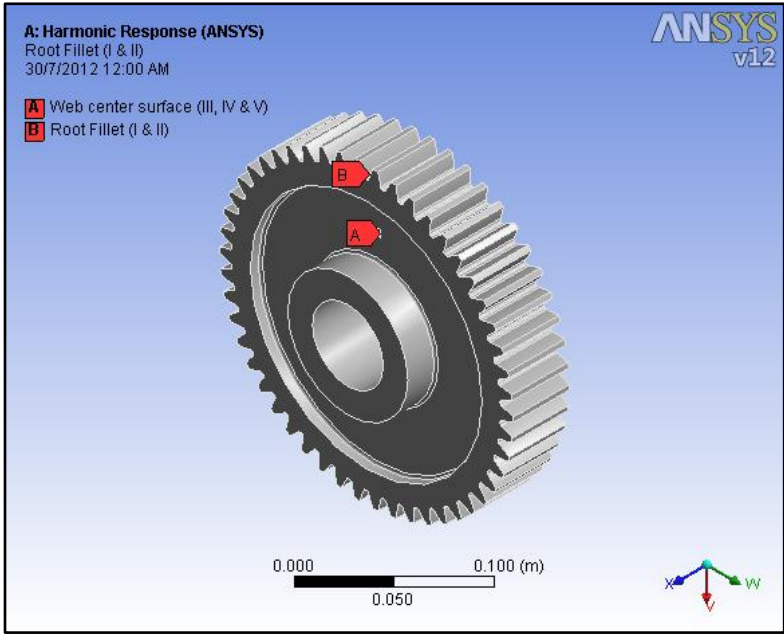


Figure 4.4: Surface probe at the root fillet and web center surface of Gear A.

Pre-stressed condition of the gear model is set in ‘ANSYS Static Structural’ with an applied torque of 289 Nm and a rotational speed of 1000 RPM as shown in Figure 4.5.

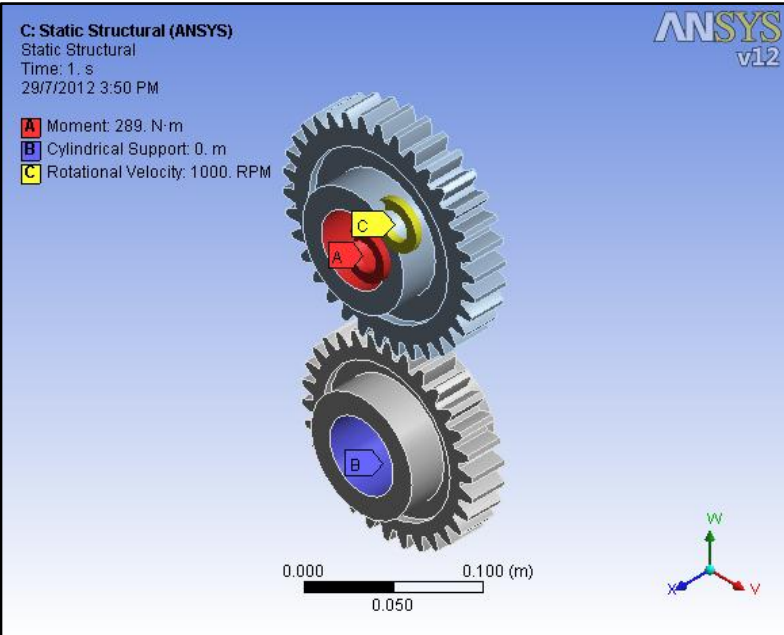


Figure 4.5: Pre-stressed conditions of the two mating spur gears.

In ANSYS workbench, ‘ANSYS harmonic response’ is selected for determining the amplitude of acceleration and the von Mises strain of the two meshing spur gears.

4.2.3 Comparison between FEA and experiment

Figure 4.6 shows the comparison of the acceleration response at the web center surface and tooth root for Gear A. The difference in acceleration response between the FEA results and the measured one is small. The acceleration response frequencies determined using both methods show close agreement.

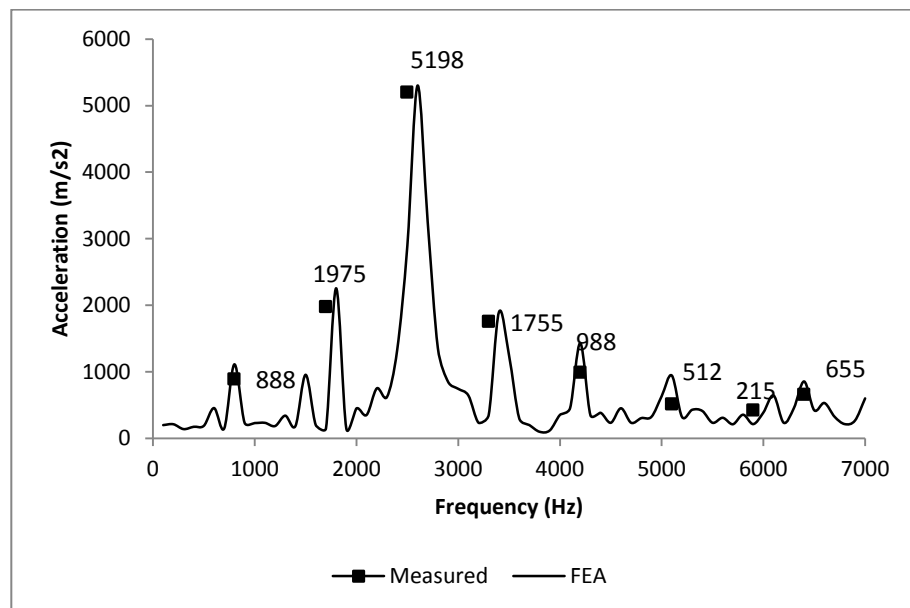


Figure 4.6: Comparison of the acceleration response at the web center surface and tooth root of Gear A (1000 RPM).

Figure 4.7 shows the comparison of the strain response at the web center surface and tooth root for Gear B. The measured strain and the strain

obtained from FEA for Gear B also have close agreement. Hence, this confirms the positioning of the probe surface at the root tooth and web center surface for the FEA models of Gear A and Gear B. With close agreement between the FEA and measured results, the FEA models of Gear A and Gear B are validated.

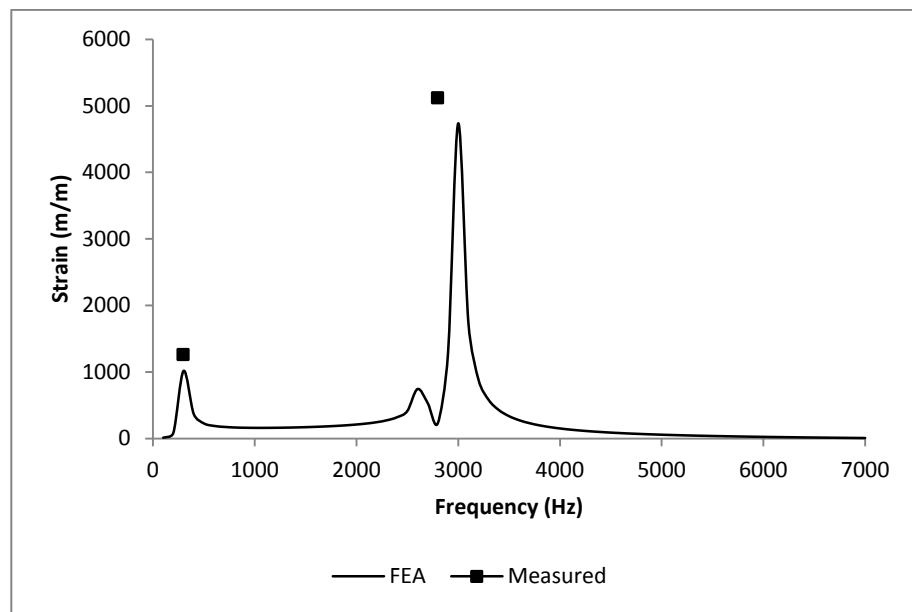


Figure 4.7: Comparison of the strain response at the web center surface and tooth root of Gear B (3119 RPM).

4.3 Effect of non-ideal loading to the gear train vibration

The effect of non-ideal loading as described in Chapter 3 is also considered in the vibration analysis of the three gear train designs. In the free vibration analysis, the input and output gear are set to cylindrical constraint which restricts the gears to rotate. The first ten mode shapes and the overall deformation of the three gear train designs are determined. The details of gear dimensions and the orientation of the three gear train designs can be referred to

Section 3.5 and Section 3.6. The three types of non-ideal loading can be referred to Section 3.7 respectively.

In the forced vibration, an additional input load excitation is applied at the input gear of the gear train models. A torsional load of 297 Nm and a rotational speed of 1000 RPM are acted on the cylindrical surface of the input gear hub while the output gear is fixed at its cylindrical hub. In the post-processing of ANSYS simulation, the amplitude of the X, Y and Z directional deformation are measured at the root fillet and the web center surface of the output gear.

4.3.1 Modal analysis of the gear train without idler gear

Figure 4.8 shows a sample of the 8th mode shape of the gear train without idler gear in normal loading, out of plane, tilt angle, and axial separation. The gear train in normal loading, out of plane, and axial separation show similar bending deformation at the output gear. However, the 8th mode shape of the gear train in tilt angle shows swaying deformation at the input gear and bending deformation at the output gear.

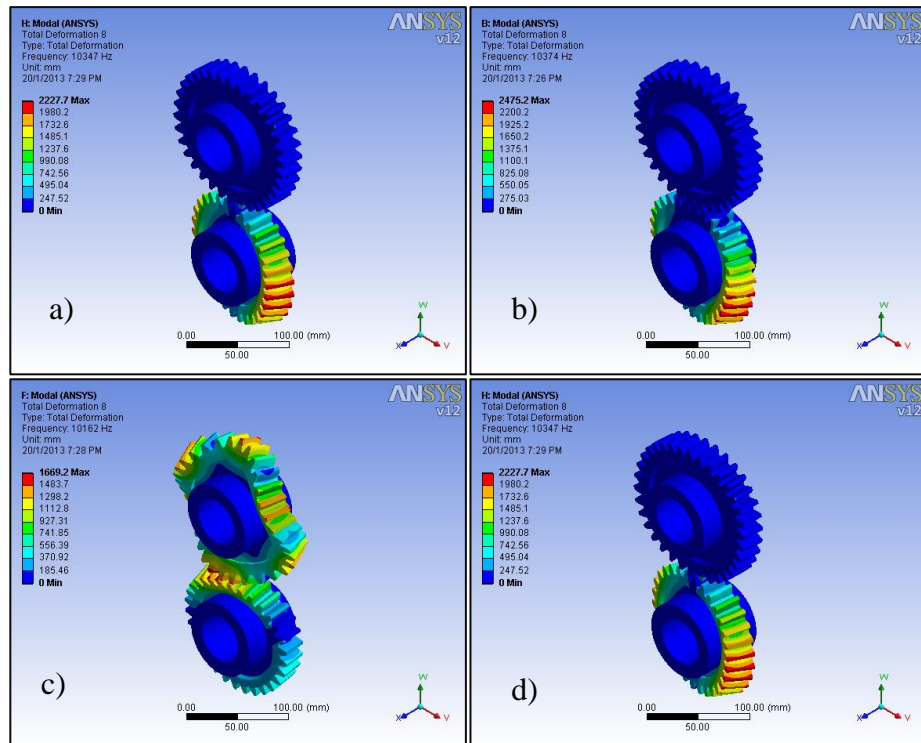


Figure 4.8: The 8th mode shape of the gear train without idler gear in a) normal loading, b) out of plane, c) tilt angle, and d) axial separation.

Table 4.2 shows the first ten mode shapes of the gear train without idler gear and a comparison between the normal gear train with the out of plane, the tilt angle, and the axial separation misalignments. The input gear exhibits the most dominant behavior in vibrations in which bending vibration occurs most frequently. There are no changes in the first ten mode shapes of the gear train when the output gear is misaligned to out of plane misalignment. Changes in the mode shapes only occur at the 8th mode shape for the tilt angle misalignment and the 10th mode shape for the axial separation. The output gear misalignment has very minimal influence on the changes in the mode shapes of the gear train under normal condition.

Table 4.2: First ten mode shapes of gear train without idler gear (IN and OT indicate the input gear and output gear respectively).

Mode	Vibrational mode shape			
	Normal	Out of plane	Tilt angle	Axial separation
1 st	Bending (IN)	Bending (IN)	Bending (IN)	Bending (IN)
2 nd	Bending (IN)	Bending (IN)	Bending (IN)	Bending (IN)
3 rd	Bending (IN)	Bending (IN)	Bending (IN)	Bending (IN)
4 th	Swaying (IN)	Swaying (IN)	Swaying (IN)	Swaying (IN)
5 th	Swaying (IN)	Swaying (IN)	Swaying (IN)	Swaying (IN)
6 th	Rotation (IN)	Rotation (IN)	Rotation (IN)	Rotation (IN)
7 th	Swaying (IN)	Swaying (IN)	Swaying (IN)	Swaying (IN)
8 th	Bending (OT)	Bending (OT)	Swaying (IN) Bending (OT)	Bending (OT)
9 th	Bending (OT)	Bending (OT)	Bending (OT)	Bending (OT)
10 th	Bending (OT)	Bending (OT)	Bending (OT)	Swaying (IN) Bending (OT)

Figure 4.9 shows the correlation between the overall deformation of the gear train without idler gear against the first ten mode shapes. All four conditions show very similar deformational amplitude at the first 7th mode. The maximum deformation occurs at the 9th mode for the normal and the out of plane whereas maximum deformation occurs at the 10th mode for the tilt angle. The misalignments of gear train start to show variation in deformation when it is between the 8th and 10th mode.

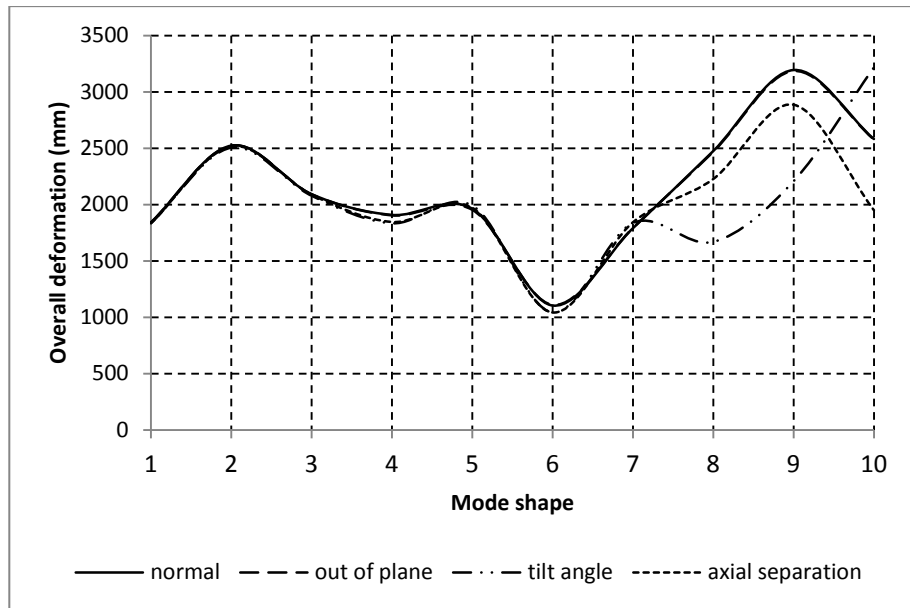


Figure 4.9: Maximum deformation of the gear train without idler gear in the first ten mode shape.

4.3.2 Modal analysis of the gear train with one idler gear

Figure 4.10 shows a sample of the 8th mode shape of the gear train with one idler gear in normal loading, out of plane, tilt angle, and axial separation. With respect to all loading conditions, the gear train shows swaying deformation at the idler gear. This indicates that the gear train with one idler gear is not affected by the non-ideal loading at its 8th mode shape.

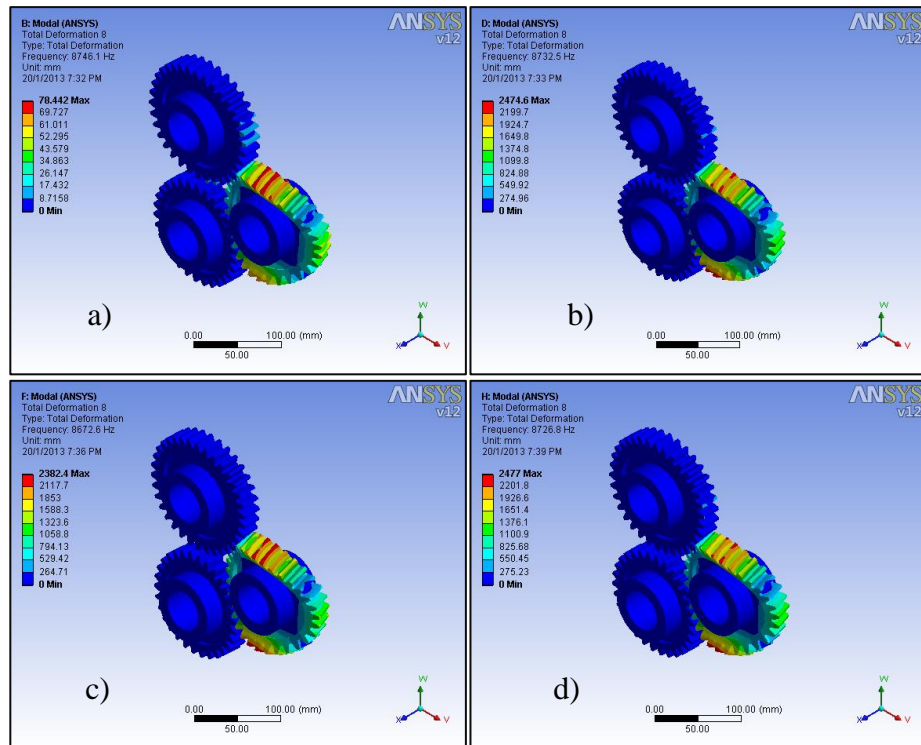


Figure 4.10: The 8th mode shape of the gear train with one idler gear in a) normal loading, b) out of plane, c) tilt angle, and d) axial separation.

Table 4.3 shows the comparisons of the vibrational mode shapes between the normal gear train with the out of plane, tilt angle, and axial separation misalignment for the gear train with one idler gear. About 60% of the vibration occurs at the input gear, 40% of the vibration occurs at the idler gear, and the output gear is less sensitive to the excitation. Swaying and bending vibrations are the most frequent vibrational behavior for the first ten mode shapes. It can also be highlighted that there is no changes in the mode shapes for all loading conditions as shown in Table 4.3.

Table 4.3: First ten mode shapes of gear train with one idler gear (IN, ID and OT indicate the input gear, idler gear and output gear respectively).

Mode	Vibrational mode shape			
	Normal	Out of plane	Tilt angle	Axial separation
1 st	Bending (IN)	Bending (IN)	Bending (IN)	Bending (IN)
2 nd	Bending (IN)	Bending (IN)	Bending (IN)	Bending (IN)
3 rd	Bending (IN)	Bending (IN)	Bending (IN)	Swaying (IN)
4 th	Swaying (IN)	Swaying (IN)	Swaying (IN)	Swaying (IN)
5 th	Swaying (IN) Bending (ID)	Swaying (IN) Bending (ID)	Swaying (IN) Bending (ID)	Swaying (IN) Bending (ID)
6 th	Bending (ID)	Bending (ID)	Bending (ID)	Bending (ID)
7 th	Bending (ID)	Bending (ID)	Bending (ID)	Bending (ID)
8 th	Swaying (ID)	Swaying (ID)	Swaying (ID)	Swaying (ID)
9 th	Rotation (IN)	Rotation (IN)	Rotation (IN)	Rotation (IN)
10 th	Swaying (ID)	Swaying (ID)	Swaying (ID)	Swaying (ID)

Figure 4.11 shows the correlation between the maximum deformations of the gear train with one idler gear against the first ten mode shapes. The gear train in normal condition have overall low deformation.

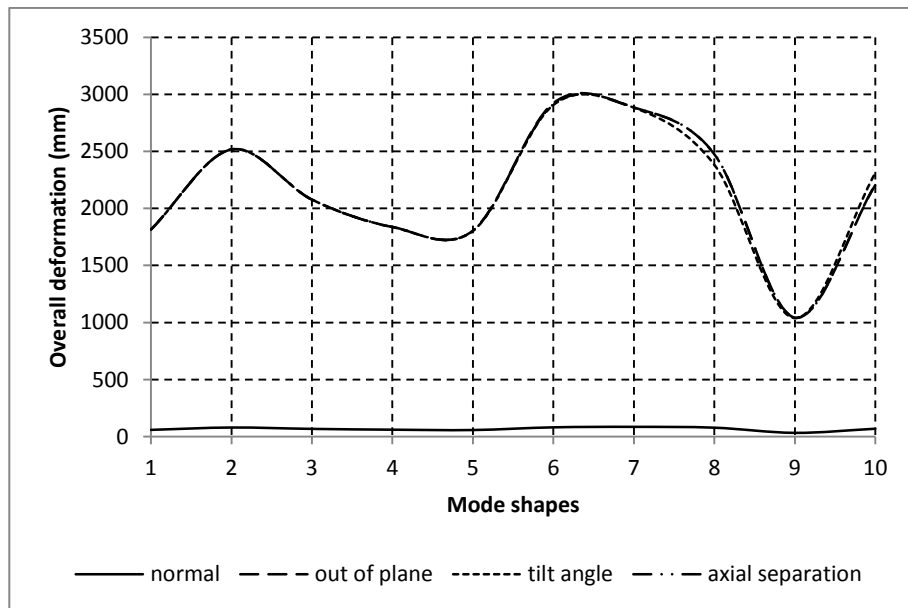


Figure 4.11: Maximum deformation of the gear train with one idler gear in the first ten mode shape.

Overall, the three misalignments cause a drastic increase in the deformation behavior of the gear train. However, the three misalignments did not cause any changes in the vibrational mode shapes of the gear train.

4.3.3 Modal analysis of the gear train with two idler gears

Figure 4.12 shows a sample of the 8th mode shape of the gear train with two idler gears in normal loading, out of plane, tilt angle, and axial separation. In the 8th mode shape, the gear train in normal loading shows bending deformation at the 1st idler gear whereas the three types of non-ideal loading show bending deformation at both idler gears.

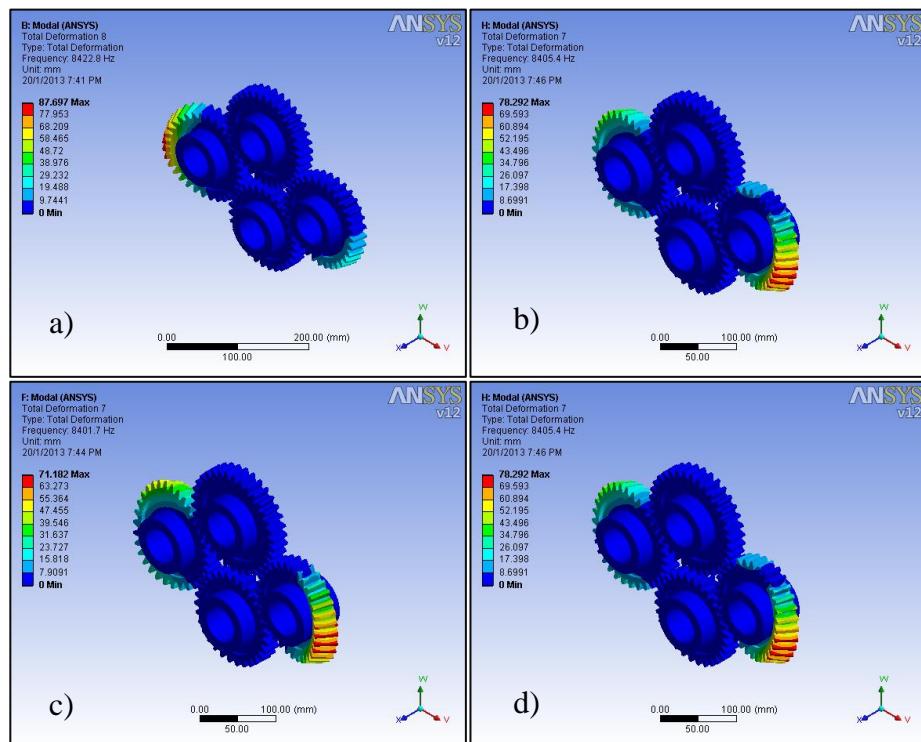


Figure 4.12: The 8th mode shape of the gear train with two idler gears in a) normal loading, b) out of plane, c) tilt angle, and d) axial separation.

Table 4.4 shows the comparison of the vibrational mode shapes between the normal gear train with the out of plane, the tilt angle, and the axial separation misalignment for the gear train with two idler gears. In comparison to the gear train in normal mode, the out of plane misalignment changes the vibrational mode shape at the 4th and 8th mode, the tilt angle misalignment changes the gear train mode shapes at the 8th, 9th and 10th mode and the axial separation misalignment changes the gear train mode shapes at the 3rd, 4th, 6th, 7th, 8th, and 9th mode.

Table 4.4: First ten mode shapes of gear train with two idler gears (IN, ID1, ID2, and OT indicate the input gear, idler gear 1, idler gear 2, and output gear respectively).

Mode	Vibrational mode shape			
	Normal	Out of plane	Tilt angle	Axial separation
1 st	Bending (IN)	Bending (IN)	Bending (IN)	Bending (IN)
2 nd	Swaying (IN)	Swaying (IN)	Swaying (IN)	Swaying (IN)
3 rd	Swaying (IN)	Swaying (IN)	Swaying (IN)	Swaying (IN) Bending (ID1 & ID2)
4 th	Swaying (IN) Bending (ID2)	Swaying (IN) Bending (ID2)	Swaying (IN) Bending (ID2)	Swaying (IN)
5 th	Swaying (ID1 & ID2)	Swaying (ID1 & ID2)	Swaying (ID1 & ID2)	Swaying (ID1 & ID2)
6 th	Swaying (ID1 & ID2)	Swaying (ID1 & ID2)	Swaying (ID1 & ID2)	Swaying (ID1) Bending (ID2)
7 th	Swaying (ID1) Bending (ID2)	Swaying (ID1) Bending (ID2)	Swaying (ID1) Bending (ID2)	Bending (ID1 & ID2)
8 th	Bending (ID1)	Bending (ID1 & ID2)	Bending (ID1 & ID2)	Bending (ID1 & ID2)
9 th	Swaying (IN, ID1 & ID2)	Swaying (IN, ID1 & ID2)	Bending (ID1) Swaying (IN & ID2)	Swaying (ID1 & ID2)
10 th	Swaying (ID1 & ID2)	Swaying (ID1 & ID2)	Swaying (ID1)	Swaying (ID1 & ID2)

Figure 4.13 shows the correlation between the maximum deformations of the gear train with two idler gears against the first ten mode shapes. Overall,

the gear train positioned in the out of plane misalignment has exceptionally higher level of deformation compared to the other three loading conditions. In this analysis, it can be remarked that the axial separation misalignment greatly influences the vibrational mode shape of the gear train in normal mode and the out of plane misalignment causes a drastic increase in the overall deformation of the gear train.

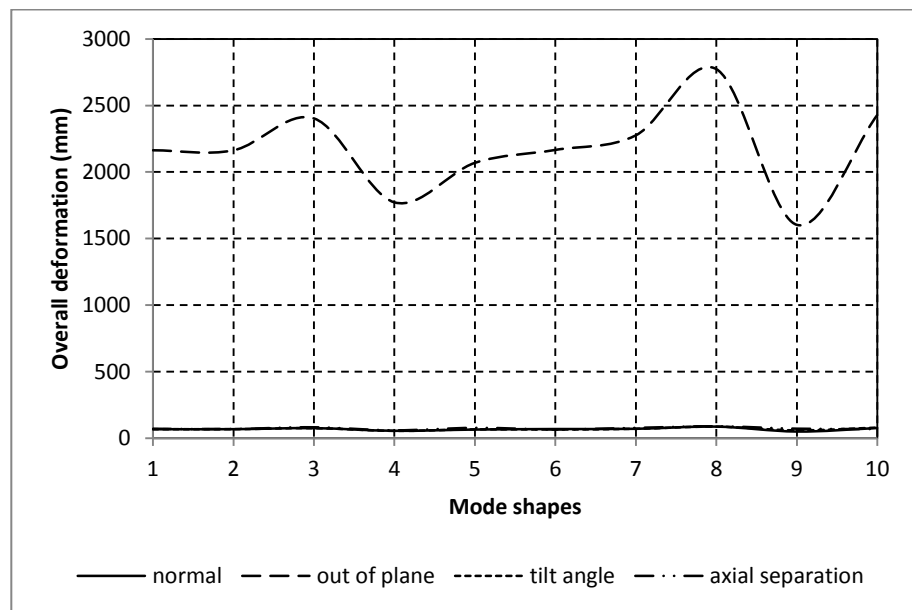


Figure 4.13: Maximum deformation of the gear train with two idler gears in the first ten mode shape.

4.3.4 Forced frequency response of the gear train without idler gear

The frequency response of gear train without idler gear in normal condition is compared with the three types of misalignment. To investigate the frequency response of the gear train in detail, the amplitude of deformation is measured in the X, Y, and Z direction against the frequency between 0 to

10000 Hz. The correlations are plotted in three separate graphs as shown in Figure 4.14, Figure 4.15 and Figure 4.16.

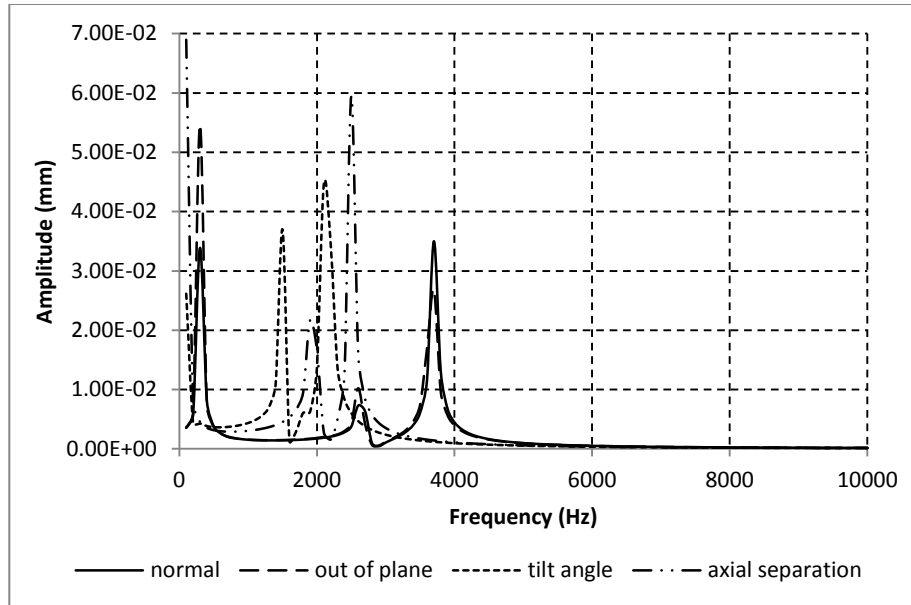


Figure 4.14: X direction deformation against frequency for the gear train without idler gear under non-ideal loading conditions.

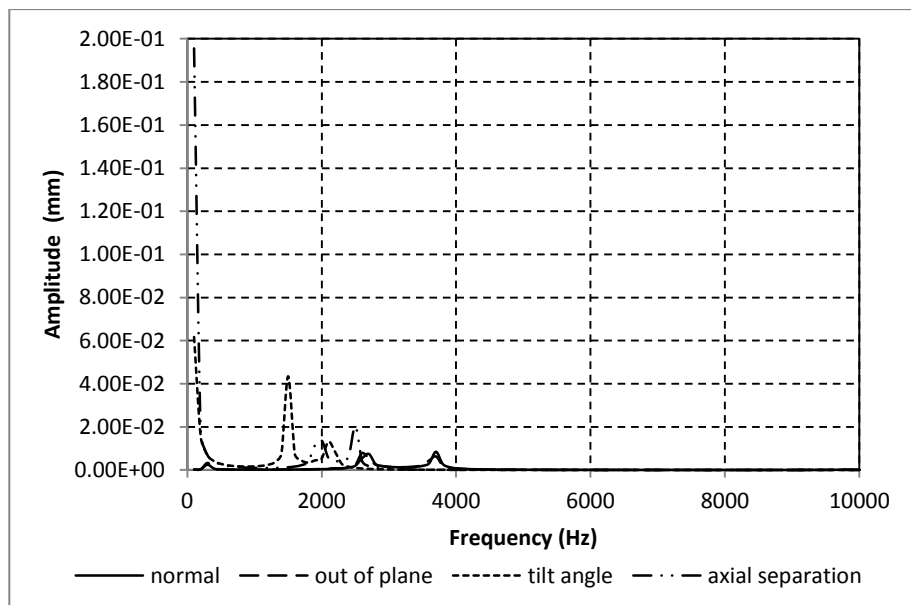


Figure 4.15: Y direction deformation against frequency for the gear train without idler gear under non-ideal loading conditions.

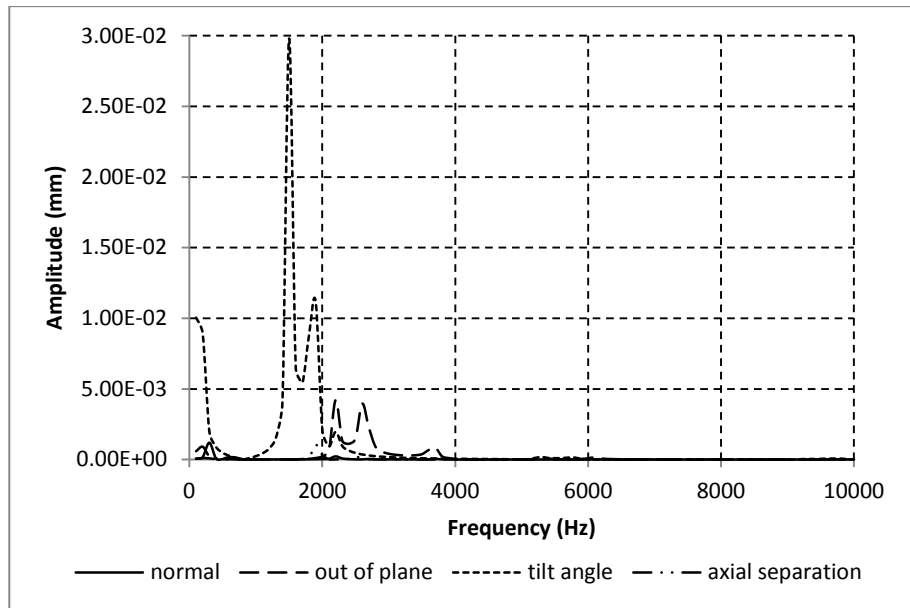


Figure 4.16: Z direction deformation against frequency for the gear train without idler gear under non-ideal loading conditions.

It can be observed that the vibrational amplitude of the gear train under ideal and non-ideal conditions occurs between the frequency responses of 0 to 4000 Hz. The axial separation misalignment in gear train contributes to overall highest vibrational amplitude in the X and Y direction whereas the tilt angle misalignment of gear train results in much higher vibrational amplitude of Z direction. The out of plane misalignment in gear train shows very similar vibrational amplitude pattern in the X, Y and Z directions when compared to the gear train in normal condition. This shows that the out of plane misalignment is less sensitive to the changes of the forced frequency response of the gear train in normal condition.

4.3.5 Forced frequency response of the gear train with one idler gear

The vibration amplitude determined in the X, Y, and Z directions is plotted against the frequency response as shown in Figure 4.17, Figure 4.18 and Figure 4.19 respectively. It can be observed that all loading conditions (normal, out of plane, tilt angle, and axial separation) are nearly in phase for the frequency response in X, Y and Z directions. However, the tilt angle misalignment shows overall highest vibration amplitude in the Z direction in which indicates that the other three conditions are less sensitive to the frequency response in the Z direction.

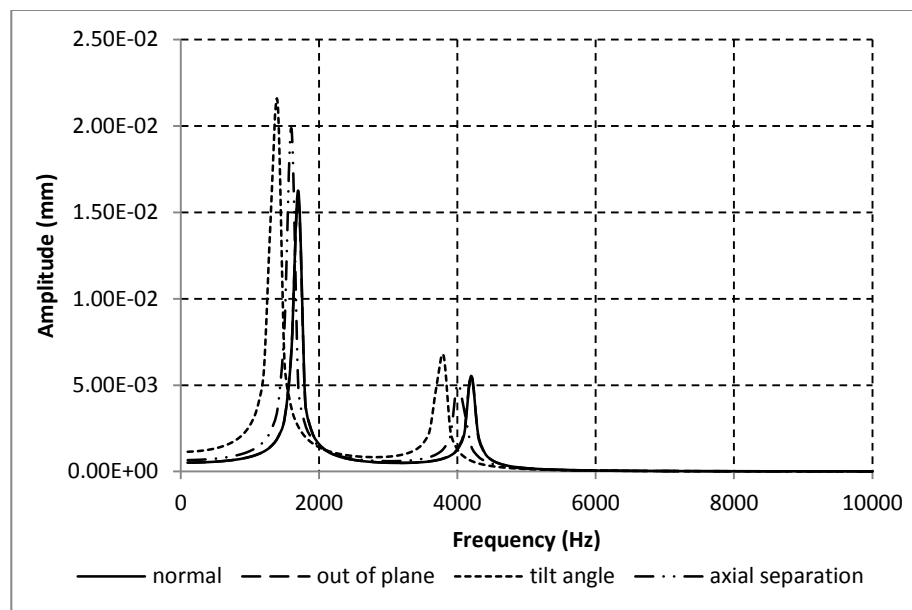


Figure 4.17: X direction deformation against frequency for the gear train with one idler gear under non-ideal loading conditions.

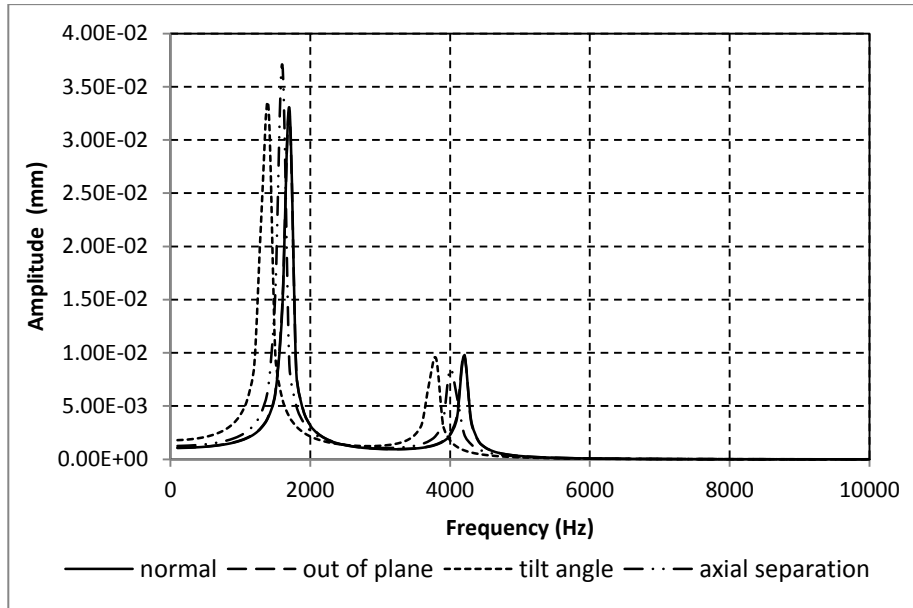


Figure 4.18: Y direction deformation against frequency for the gear train with one idler gear under non-ideal loading conditions.

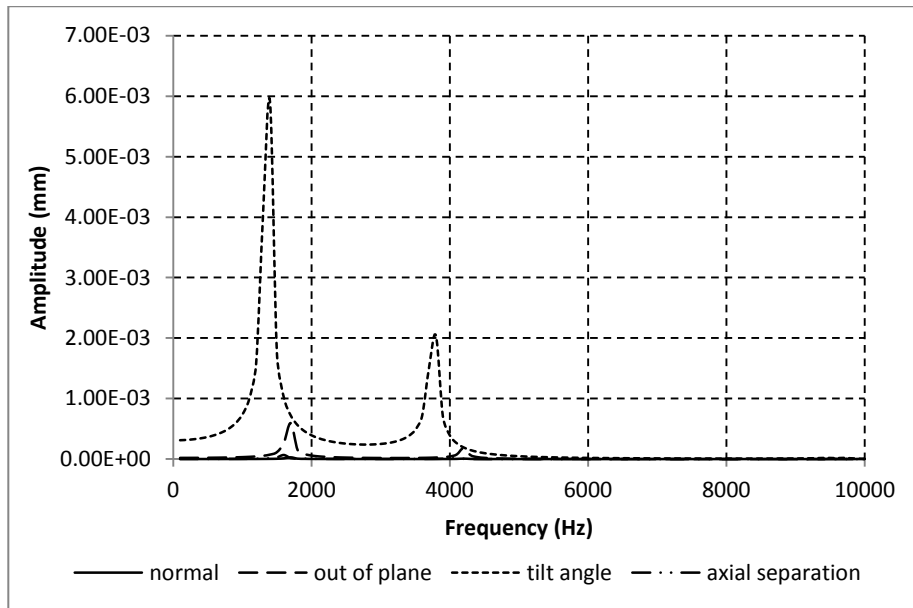


Figure 4.19: Z direction deformation against frequency for the gear train with one idler gear under non-ideal loading conditions.

In comparison to the X, Y, and Z deformations behavior of gear train with one idler gear, the tilt angle misalignment exhibits the highest amplitude in the X and Z direction whereas the axial separation misalignment exhibits the

highest amplitude in the Y direction. Overall, the three types of misalignment exhibit similar frequency response in the X and Y directions when compared to the gear train in normal condition. This shows that all three misalignments minimally affect the deformation of the gear train in X and Y directions.

4.3.6 Forced frequency response of the gear train with two idler gears

The vibration amplitude of the gear train with two idler gears is plotted in the X, Y, and Z directions against the frequency response as shown in Figure 4.20, Figure 4.21 and Figure 4.22. For the frequency response in X direction, it is observed that all loading conditions of the gear train exhibit two peak amplitudes at approximately 2000 Hz and 4000 Hz. The three types of misalignments in the gear train tend to reduce the peak amplitudes of the gear train in normal condition.

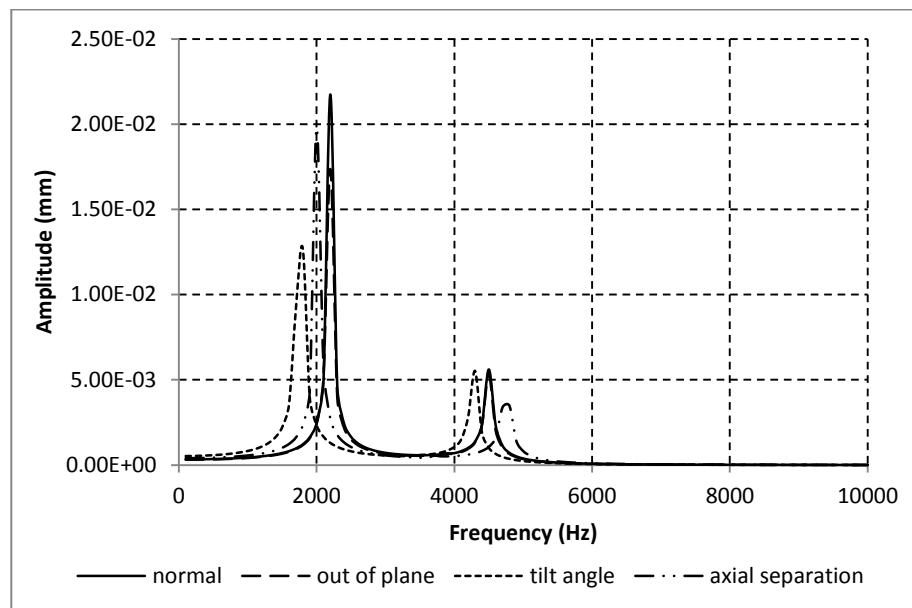


Figure 4.20: X direction deformation against frequency for the gear train with two idler gears under non-ideal loading conditions.

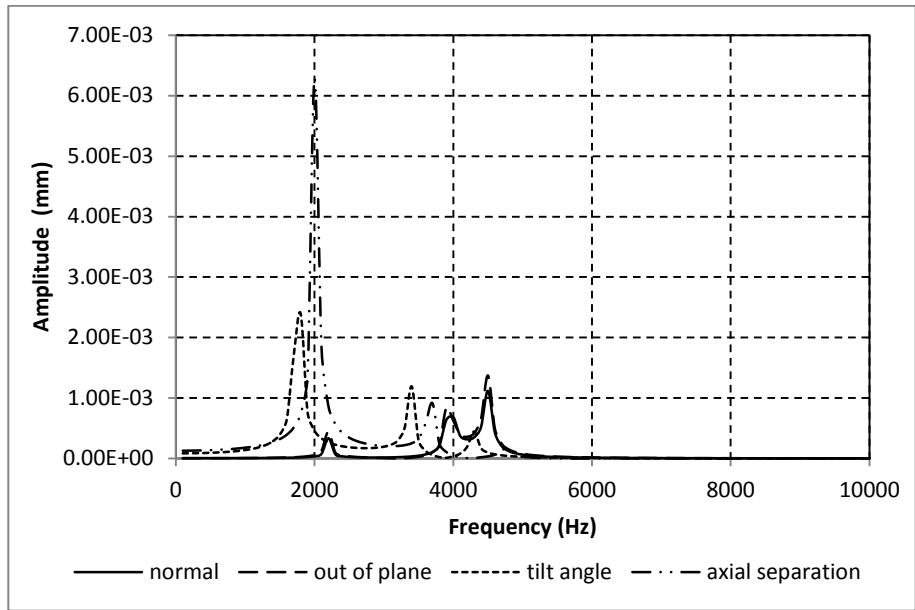


Figure 4.21: Y direction deformation against frequency for the gear train with two idler gears under non-ideal loading conditions.

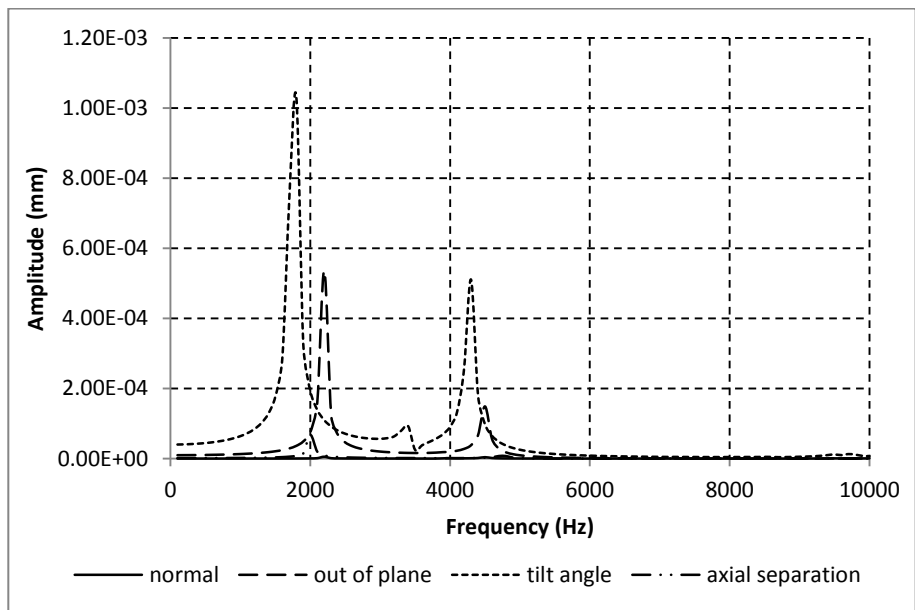


Figure 4.22: Z direction deformation against frequency for the gear train with two idler gears under non-ideal loading conditions.

The axial separation misalignment shows the highest peak amplitude at 2000 Hz in the Y direction frequency response. The gear train in normal condition is excited with low vibration amplitudes in the Y direction. This shows that the misalignment effects are sensitive in the Y direction of the frequency response. In the Z direction frequency response, the tilt angle exhibits the highest amplitude frequency at 1700 Hz. The peak amplitudes of the gear train in normal condition are also very low in the Z direction. This also indicates that the misalignment effects are sensitive in the Z direction of the frequency response.

4.4 Conclusion

In the modal analysis, bending and swaying are the most dominant mode shapes for the gear train without idler gear and gear train with one idler gear. The first ten mode shapes of the gear train without idler gear and the gear train with one idler gear are not affected by the three types of non-ideal loading. However, the tilt angle and axial separation non-ideal loading affect the first ten mode shapes of the gear train with two idler gears.

Table 4.5 shows a summary of the influence of the three different misalignments to the overall amplitude of the three gear train designs in free vibration and forced vibration (forced harmonic response). The overall amplitude of the gear train with one idler gear in free vibration is increased drastically when subjected to three different misalignments. The tilt angle and axial separation misalignment caused a reduction in the overall amplitude of the gear train without idler gear in free vibration.

Table 4.5: The effect of the three different misalignments to the overall amplitude of the three gear train designs in free and forced vibration.

	Non-ideal loading	Types of gear train		
		No idler gear	One idler gear	Two idler gears
Overall amplitude in free vibration	Out of plane	No changes	Drastic increase	Drastic increase
	Tilt angle	Decrease	Drastic increase	No changes
	Axial separation	Decrease	Drastic increase	No changes
Overall amplitude in forced vibration	Out of plane	Increase	Increase	Drastic increase
	Tilt angle	Slight increase	Increase	Increase
	Axial separation	Slight increase	Increase	Increase

In the forced vibration, all three gear train designs are excited to very high deformation amplitude in a frequency range between 0 Hz to 5000 Hz. The gear train with one idler gear and the gear train with two idler gears exhibit very similar harmonic response even with the presence of non-ideal loading. The overall amplitude of the gear train with one idler gear and the gear train with two idler gears are significantly increased when subjected to three different misalignments. The three misalignments caused an increase in the overall amplitude of the three gear train designs in forced vibration. In comparison between the three gear train designs in free vibration and forced vibration, the gear train without idler gear is the least affected by the three different misalignments.

CHAPTER 5

PARAMETRIC OPTIMIZATION OF THE HOLLOW SHAFT WITH RIB

5.1 Introduction

The research overview of this chapter is shown in Figure 5.1. The steps are carried out in sequence for optimizing the proposed hollow shaft with rib for the output shaft of the portal axle.

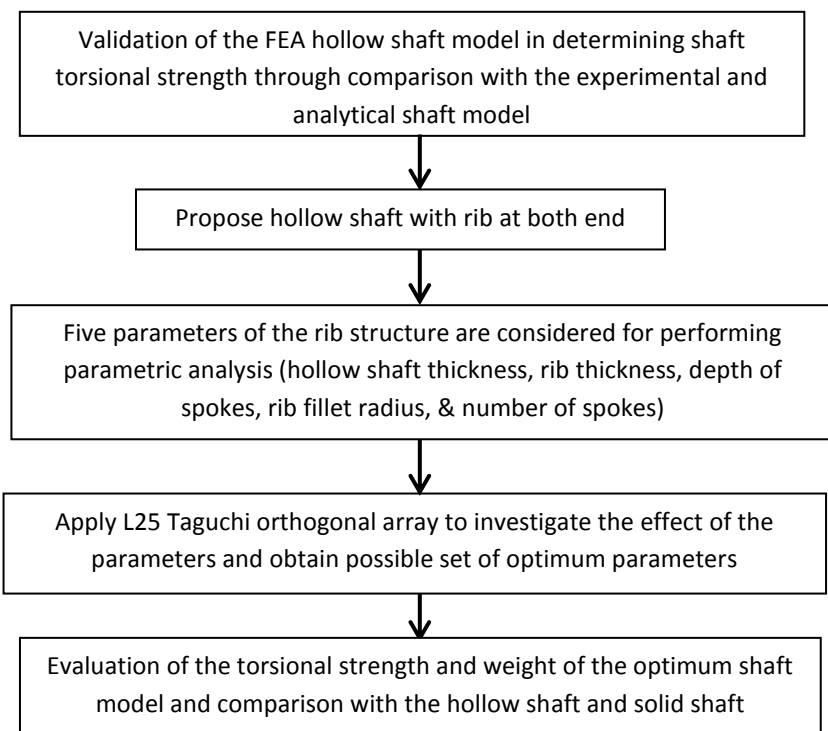


Figure 5.1: Procedure for determining the optimum set of parameters of the hollow shaft with rib.

5.2 Validation of FEA hollow shaft model

The FEA model of a hollow shaft is validated through comparison with the experiment test before modelling the hollow shaft with rib using FEA. The maximum torsional stress of the hollow shaft determined by FEA, experiment test, and analytical method are compared.

5.2.1 Torsional stress evaluation by using FEA

ANSYS software is used to determine the maximum torsional stress of the hollow shaft. Firstly, a 3D hollow shaft of 3 mm in thickness, length of 210 mm and 37 mm outer diameter is modelled by using Autodesk Inventor Professional 2010 software.

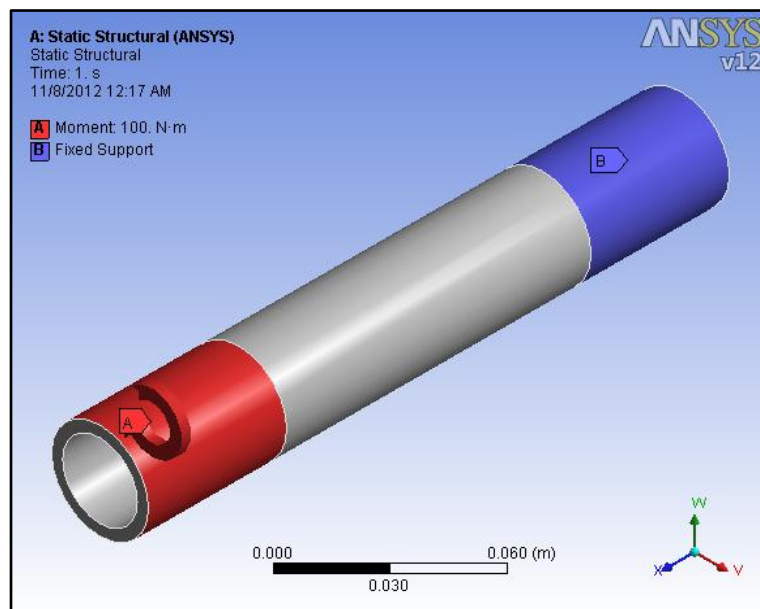


Figure 5.2: Boundary condition settings on the hollow shaft model.

The surface boundary conditions are applied to the shaft model as shown in Figure 5.2. A fixed support is applied at one end shaft and 100 Nm of torsion is applied at one end of the shaft. In the ANSYS mesh settings, hexahedron (brick) element is selected to generate mesh for the hollow shaft model. The convergence of the mesh element size for the FEA shaft model is determined by plotting the maximum torsional stress against decreasing mesh element size as shown in Figure 5.3.

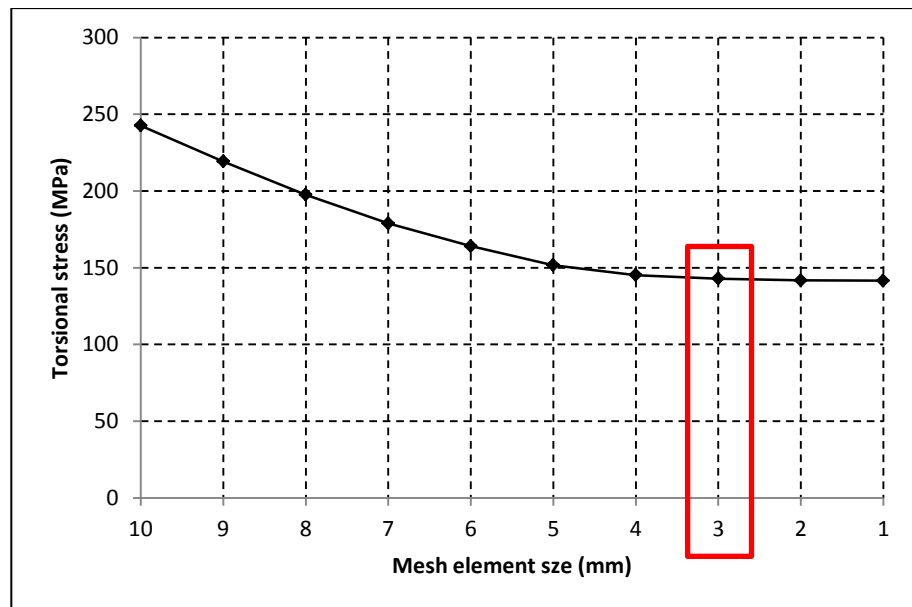


Figure 5.3: Convergence of torsional stress at 3 mm mesh element size for the hollow shaft model.

From Figure 5.3, the optimum element mesh size for the hollow shaft model is 3 mm and the maximum torsional stress is 141.76 MPa. The mesh model of the hollow shaft is generated as shown in Figure 5.4. The number of nodes and elements generated for the hollow shaft model are 11212 and 5678 respectively. ‘Static Structural’ type of analysis is selected in the ANSYS workbench to simulate the torsional stress on the hollow shaft model.

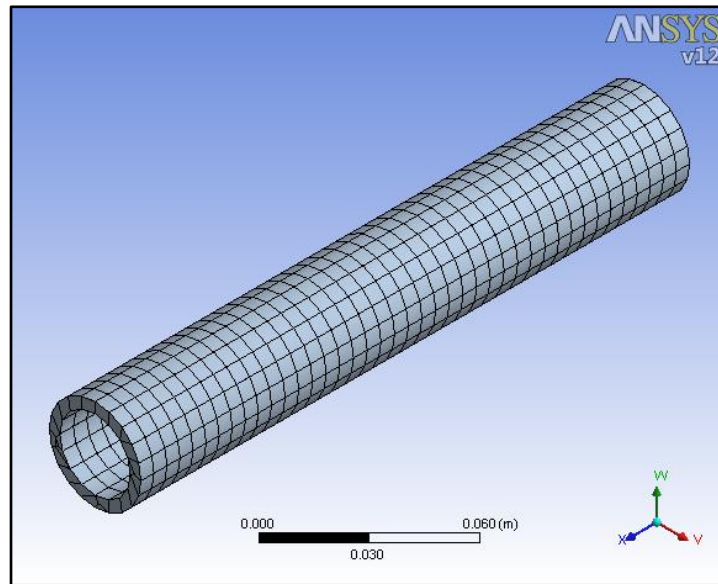


Figure 5.4: Mesh model of the hollow shaft.

Figure 5.5 shows the maximum torsional stress occurred at the discontinuity surface close to the fixed support. The maximum von Mises stress (torsional stress) of the hollow shaft model determined using ANSYS software is 141.76 MPa.

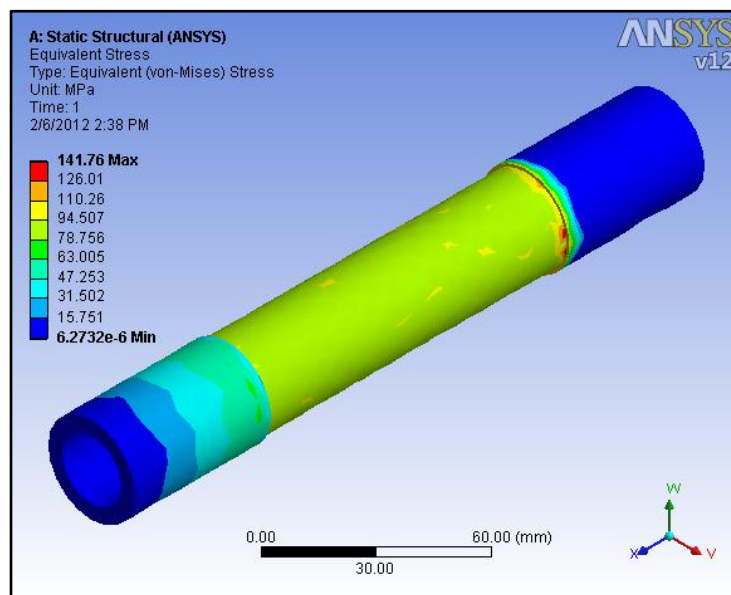


Figure 5.5: Maximum torsional stress of the hollow shaft model.

5.2.2 Torsional stress evaluation by using Distortion Energy Theory

A 2D schematic diagram of the shaft of the hollow shaft is constructed as shown in Figure 5.6. Since torque is only applied on the shaft by the output gear, there is no bending moment. The weight effect of the gear, shaft and bearings are neglected in this analysis.

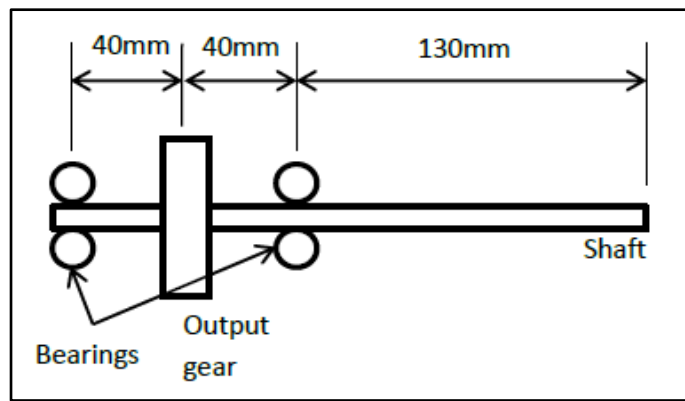


Figure 5.6: Layout diagram of the hollow shaft in 2D.

Distortion energy theory (DET) is applied to determine the von Mises stress of the hollow shaft. DET postulates that failure is caused by the elastic energy associated with shear deformation in which the shaft is assumed to be made of ductile material. DET considers the normal stress σ_x in the x direction (parallel to the direction of shaft axis) caused by bending moment and the maximum shear stress τ_{xy} caused by torque. For a hollow shaft, the normal stress in the x direction is:

$$\sigma_x = \frac{32MD}{\pi(D^4 - d^4)}$$

(12)

Similarly, the maximum shear stress is,

$$\tau_{xy} = \frac{16TD}{\pi(D^4 - d^4)} \quad (13)$$

Where M is the bending moment, T is the applied torque, D is the external diameter of the hollow shaft, and d is the internal diameter of the hollow shaft.

The principal stresses can be determined with the know value of σ_x , σ_y and τ_{xy} as in the following,

$$\sigma_{1,2} = \frac{\sigma_x + \sigma_y}{2} \pm \sqrt{\left(\frac{\sigma_x - \sigma_y}{2}\right)^2 + \tau_{xy}^2} \quad (14)$$

Finally, the general equation for calculating the von Mises stress of the shaft is,

$$\sigma_e = \left(\sigma_1^2 - \sigma_1\sigma_2 + \sigma_2^2\right)^{\frac{1}{2}} \quad (15)$$

5.2.3 Torsional stress evaluation by using experiment

The Tinius Olsen torsion tester is used to apply torsion to the hollow shaft. Firstly, the long rod of normalized AISI 4340 alloy steel with one and a half inch in outer diameter and 3 mm hollow shaft thickness is cut to a length of 210 mm. The cylindrical surface of the hollow shaft is slightly machined to approximately 37 mm in outer diameter and also for smoother surface finish by using the CNC lathe machine. The hollow shaft is then pre-assembled with a strain gage rosettes that provide shear strain data. When torsion is applied to

the shaft causing it to twist, shear stresses are induced. The stresses are measured by bonding the strain gauges at 45° to the horizontal torque axis. Figure 5.7 shows the bonding of the strain gauge on the hollow shaft.

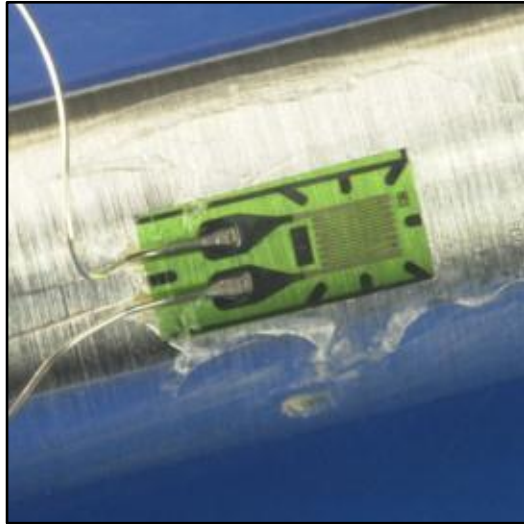


Figure 5.7: Bonding of the strain gauge on the polished surface of the hollow shaft.

Figure 5.8 shows the mounting of the hollow shaft on the Tinius Olsen torsion tester. Both ends of the shaft are gripped and tightened using the jaw and chuck. This machine comes with a built-in data acquisition system where a notebook retrieves all the measured data required. The LabView program read all data and writes to a text file that is readable into Microsoft Excel format sheet.



Figure 5.8: Mounting of the hollow shaft on the Tinius Olsen torsion tester.

Figure 5.9 shows the schematic diagram of the process flow in obtaining the shaft torsional stress. In the LabView software, the initial torque load was set at 100 Nm with an increment of 20 Nm until the first ten load points. All of the data files were recorded in LabView and the experimental results of the measured shear stress of the shaft are collected and plotted. The results are directly imported into ‘Microsoft Excel’ sheet file for analysis of the results.

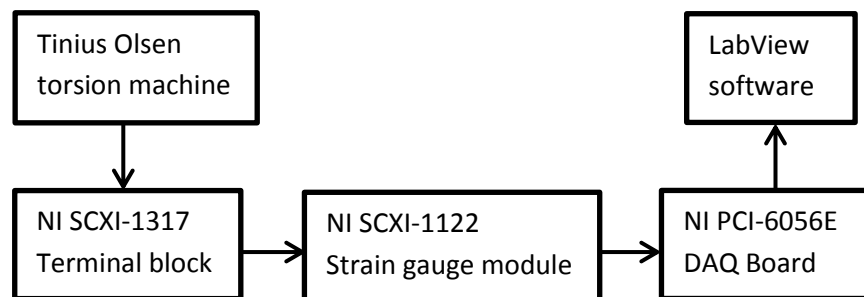


Figure 5.9: Strain measurement system of the torsion tester machine.

5.2.4 Results comparison

The FEA model is compared with the experimental and the analytical model. With the same size and dimension of the solid shaft, the torsional stresses of the models were plotted against the increasing torque as shown in Figure 5.10. All models show linear relationship between the torsional stress and the increment of torque.

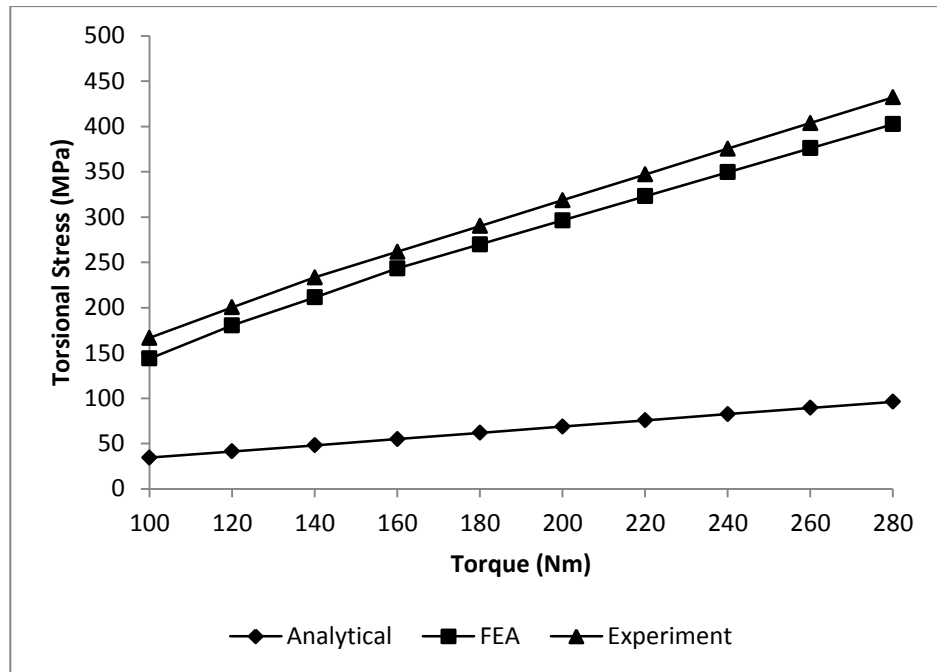


Figure 5.10: Torsional stress comparison between the FEA model, experimental model, and the analytical model.

The experimental model has higher torsional stress compared to the FEA model and the analytical model. However, the torsional stress calculated for the FEA model is quite close to the torsional stress measured from the experimental model. The average percentage of difference between them is only 9.83%. This shows the FEA model agree well with the experimental

model. A huge difference between the analytical model with the FEA and experimental models is due to the consideration of the shaft analysis of the shaft in 2D and many assumptions are made to perform the calculations. This shows that FEA model is a more acceptable method for evaluation of the shaft torsional stress.

5.3 Model of the hollow shaft with rib

A hollow shaft with rib at both ends is proposed for the output shaft of the portal axle and is also used as a benchmarking shaft for comparison in the later section. The benchmarking shaft with five types of parameter is modelled as shown in Figure 5.11. Table 5.1 shows the material properties and the dimension used for modelling the shaft.

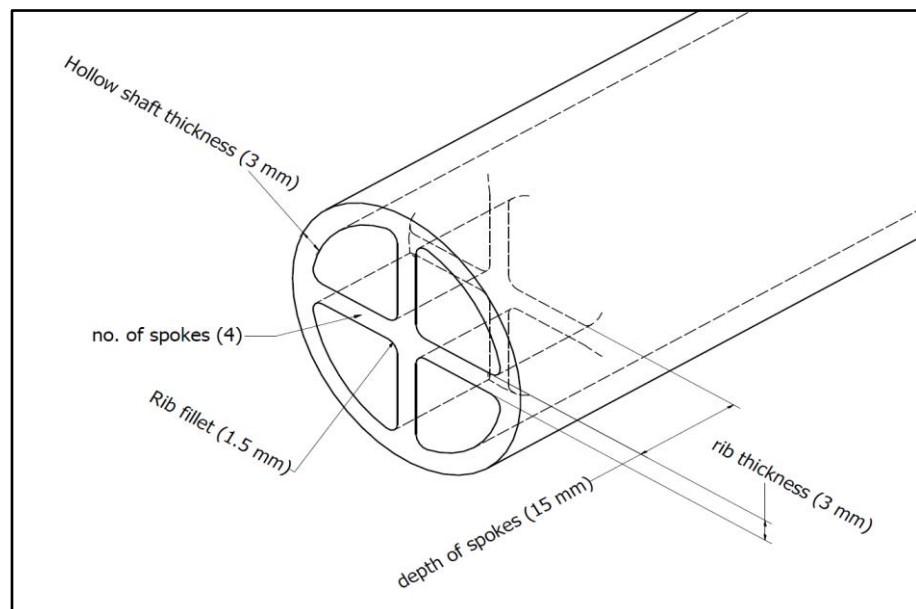


Figure 5.11: Model of the hollow shaft with rib with five types of parameter.

Table 5.1: Dimensions and material properties of the hollow shaft with rib.

Length	210 mm
Outer diameter	37 mm
Material	ANSI 4340 alloy steel (normalized at 870°C)
Ultimate tensile strength (UTS)	1279.0 MPa
Yield strength	861.8 MPa
Young's Modulus	200 GPa
Poisson's Ratio	0.3
Density	7850 kg/m ³

5.4 Parametric analysis of the hollow shaft with rib

The effect of the hollow shaft thickness, rib thickness, depth of spokes, rib fillet radius, and the number of spokes to the torsional stress of the hollow shaft with rib are investigated. The proposed shaft is used as a benchmarking shaft for modifying the values of the parameter. In the study on the effect of one parameter, the other parameters of the benchmark shaft remain constant. Each of the following sections discusses the effect of each parameter separately:

5.4.1 Effect of the hollow shaft thickness

Figure 5.12 shows an exponential correlation between the torsional stress and the hollow shaft thickness. There is a drastic decrease in the torsional stress when the hollow shaft thickness increases from 1 mm to 3 mm. This indicates that the increase in hollow shaft thickness contributes to the increase in torsional strength of the hollow shaft with rib. However, the torsional stress decreases slightly when the hollow shaft thickness is increased from 3 mm to 5

mm. This indicates that the torsional stress is converging when the hollow shaft thickness is increased beyond 4 mm.

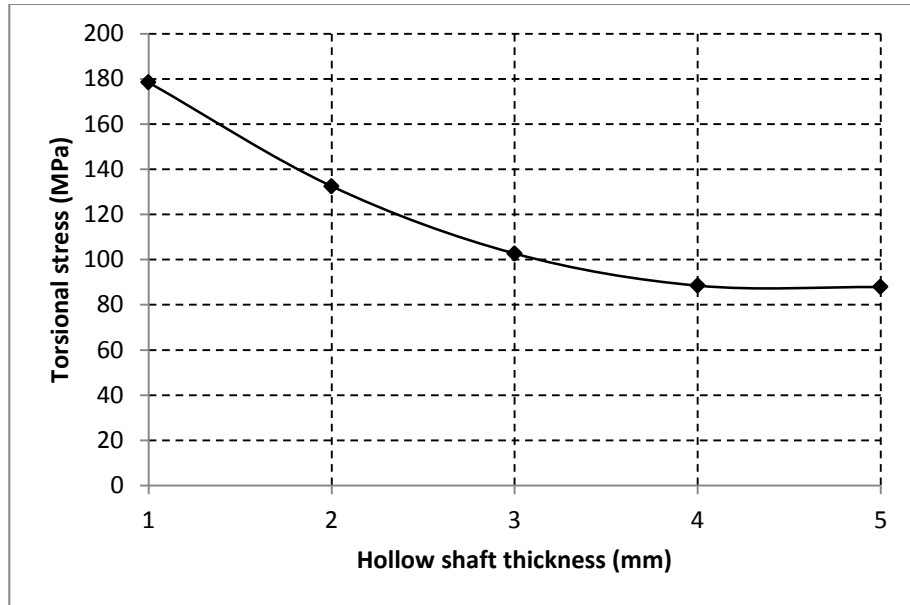


Figure 5.12: Torsional stress versus hollow shaft thickness of the hollow shaft with rib.

5.4.2 Effect of the rib thickness

Figure 5.13 shows an inverse proportional relationship between the torsional stress and the rib thickness. There is a gradual decrement in the torsional stress with the increasing rib thickness. With every increment of 1 mm rib thickness, the torsional stress reduces by an average of 10 MPa. This shows that the rib thickness significantly affects the torsional strength of the hollow shaft with rib.

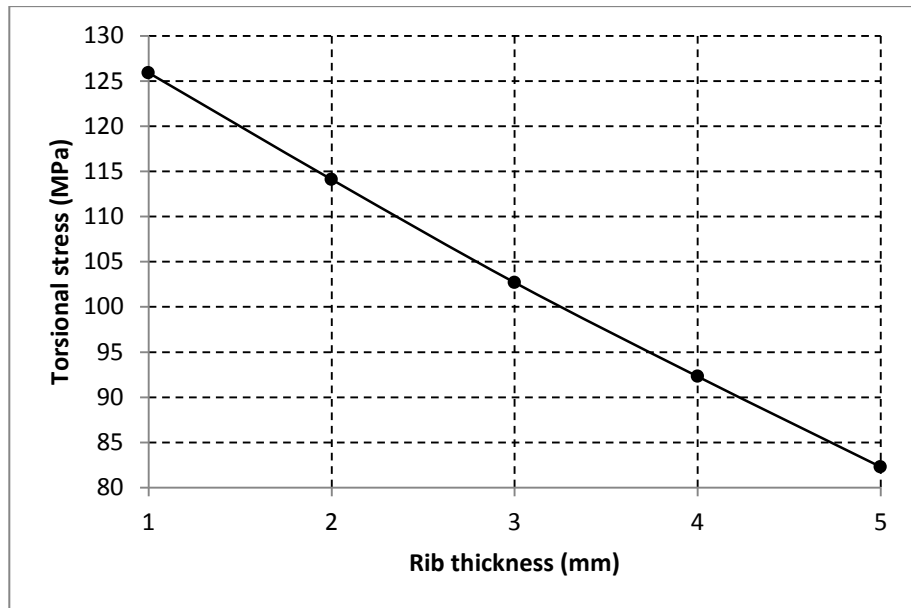


Figure 5.13: Torsional stress versus rib thickness of the hollow shaft with rib.

5.4.3 Effect of the depth of spokes

Figure 5.14 shows an inverse exponential correlation between the shaft torsional stress and the depth of spokes. There is a huge reduction in the torsional stress when the depth of spokes is increased from 5 mm to 15 mm which indicates significant reduction in the shaft torsional strength. However, the reduction in torsional stress is less significant when the depth of spokes is increased from 15 mm to 25 mm.

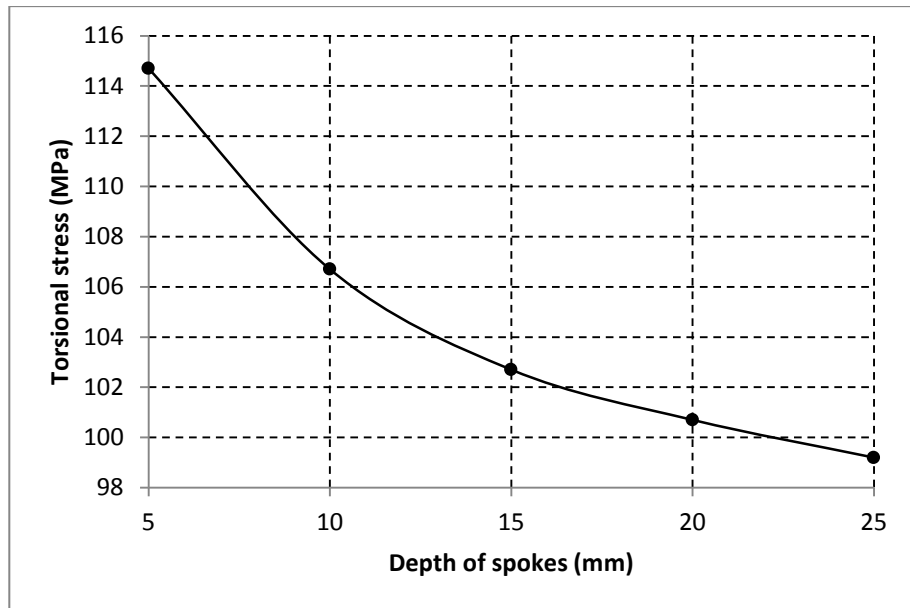


Figure 5.14: Torsional stress versus depth of spokes of the hollow shaft with rib.

5.4.4 Effect of the rib fillet radius

Figure 5.15 shows an almost inverse proportional relationship between the torsional stress and the radius of the rib. It can be seen that increasing the rib fillet radius from 1 mm to 1.75 mm yields to linear reduction in the torsional stress. In Figure 5.15, it can be remarked that the rib fillet radius significantly affect the torsional strength of the hollow shaft with rib. For every increment of 0.5 mm in rib fillet radius, the average reduction in the torsional stress is 7 MPa.

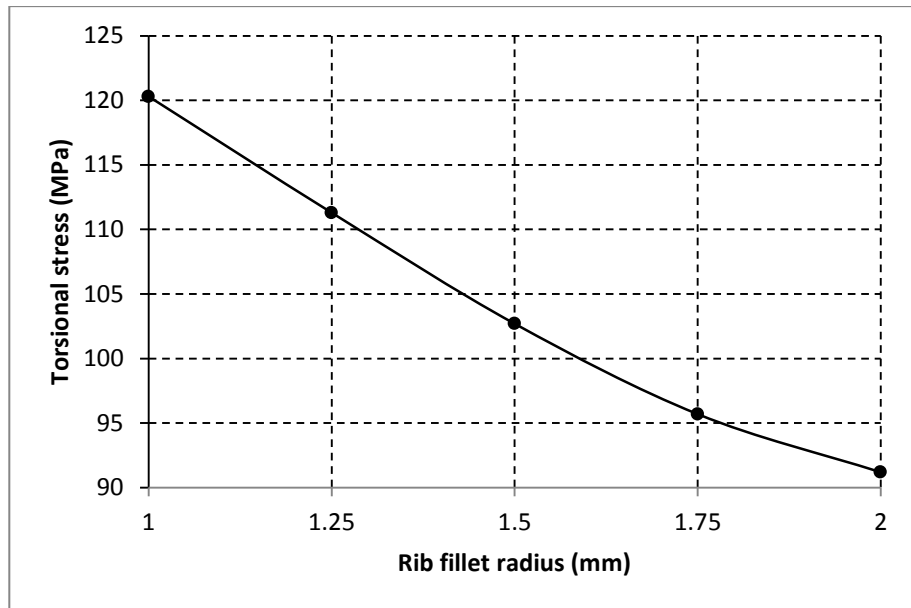


Figure 5.15: Torsional stress versus rib fillet radius of the hollow shaft with rib.

5.4.5 Effect of the number of spokes

Figure 5.16 shows the correlation between the torsional stress and the number of spokes. The torsional stress decreases exponentially with the increasing number of spokes. When the number of spokes increases, the average reduction in the torsional stress is only 2.5 MPa. The percentage difference of the torsional stress between the shaft with 2 spokes and 6 spokes is only 9%. This shows that the number of spokes of the rib of the hollow shaft has minimal effect to the shaft torsional strength.

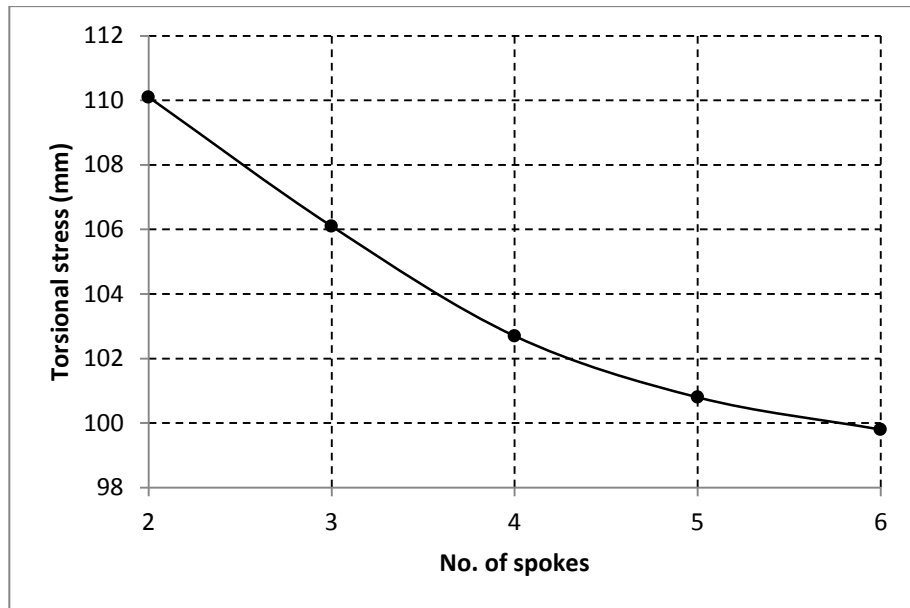


Figure 5.16: Torsional stress versus the number of spokes of the hollow shaft with rib.

5.5 Parametric optimization of the hollow shaft with rib

5.5.1 L25 Taguchi Orthogonal Array

The L25 Taguchi OA is applied to determine the optimum combination of the five types of parameters (the hollow shaft thickness, rib thickness, depth of spokes, rib fillet radius, and the number of spokes) that will result in the lowest torsional stress. Minitab 16 statistical software is applied to run the L25 Taguchi OA. Firstly, the factorial design is set by selecting five factors (five parameters) with five levels (five variables) as shown in Table 5.2. Table 5.3 shows twenty five unique sets of parametric combination that are randomly generated for L25 Taguchi OA when five factors with five different variables are selected. The 3D benchmarking shaft model is modified in the Autodesk

Inventor software before importing the model to ANSYS software for evaluating the shaft torsional stress.

Table 5.2: Factorial design of the shaft model with five factors and five levels.

	Factor	Unit	Type	Level 1	Level 2	Level 3	Level 4	Level 5
A	hollow shaft thickness	mm	Qualitative	1	2	3	4	5
B	rib thickness	mm	Qualitative	1	2	3	4	5
C	depth of spokes	mm	Qualitative	5	10	15	20	25
D	rib fillet radius	mm	Qualitative	1	1.25	1.5	1.75	2
E	no. of spokes	-	Qualitative	2	3	4	5	6

Table 5.3: L25 Taguchi Orthogonal Array design factors of the shaft model.

Standard order	Run order	Hollow shaft thickness (mm)	Rib thickness (mm)	Depth of spokes (mm)	Rib fillet radius (mm)	No. of spokes	von Mises stress (Mpa)
23	1	5	3	10	1	6	119.1
13	2	3	3	25	1.25	5	215.5
19	3	4	4	10	2	4	88.56
5	4	1	5	25	2	6	263.6
24	5	5	4	15	1.25	2	109.9
14	6	3	4	5	1.5	6	123.8
3	7	1	3	15	1.5	4	270.4
2	8	1	2	10	1.25	3	293.1
1	9	1	1	5	1	2	226.8
22	10	5	2	5	2	5	121.2
8	11	2	3	20	2	2	206.7
17	12	4	2	25	1.5	2	135.3
7	13	2	2	15	1.75	6	193.8
25	14	5	5	20	1.5	3	92.24
11	15	3	1	15	2	3	158.5
16	16	4	1	20	1.25	6	186
18	17	4	3	5	1.75	3	132.1
21	18	5	1	25	1.75	4	129
12	19	3	2	20	1	4	149.7
10	20	2	5	5	1.25	4	194.8
6	21	2	1	10	1.5	5	186.5
15	22	3	5	10	1.75	2	147.3
4	23	1	4	20	1.75	5	229.7
20	24	4	5	15	1	5	126.9
9	25	2	4	25	1	3	179.4

In the next step, Analysis of Variance (ANOVA) is generated to determine the 'F Ratio' and 'P value' so that the level of significance of the parameters to the output (objective) can be distinguished. Table 5.4 shows the ANOVA of the five parameters. The lowest P value indicates that the highest level of significance to the output response. From the ANOVA table, the level of significance in the ascending order is the number of spokes, depth of spokes, rib thickness, rib fillet radius, and hollow shaft thickness. In comparisons, the hollow shaft thickness affect the torsional stress of the shaft the most.

Table 5.4: Analysis of Variance of the five parameters.

Source of Variation	Degrees of Freedom	Sum of Squares [Partial]	Mean Squares [Partial]	F Ratio	P Value
Model	20	7.56E+04	3780.4376	15.2389	0.0085
A: hollow shaft thickness	4	6.27E+04	1.57E+04	63.2162	0.0007
B: rib thickness	4	5307.9926	1326.9982	5.3491	0.0666
C: depth of spokes	4	1657.4014	414.3504	1.6702	0.3157
D: rib fillet radius	4	5325.5358	1331.384	5.3668	0.0663
E: no. of spokes	4	587.819	146.9548	0.5924	0.6878
Residual	4	992.3096	248.0774	-	-
Lack of Fit	4	992.3096	248.0774	-	-
Total	24	7.66E+04	-	-	-

Finally, diagnostic analysis is carried out as shown in Table 5.5 to determine the actual value based on the results obtained earlier in Table 5.3. The one highlighted in green is the optimum design parameters where the actual value corresponds to the lowest torsional stress whereas the highlighted red corresponds to the highest actual value of the torsional stress. Therefore, referring to Table 5.5, "standard order 19" is the optimum set of parameter for the hollow shaft with rib in which the hollow shaft thickness is 4 mm, the rib thickness is 4 mm, the depth of spokes is 10 mm, the rib fillet is 2 mm, and the

number of spokes is 4. The torsional stress of the optimized shaft model is 88.56 MPa.

Table 5.5: Diagnostic analysis of the L25 Taguchi OA design factor.

Run Order	Standard Order	Actual Value (Y)	Fitted Value (YF)
1	23	119.1	122.816
2	13	215.5	223.316
3	19	88.56	96.376
4	5	263.6	266.436
5	24	109.9	112.736
6	14	123.8	119.096
7	3	270.4	260.736
8	2	293.1	288.396
9	1	226.8	234.616
10	22	121.2	111.536
11	8	206.7	201.996
12	17	135.3	139.016
13	7	193.8	201.616
14	25	92.24	100.056
15	11	158.5	162.216
16	16	186	176.336
17	18	132.1	134.936
18	21	129	124.296
19	12	149.7	152.536
20	10	194.8	198.516
21	6	186.5	189.336
22	15	147.3	137.636
23	4	229.7	233.416
24	20	126.9	122.196
25	9	179.4	169.736

5.5.2 Strength and weight comparison of the optimized shaft

The torsional strength and weight reduction of the optimized shaft, the benchmarking shaft, the hollow shaft, and the solid shaft are obtained for comparison. The torsional stress and the weight of the four types of shaft are determined by using ANSYS software. Table 5.6 shows the torsional stress and the weight reduction comparisons between the four types of shaft. The weight reduction is calculated with reference to the mass of the solid shaft in which it is the heaviest among the other shafts.

Table 5.6: Comparison of shaft models based on strength and weight reduction.

	Optimized shaft	Benchmark shaft	Hollow shaft	Solid shaft
Length (mm)	210			
Diameter (mm)	37			
Material	AISI 4340 alloy steel (normalized at 870°C)			
Torque (Nm)	100			
Hollow shaft thickness (mm)	4	3	3	-
Rib thickness (mm)	4	3	-	-
Depth of spokes (mm)	10	15	-	-
Rib fillet radius (mm)	2	1.5	-	-
Number of spokes	4	4	-	-
Torsional stress (MPa)	88.56	102.70	141.76	81.28
Weight (kg)	0.744	0.595	0.552	1.796
Weight reduction (kg) compared to solid shaft	1.052	1.201	1.244	-
Stress to weight reduction ratio	84.18	85.51	113.96	-

From the shaft comparisons in Table 5.6, the optimized shaft has lower torsional stress compared to the benchmark shaft and the hollow shaft. The weight of the shaft is measured by using ANSYS software to determine the percentage of weight reduction. The hollow shaft is the lightest among the four shafts, thus having the highest weight reduction. In order to evaluate the shaft with overall most improved strength and amount of weight reduction, the stress to weight reduction ratio is calculated for each shaft. The optimized shaft has the lowest stress to weight reduction compared to the benchmarking shaft and the hollow shaft. This indicates that the optimized shaft has the most improved torsional strength and weight reduction. The optimized shaft has an improved strength by 13.77% but an increase of 20% in weight compared to the benchmarking shaft.

5.6 Conclusion

The hollow shaft thickness was the most dominant parameter which greatly affects the torsional strength of the hollow shaft with rib. However, the number of spokes was the least dominant parameter to the torsional strength of the hollow shaft with rib. The optimum set of parameters for the hollow shaft with rib was determined in which the hollow shaft thickness is 4 mm, the rib thickness is 4mm, the depth of spokes is 10 mm, the rib fillet radius is 2 mm, and the number of spokes is 4. The optimized shaft has an improvement in strength of 13.77% but a 20% increase in weight compared to the benchmarking shaft. The optimized shaft has the most improved “strength to weight reduction ratio” compared to the solid shaft and the hollow shaft. The L25 Taguchi OA method has been proven effective in determining the optimum parameters for the hollow shaft with rib.

CHAPTER 6

CONCLUSIONS AND FUTURE WORK

6.1 Conclusions

The 3D models of the three types of gear train developed by using the ANSYS FEA software are able to predict the bending and the contact stress at the output gear with increasing angular position. All three types of non-ideal loading in gear train caused a drastic increase in the bending stress and the contact stress of the output gear. The tilt angle misalignment is found to be the most dominant in causing a tremendous increase in the stresses at the output gear. The difference between ideal and non-ideal cases was found to be as much as 44.45% for the bending stress and 25.15% for the contact stress. A tremendous increase in the bending stress and the contact stress at the output gear of the gear train would lead to gear failure sooner than expected.

The 3D models developed are also able to effectively predict the mode shapes and the harmonic response frequency of the three gear train designs. In the modal analysis, bending and swaying are found to be the most dominant mode shapes for the gear train without idler gear and the gear train with one idler gear. The three types of non-ideal loading changed the mode shapes of the gear train without idler gear and the gear train with two idler gears. The three types of non-ideal loading increased the overall deformation of the gear trains but the overall deformation of the gear train without idler gear is the least affected. The three types of non-ideal loading caused a huge change in the

harmonic response frequency of the gear train without idler gear and the gear train with two idler gears.

The 3D shaft model developed by using ANSYS software can effectively predict the shaft torsional strength. The hollow shaft thickness is found to be the dominant parameter which greatly affects the torsional strength of the hollow shaft with rib. The optimum set of parameters for the hollow shaft with rib was successfully determined by using L25 Taguchi OA. The optimized shaft has the highest “strength to weight reduction ratio” with an improvement in strength of 13.77% but a 20% increase in weight compared to the benchmarking shaft. The L25 Taguchi OA method has been proven effective in determining the optimum parameters for the hollow shaft with rib.

6.2 Contributions

This thesis has contributed to developing the 3D gear train models for a portal axle using FEA that can accurately evaluate the bending and contact strength of the gears in the gear train of the portal axle. With the procedures and techniques presented for modelling and simulation of the gear train models using FEA, design engineers can accurately predict the increase in both bending and contact stress and also design gears closer to safety factors for a more optimized gear train. The investigation of the gear stress analysis and vibration analysis in ideal loading and non-ideal loading conditions for the gear train models also contributed to the understanding of how the gear stresses and vibrational behaviour of the gear train models of the portal axle can be affected. In the analysis of the output shaft of the portal axle, the developed

FEA model of the hollow shaft with rib and the parametric optimization of the rib using Taguchi method provided an effective solution for optimizing the design parameters of the shaft model that can significantly improve its torsional strength. The presented methodology for determining the shaft torsional stress and the optimum set of parameters for shaft can be used as a guideline for design engineers in optimizing shaft design.

6.3 Future Work

The research in portal axle is still in infancy stage and there is possibility of more in depth research work can be done to improve the mechanical design and performance of the portal axle. As computer capabilities increase from time to time, finite element analysis investigations should be applied on the following areas:

- A whole gearbox with all elements in the system such as the bearing and the gear casing,
- Three-dimensional model of the portal axle gear train simulations consisting of helical gears,
- An optimization of the gear shape to reduce bending stress, contact stress and wear depth would benefit the gear design community.

REFERENCES

- Arafa, M.H. and Megahed, M.M., 1999. Evaluation of Spur Gear Mesh Compliance Using the Finite Element Method. *Proceedings of Institution of Mechanical Engineers*, 3, pp. 569-579.
- Archard, J.F., 1953. Contact and Rubbing of Flat Surfaces. *Journal of Applied Physics*, 24 (8), pp. 981-988.
- Arikan, S., 2002. Direct Calculation of AGMA Geometry Factor J by Making use of Polynomial Equations. *Journal of Mechanics Research Communications*, 29 (4), pp. 257-268.
- Axle Tech Bolt On Portal Axle For 14 Bolt & Dana 60 Axles, 2009, *Lift-N-Gears 4Wheel & Off-Road* [Online]. Available at: http://www.4wheeloffroad.com/techarticles/drivetrain/131_0908_axletech_bolt_on_portal_axles_dana_60_14_bolt/index.html [Accessed: 9 March 2011].
- Barone, S., Borgianni, L. and Forte, P., 2003. Evaluation of the Effect of Misalignment and Profile Modification in Face Gear Drive by a Finite Element Meshing Simulation. *Proceedings of the ASME Design Engineering Conference*, pp. 657-664.
- Bayrakceken, H., Tasgetiren, S. and Yavuz, I., 2007. Two cases of failure in the power transmission system on vehicles: A universal joint yoke and a drive shaft. *Journal of Engineering Failure Analysis*, 14 (4), pp. 716-724.
- Berlioz, A. and Trompette, P., 2010. *Solid mechanics using the finite element method*, ISTE Ltd and John Wiley & Sons, Inc.
- Black, P.H., 1936. An Investigation of Relative Stresses in Solid Spur Gears by the Photoelastic Method. *Proceedings of Engineering Experiment Station Bulletin Series No. 288*, University of Illinois, Urbana-Champaign.
- Box, G. and Bisgaard, S., 1988. Statistical Tools for Improving Designs. *Proceedings of Mechanical Engineering*, 110 (1), pp. 32-40.
- Bruns, T., 2007. Modelling and identification of an all-terrain vehicle. *Journal of Vehicle Systems Modeling and Testing*, 2 (3), pp. 276-295.
- Byrne, D.M. and Taguchi, S., 1987. The Taguchi approach to parameter design. *Proceedings of Quality Progress*, 20 (12), pp. 19-26.

- Cavdar, K., Karpat, F. and Babalik, F., 2005. Computer Aided Analysis of Bending Strength of Involute Spur Gears with Asymmetric Profile. *Journal of Mechanical Design*, 127 (1), pp. 477-484.
- Chen, Y. and Tsay, C., 2002. Stress analysis of a helical gear set with localized bearing Contact. *Journal of Finite Elements in Analysis and Design*, 38 (8), pp. 707–723.
- Choi, S.H., Glienicke, J., Han, D.C. and Ulrichs, K., 1999. Dynamic gear loads due to coupled lateral, torsional and axial vibrations in a helical geared system. *Journal of Vibration and Acoustics*, 121, pp. 141–148.
- Chong, T.H., Bae, I. and Park, G., 2002. A new and generalized methodology to design multi-stage gear drives by integrating the dimensional and the configuration design process. *Journal of Mechanism and Machine Theory*, 37 (3), pp. 295-310.
- Crivelli, D., Ghelichi, R. and Guagliano, M., 2011. Failure analysis of a shaft of a car lift system. *Journal of Procedia Engineering*, 10, pp. 3683–3691.
- Dolan, T.J. and Broghamer, E.L., 1942. A Photoelastic Study of Stresses in Gear Tooth Fillets. *Proceedings of Engineering Experiment Station Bulletin Series No. 335*, University of Illinois, Urbana-Champaign.
- Draca, S., 2006. *Finite element model of a double-stage helical gear reduction*. Master Thesis, University of Windsor, Canada.
- Eritenel, T. and Parker, R.G., 2009. Modal properties of three-dimensional helical planetary gears. *Journal of Sound and Vibration*, 32 (5), pp. 397-420.
- Errichello, R., 1979. State-of-art review: gear dynamics. *Journal of Mechanical Design*, 101 (3), pp. 368-372.
- Exaxt, 2002, *EXAXT Extreme Axle Technology Ltd.* [Online]. Available at: http://www.exaxt.ca/contact_us.asp [Accessed: 15 March 2011].
- Flodin, A. and Andersson, S., 1997. Simulation of Mild Wear in Spur Gears. *Journal of Wear*, 207 (1), pp. 16-23.
- Göksenli, A. and Eryürek, I.B., 2009. Failure analysis of an elevator drive shaft. *Journal of Engineering Failure Analysis*, 16 (4), pp. 1011–1019.
- Gunes, S., Manay, E., Senyigit, E. and Ozceyhan, V., 2011. A Taguchi approach for optimization of design parameters in a tube with coiled wire inserts. *Journal of Applied Thermal Engineering*, 31 (14-15), pp. 2568-2577.

- Hassan, A.R., 2009, *Contact Stress Analysis of Spur Gear Teeth Pair*, World Academy of Science, Engineering and Technology [Online]. Available at: <http://www.scribd.com/doc/29351224/Contact-Stress-Analysis-of-Spur-Gear-Teeth-Pair> [Accessed: 26 March 2011].
- Heisler, H., 1999. *Vehicle and engine technology*, 2nd ed. London: SAE International.
- Hertz, H.R., 1882. Ueber die Beruehrung elastischer Koeper (On Contact Between Elastic Bodies), in *Gesammelte Werke (Collected Works)*. Vol. 1, Leipzig, Germany.
- Hu, Y., Shao, Y., Chen, Z. and Zuo, M.J., 2011. Transient meshing performance of gears with different modification coefficients and helical angles using explicit dynamic FEA. *Journal of Mechanical Systems and Signal Processing*, 25 (1), pp. 1786-1802.
- Jianping, J. and Guang, M., 2008. Investigation on the failure of the gear shaft connected to extruder. *Journal of Engineering Failure Analysis*, 15 (4), pp. 420–429.
- Kahraman, A., Kienzle, K., Kubur, M. and Zini, D.M., 2004. Dynamic analysis of a multi- shaft helical gear transmission by finite elements: Model and experiment. *Journal of Vibration and Acoustics*, 126 (3), pp. 398–406.
- Kang, J.S. and Choi, Y., 2008. Optimization of helix angle for helical gear system. *Journal of Mechanical Science and Technology*, 22, pp. 2393-2402.
- Kapelevich, A., 2000. Geometry and Design of Involute Spur Gears with Asymmetric Teeth. *Journal of Mechanism and Machine Theory*, 35 (1), pp. 117-130.
- Kawalec, A., Wiktor, J. and Ceglarec, D., 2006. Comparative Analysis of Tooth-Root Strength using ISO and AGMA Standards in Spur and Helical Gears with FEM Based Verification. *Journal of Mechanical Design*, 128 (1).
- Kotcioglu, I., Cansiz, A. and Nasirikhajaji, M., 2012. Experimental investigation for optimization of design parameters in a rectangular duct with Plate Fins heat exchanger by Taguchi Method. *Journal of Applied Thermal Engineering, In Press, Accepted Manuscript*.
- Lewis, W., 1893. Investigation of the Strength of Gear Teeth. *Proceedings of Engineering Club*, Philadelphia, pp. 16-23.
- Li, S., 2007. Finite element analyses for contact strength and bending strength of a pair of spur gears with machining errors, assembly errors and tooth modifications. *Journal of Mechanism and Machine Theory*, 42, pp. 88–114.

- Li, S., 2008. Experimental investigation and FEM analysis of resonance frequency behaviour of three-dimensional, thin-walled spur gears with a power-circulating test rig. *Journal of Mechanism and Machine Theory*, 43 (1), pp. 934-936.
- Li, Q., Steven, G.P., Querin, O.M. and Xie, Y.M., 2001. Stress based optimization of torsional shafts using an evolutionary procedure. *Journal of Solids and Structures*, 38 (32-33), pp. 5661-5677.
- Lin, T., Ou, H. and Li, R., 2007. A finite element method for 3D static and dynamic contact/impact analysis of gear drives. *Journal of Computer Methods in Applied Mechanics and Engineering*, 196 (9-12), pp. 1716-1728.
- Lim, T.C. and Singh, R., 1991. Vibration Transmission Through Rolling Element Bearings. Part III: Geared Rotor System Studies. *Journal of Sound and Vibration*, 151 (1), pp. 31-54.
- Liu, C., Chen, Y. and Lin, S., 2010. Contact Stress Analysis of Straight Concave Conical Involute Gear Pairs with Small Intersected Angles. *Proceedings of the International MultiConference of Engineers and Computer Scientists*, 3, pp. 1722-1727.
- Mao, K., 2007. Gear tooth contact analysis and its application in the reduction of fatigue wear. *Journal of Wear*, 262 (11), pp. 1281-1288.
- Mark, W.D., 1978. Analysis of the vibratory excitation of gear system: Basic theory. *Journal of Acoustical Society of America*, 63, pp. 1409-1430.
- Marks 4WD Adaptors, 2002, *Nissan Portal History/Components and Testing* [Online]. Available at: <http://www.marks4wd.com/images/products/gearmaster/Portals/PICT1158.JPG> [Accessed: 15 March 2011].
- Mutasher, S.A., 2009. Prediction of the torsional strength of the hybrid aluminum/composite drive shaft. *Journal of Materials and Design*, 30 (2), pp. 215-220.
- Ooi, J.B., Wang, X., Tan, C.S., Ho, J.H., and Lim, Y.P., 2012. Modal and stress analysis of gear train design in portal axle using finite element modeling and simulation. *Journal of Mechanical Science and Technology*, 26 (2), pp. 575-589.
- Otto, K.N. and Antonsson, E.K., 1991. Extensions to the Taguchi Method of Product Design. *Journal of Mechanical Design*, 115, pp. 5-13.
- Ozguven, H.N. and Houser, D.R., 1988. Mathematical models used in gear dynamics—a review. *Journal of Sound and Vibration*, 121 (3), pp. 383-411.

- Parey, A. and Tandon, N., 2003. Spur Gear Dynamic Models Including Defects - A Review. *The Shock and Vibration Digest*, 36 (6), pp. 465-478.
- Perret-Liaudet, J. and Sabot, J., 1994. Dynamics of Truck Gearbox. *Proceedings of the 6th International Power Transmission and Gearing Conference*, pp.249-258.
- Ross, P.J., 1996. *Taguchi Techniques for Quality Engineering: Loss Function, Orthogonal Experiments, Parameter and Tolerance Design*, 2nd ed., New York, NY: McGraw-Hill.
- Sackfield, A. and Hills, D.A., 1983. Some Useful Results in the Classical Hertz Contact Problem. *The Journal of Strain Analysis for Engineering Design*, 18 (2), pp. 101-105.
- Sanders, A.A., 2010. *An Experimental Investigation of the Influence of Elliptical Root Shapes and Asymmetric Teeth on Root Stresses and Bending Fatigue Lives*. Master Thesis, The Ohio State University, United States.
- Shigley, J.E. and Mitchell, L.D., 1983. *Mechanical Engineering Design*, 4th ed. New York: McGraw Hill.
- Shimamura, S. and Noguchi, Y., 1965. An Analytical Determination of Speed Factor in Gear Designs,. *Proceedings of the Second SESA International Congress on Experimental Mechanics*, Washington, D.C.
- Simon, V., 2000. FEM stress analysis in hypoid gears. *Journal of Mechanism and Machine Theory*, 35 (9), pp. 1197-1220.
- Stoker, K.C., 2009. *A finite element approach to spur gear response and wear under non ideal loading*. Master Thesis, University of Florida, United States.
- THC Gears Standards, 1998, *List of Gear Standards*, Beijing THC Limited [Online]. Available at: http://www.gearandrack.com/gear_information/gear_standards.html [Accessed 9 March 2011].
- The Unimog Centre.com, 2004, *Mercedes Benz Unimog Co.* [Online]. Available at: <http://unimogcentre.com/unimogprinc.html#portalaxle> [Accessed: 9 March 2011].
- Tom, B., 2007, *Comparison between normal and portal axles* [Online]. Available at: <http://en.wikipedia.org/wiki/File:NormalVsPortalAxle.svg> [Accessed: 15 March 2011].
- Townsend, D.P. and Coy, J.J., 1985. *Gearing*, NASA Reference Publication: AVSCOM Technical Report 84-C-15.

- Velex, P. and Maatar, M., 1996. A Mathematical Model for Analyzing the Influence of Shape Deviations and Mounting Errors on Gear Dynamic Behaviour. *Journal of Sound and Vibration*, 191 (5), pp. 629-660.
- Vijayarangan, S. and Ganesan, N., 1993. A Study of Dynamic Stresses in a Spur Gear Under a Moving Line Load and Impact Load Conditions by a Three-dimensional Finite Element Method. *Journal of Sound and Vibration*, 162 (1), pp. 185-189.
- Wang, J. and Howard, I., 2005. Finite Element Analysis of High Contact Ratio Spur Gears in Mesh. *Journal of Tribology*, vol. 127 (3), pp. 469-483.
- Wei, Z., 2004. *Stresses and Deformations in Involute Spur Gears by Finite Element Method*. Master Thesis, University of Saskatchewan, Canada.
- Xiaolei, X., Zhiwei, Y. and Hongxin, D., 2011. Failure analysis of a diesel engine gear-shaft. *Journal of Engineering Failure Analysis*, 13 (8), pp. 672-678.
- Xu, R., 2008. *Finite element modelling and simulation on the quenching effect for spur gear design optimization*. Master Thesis, University of Akron, Canada.

APPENDIX A

DATA INPUT IN THE ANSYS SOFTWARE OF THE GEAR TRAIN

MODEL



First Saved	Tuesday, April 10, 2011
Last Saved	Monday, August 20, 2011
Product Version	12.0.1 Release

Units

TABLE 1

Unit System	Metric (m, kg, N, s, V, A) Degrees RPM Celsius
Angle	Degrees
Rotational Velocity	RPM
Temperature	Celsius

Model (A4, B4, C4)

Geometry

TABLE 2
Model (A4, B4, C4) > Geometry

Object Name	<i>Geometry</i>
State	Fully Defined
Definition	
Source	C:\Users\user\Desktop\vibration analysis\design 1 (normal).stp
Type	Step
Length Unit	Meters
Element Control	Program Controlled
Display Style	Part Color
Bounding Box	
Length X	0.15202 m
Length Y	0.28122 m
Length Z	6.54e-002 m
Properties	
Volume	8.0204e-004 m ³
Mass	6.296 kg
Scale Factor Value	1.
Statistics	

Bodies	2
Active Bodies	2
Nodes	12102
Elements	6397
Mesh Metric	None
Preferences	
Import Solid Bodies	Yes
Import Surface Bodies	Yes
Import Line Bodies	No
Parameter Processing	Yes
Personal Parameter Key	DS
CAD Attribute Transfer	No
Named Selection Processing	No
Material Properties Transfer	No
CAD Associativity	Yes
Import Coordinate Systems	No
Reader Save Part File	No
Import Using Instances	Yes
Do Smart Update	No
Attach File Via Temp File	Yes
Temporary Directory	C:\Users\user\AppData\Local\Temp
Analysis Type	3-D
Mixed Import Resolution	None
Enclosure and Symmetry Processing	Yes

TABLE 3
Model (A4, B4, C4) > Geometry > Parts

Object Name	<i>Idler Gear</i>	<i>Spur Gear1</i>
State	Meshed	
Graphics Properties		
Visible	Yes	
Transparency	1	
Definition		
Suppressed	No	
Stiffness Behavior	Flexible	
Coordinate System	Default Coordinate System	
Reference Temperature	By Environment	
Material		
Assignment	Structural Steel	
Nonlinear Effects	Yes	
Thermal Strain Effects	Yes	
Bounding Box		
Length X	0.13596 m	0.15202 m
Length Y	0.13637 m	0.15239 m
Length Z	6.54e-002 m	
Properties		
Volume	3.6375e-004 m ³	4.3829e-004 m ³
Mass	2.8554 kg	3.4406 kg
Centroid X	6.6479e-003 m	-2.7172e-007 m
Centroid Y	-0.13684 m	1.732e-006 m
Centroid Z	1.2692e-002 m	1.2694e-002 m
Moment of Inertia Ip1	3.3496e-003 kg·m ²	4.8248e-003 kg·m ²

Moment of Inertia Ip2	3.3495e-003 kg·m ²	4.8247e-003 kg·m ²
Moment of Inertia Ip3	5.4758e-003 kg·m ²	8.3767e-003 kg·m ²
Statistics		
Nodes	5891	6211
Elements	3125	3272
Mesh Metric	None	

Coordinate Systems

TABLE 4
Model (A4, B4, C4) > Coordinate Systems > Coordinate System

Object Name	<i>Global Coordinate System</i>
State	Fully Defined
Definition	
Type	Cartesian
Ansys System Number	0.
Origin	
Origin X	0. m
Origin Y	0. m
Origin Z	0. m
Directional Vectors	
X Axis Data	[1. 0. 0.]
Y Axis Data	[0. 1. 0.]
Z Axis Data	[0. 0. 1.]

Connections

TABLE 5
Model (A4, B4, C4) > Connections

Object Name	<i>Connections</i>
State	Fully Defined
Auto Detection	
Generate Contact On Update	Yes
Tolerance Type	Slider
Tolerance Slider	0.
Tolerance Value	8.1575e-004 m
Face/Face	Yes
Face/Edge	No
Edge/Edge	No
Priority	Include All
Group By	Bodies
Search Across	Bodies
Revolute Joints	Yes
Fixed Joints	Yes
Transparency	
Enabled	Yes

TABLE 6
Model (A4, B4, C4) > Connections > Contact Regions

Object Name	<i>Contact Region</i>
State	Fully Defined
Scope	
Scoping Method	Geometry Selection

Contact	2 Faces
Target	2 Faces
Contact Bodies	Idler Gear
Target Bodies	Spur Gear1
Definition	
Type	Bonded
Scope Mode	Automatic
Behavior	Symmetric
Suppressed	No
Advanced	
Formulation	Pure Penalty
Normal Stiffness	Program Controlled
Update Stiffness	Never
Pinball Region	Program Controlled

Mesh

TABLE 7
Model (A4, B4, C4) > Mesh

Object Name	<i>Mesh</i>
State	Solved
Defaults	
Physics Preference	Mechanical
Relevance	0
Sizing	
Use Advanced Size Function	Off
Relevance Center	Coarse
Element Size	Default
Initial Size Seed	Active Assembly
Smoothing	Medium
Transition	Fast
Span Angle Center	Coarse
Minimum Edge Length	3.0475e-003 m
Inflation	
Use Automatic Tet Inflation	None
Inflation Option	Smooth Transition
Transition Ratio	0.272
Maximum Layers	5
Growth Rate	1.2
Inflation Algorithm	Pre
View Advanced Options	No
Advanced	
Shape Checking	Standard Mechanical
Element Midside Nodes	Program Controlled
Straight Sided Elements	No
Number of Retries	Default (4)
Rigid Body Behavior	Dimensionally Reduced
Mesh Morphing	Disabled
Pinch	
Pinch Tolerance	Please Define
Generate on Refresh	No
Statistics	
Nodes	12102

Elements	6397
Mesh Metric	None

Static Structural (C5)

TABLE 34
Model (A4, B4, C4) > Analysis

Object Name	<i>Static Structural (C5)</i>
State	Solved
Definition	
Physics Type	Structural
Analysis Type	Static Structural
Solver Target	ANSYS Mechanical
Options	
Environment Temperature	22. °C
Generate Input Only	No

TABLE 35
Model (A4, B4, C4) > Static Structural (C5) > Analysis Settings

Object Name	<i>Analysis Settings</i>
State	Fully Defined
Step Controls	
Number Of Steps	1.
Current Step Number	1.
Step End Time	1. s
Auto Time Stepping	Program Controlled
Solver Controls	
Solver Type	Program Controlled
Weak Springs	Program Controlled
Large Deflection	Off
Inertia Relief	Off
Nonlinear Controls	
Force Convergence	Program Controlled
Moment Convergence	Program Controlled
Displacement Convergence	Program Controlled
Rotation Convergence	Program Controlled
Line Search	Program Controlled
Output Controls	
Calculate Stress	Yes
Calculate Strain	Yes
Calculate Results At	All Time Points
Analysis Data Management	
Solver Files Directory	C:\Users\user\Desktop\Master Work\Paper 1\ANSYS vibration\Design 1_files\dp0\SYS-8\MECH\
Future Analysis	None
Scratch Solver Files Directory	
Save ANSYS db	No
Delete Unneeded Files	Yes
Nonlinear Solution	No
Solver Units	Active System

Solver Unit System	mks
--------------------	-----

TABLE 36
Model (A4, B4, C4) > Static Structural (C5) > Loads

Object Name	<i>Cylindrical Support</i>	<i>Moment</i>
State	Fully Defined	
Scope		
Scoping Method	Geometry Selection	
Geometry	1 Face	
Definition		
Type	Cylindrical Support	Moment
Radial	Fixed	
Axial	Fixed	
Tangential	Fixed	
Suppressed	No	
Define By		Vector
Magnitude		100. N·m (ramped)
Direction		Defined
Behavior		Deformable
Advanced		
Pinball Region		All

Solution (C6)

TABLE 37
Model (A4, B4, C4) > Static Structural (C5) > Solution

Object Name	<i>Solution (C6)</i>
State	Solved
Adaptive Mesh Refinement	
Max Refinement Loops	1.
Refinement Depth	2.

TABLE 38
Model (A4, B4, C4) > Static Structural (C5) > Solution (C6) > Solution Information

Object Name	<i>Solution Information</i>
State	Solved
Solution Information	
Solution Output	Solver Output
Newton-Raphson Residuals	0
Update Interval	2.5 s
Display Points	All

TABLE 39
Model (A4, B4, C4) > Static Structural (C5) > Solution (C6) > Results

Object Name	<i>Equivalent Stress</i>
State	Solved
Scope	
Scoping Method	Geometry Selection
Geometry	All Bodies
Definition	
Type	Equivalent (von-Mises) Stress
By	Time

Display Time	Last
Calculate Time History	Yes
Use Average	Yes
Identifier	
Results	
Minimum	1308.1 Pa
Maximum	1.1274e+008 Pa
Minimum Occurs On	Idler Gear
Maximum Occurs On	Spur Gear1
Information	
Time	1. s
Load Step	1
Substep	1
Iteration Number	1

Harmonic Response (A5)

TABLE 8
Model (A4, B4, C4) > Analysis

Object Name	<i>Harmonic Response (A5)</i>
State	Solved
Definition	
Physics Type	Structural
Analysis Type	Harmonic Response
Solver Target	ANSYS Mechanical
Options	
Environment Temperature	22. °C
Generate Input Only	No

TABLE 9
Model (A4, B4, C4) > Harmonic Response (A5) > Analysis Settings

Object Name	<i>Analysis Settings</i>
State	Fully Defined
Options	
Range Minimum	0. Hz
Range Maximum	10000 Hz
Solution Intervals	100
Solution Method	Mode Superposition
Cluster Results	No
Modal Frequency Range	Program Controlled
Store Results At All Frequencies	Yes
Output Controls	
Calculate Stress	Yes
Calculate Strain	Yes
Damping Controls	
Constant Damping Ratio	1.e-002
Beta Damping Define By	Direct Input
Beta Damping Value	0.
Analysis Data Management	
Solver Files Directory	C:\Users\user\Desktop\Master Work\Paper 1\ANSYS vibration\Design 1_files\dp0\SYS\MECH\

Future Analysis	None
Scratch Solver Files Directory	
Save ANSYS db	No
Delete Unneeded Files	Yes
Solver Units	Active System
Solver Unit System	mks

TABLE 10
Model (A4, B4, C4) > Harmonic Response (A5) > Loads

Object Name	<i>Fixed Support</i>	<i>Moment</i>
State	Fully Defined	
Scope		
Scoping Method	Geometry Selection	
Geometry	1 Face	
Definition		
Type	Fixed Support	Moment
Suppressed	No	
Define By		Vector
Magnitude		100. N·m
Direction		Defined
Behavior		Deformable
Advanced		
Pinball Region		All

Solution (A6)

TABLE 11
Model (A4, B4, C4) > Harmonic Response (A5) > Solution

Object Name	<i>Solution (A6)</i>
State	Solved
Adaptive Mesh Refinement	
Max Refinement Loops	1.
Refinement Depth	2.

TABLE 12
Model (A4, B4, C4) > Harmonic Response (A5) > Solution (A6) > Solution Information

Object Name	<i>Solution Information</i>
State	Solved
Solution Information	
Solution Output	Solver Output
Newton-Raphson Residuals	0
Update Interval	2.5 s
Display Points	All

TABLE 13
Model (A4, B4, C4) > Harmonic Response (A5) > Solution (A6) > Result Charts

Object Name	<i>Frequency Response</i>	<i>Frequency Response 2</i>	<i>Frequency Response 3</i>	<i>Frequency Response 4</i>	<i>Frequency Response 5</i>
State	Solved				
Scope					

Geometry	2 Faces				
Spatial Resolution	Use Average				
Definition					
Type	Directional Deformation			Normal Stress	
Orientation	X Axis	Y Axis	Z Axis	X Axis	Y Axis
Options					
Frequency Range	Use Parent				
Minimum Frequency	0. Hz				
Maximum Frequency	10000 Hz				
Display	Amplitude				
Results					
Maximum Amplitude	3.5007e-005 m	8.4401e-006 m	1.1969e-006 m	3.8498e+007 Pa	8.7188e+007 Pa
Frequency	3700. Hz		300. Hz	3700. Hz	
Phase Angle	98.737 °	101.14 °	-4.9318 °	99.038 °	98.601 °
Real	-5.3176e-006 m	-1.6302e-006 m	1.1925e-006 m	-6.0477e+006 Pa	-1.304e+007 Pa
Imaginary	3.46e-005 m	8.2812e-006 m	-1.029e-007 m	3.802e+007 Pa	8.6207e+007 Pa

TABLE 14
Model (A4, B4, C4) > Harmonic Response (A5) > Solution (A6) > Result Charts

Object Name	<i>Frequency Response 6</i>
State	Solved
Scope	
Geometry	2 Faces
Spatial Resolution	Use Average
Definition	
Type	Normal Stress
Orientation	Z Axis
Options	
Frequency Range	Use Parent
Minimum Frequency	0. Hz
Maximum Frequency	10000 Hz
Display	Amplitude
Results	
Maximum Amplitude	1.5283e+007 Pa
Frequency	2700. Hz
Phase Angle	33.258 °
Real	1.278e+007 Pa
Imaginary	8.3812e+006 Pa

FIGURE 7
Model (A4, B4, C4) > Harmonic Response (A5) > Solution (A6) > Frequency Response 6

Modal (B5)

TABLE 15
Model (A4, B4, C4) > Analysis

Object Name	<i>Modal (B5)</i>
State	Solved
Definition	
Physics Type	Structural
Analysis Type	Modal
Solver Target	ANSYS Mechanical
Options	
Environment Temperature	22. °C
Generate Input Only	No

TABLE 16
Model (A4, B4, C4) > Modal (B5) > Initial Condition

Object Name	<i>Pre-Stress (None)</i>
State	Fully Defined
Definition	
Pre-Stress Environment	None

TABLE 17
Model (A4, B4, C4) > Modal (B5) > Analysis Settings

Object Name	<i>Analysis Settings</i>
State	Fully Defined
Options	
Max Modes to Find	10
Limit Search to Range	No
Solver Controls	
Solver Type	Program Controlled
Output Controls	
Calculate Stress	No
Calculate Strain	No
Analysis Data Management	
Solver Files Directory	C:\Users\user\Desktop\Master Work\Paper 1\ANSYS vibration\Design 1_files\dp0\SYS-1\MECH\
Future Analysis	None
Scratch Solver Files Directory	
Save ANSYS db	No
Delete Unneeded Files	Yes
Solver Units	Active System
Solver Unit System	mks

TABLE 18
Model (A4, B4, C4) > Modal (B5) > Loads

Object Name	<i>Fixed Support</i>
State	Fully Defined
Scope	
Scoping Method	Geometry Selection
Geometry	2 Faces
Definition	
Type	Fixed Support
Suppressed	No

Solution (B6)

TABLE 19
Model (A4, B4, C4) > Modal (B5) > Solution

Object Name	<i>Solution (B6)</i>
State	Solved
Adaptive Mesh Refinement	
Max Refinement Loops	1.
Refinement Depth	2.

TABLE 20
Model (A4, B4, C4) > Modal (B5) > Solution (B6)

Mode	Frequency [Hz]
1.	6766.6
2.	6864.4
3.	7045.7
4.	7336.5
5.	8655.
6.	9234.2
7.	10038
8.	10374
9.	10427
10.	10604

TABLE 21
Model (A4, B4, C4) > Modal (B5) > Solution (B6) > Solution Information

Object Name	<i>Solution Information</i>
State	Solved
Solution Information	
Solution Output	Solver Output
Newton-Raphson Residuals	0
Update Interval	2.5 s
Display Points	All

TABLE 22
Model (A4, B4, C4) > Modal (B5) > Solution (B6) > Results

Object Name	<i>Total Deformation</i>	<i>Total Deformation</i> 2	<i>Total Deformation</i> 3	<i>Total Deformation</i> 4	<i>Total Deformation</i> 5
State	Solved				
Scope					
Scoping Method	Geometry Selection				
Geometry	All Bodies				
Definition					
Type	Total Deformation				
Mode	1.	2.	3.	4.	5.
Identifier					
Results					
Minimum	0. m				
Maximum	1.8422 m	2.5233 m	2.0916 m	1.9082 m	1.9628 m
Minimum Occurs On	Idler Gear				

Maximum Occurs On	Spur Gear1				
Information					
Reported Frequency	6766.6 Hz	6864.4 Hz	7045.7 Hz	7336.5 Hz	8655. Hz

TABLE 23
Model (A4, B4, C4) > Modal (B5) > Solution (B6) > Total Deformation

Mode	Frequency [Hz]
1.	6766.6
2.	6864.4
3.	7045.7
4.	7336.5
5.	8655.
6.	9234.2
7.	10038
8.	10374
9.	10427
10.	10604

TABLE 24
Model (A4, B4, C4) > Modal (B5) > Solution (B6) > Total Deformation 2

Mode	Frequency [Hz]
1.	6766.6
2.	6864.4
3.	7045.7
4.	7336.5
5.	8655.
6.	9234.2
7.	10038
8.	10374
9.	10427
10.	10604

TABLE 25
Model (A4, B4, C4) > Modal (B5) > Solution (B6) > Total Deformation 3

Mode	Frequency [Hz]
1.	6766.6
2.	6864.4
3.	7045.7
4.	7336.5
5.	8655.
6.	9234.2
7.	10038
8.	10374
9.	10427
10.	10604

TABLE 26
Model (A4, B4, C4) > Modal (B5) > Solution (B6) > Total Deformation 4

Mode	Frequency [Hz]
1.	6766.6
2.	6864.4

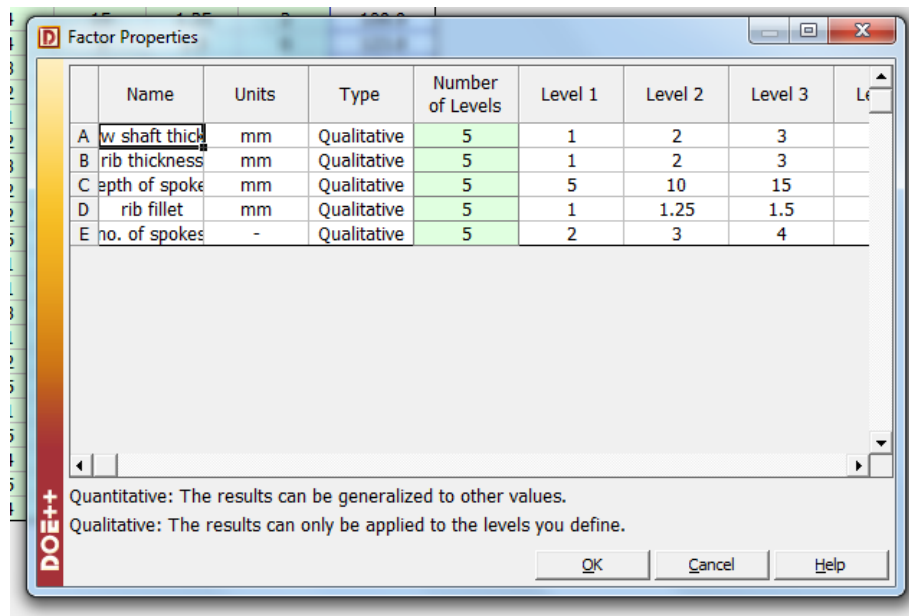
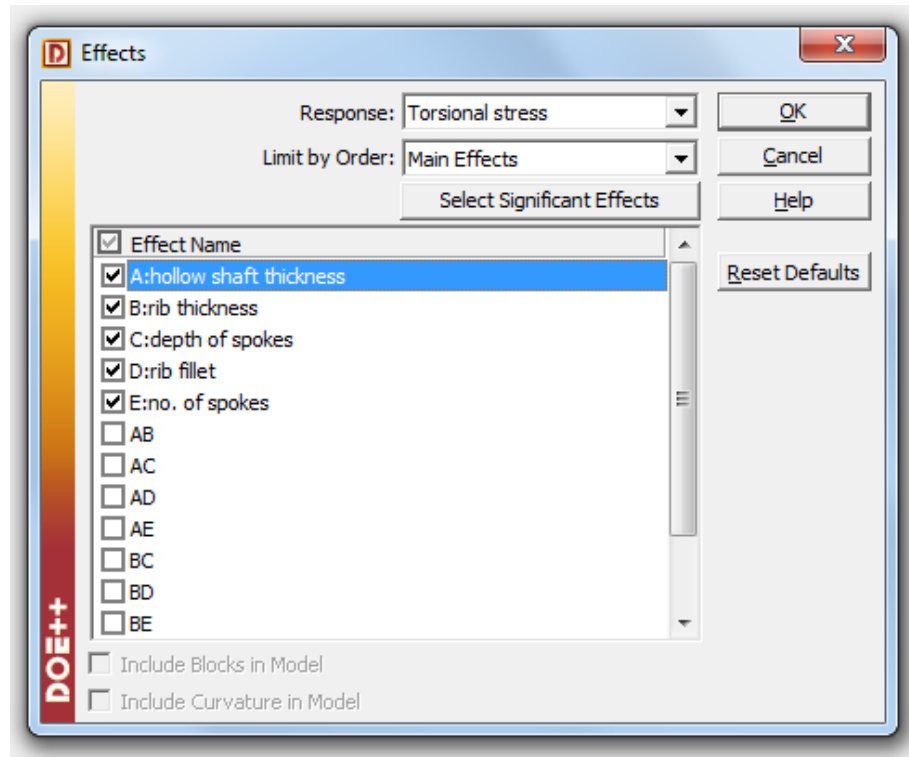
3.	7045.7
4.	7336.5
5.	8655.
6.	9234.2
7.	10038
8.	10374
9.	10427
10.	10604

TABLE 27
Model (A4, B4, C4) > Modal (B5) > Solution (B6) > Total Deformation 5

Mode	Frequency [Hz]
1.	6766.6
2.	6864.4
3.	7045.7
4.	7336.5
5.	8655.
6.	9234.2
7.	10038
8.	10374
9.	10427
10.	10604

APPENDIX B

DATA INPUT OF THE L25 TAGUCHI ORTHOGONAL ARRAY IN THE DOE++ PROGRAM



ReliaSoft DOE++ - [Folio: Folio1 (Design)]

File Edit View Project Sheet Data Tools Window Help

optimization shaft

- Standard Folios
 - Folio1
 - Additional Plots
 - Other Tools
 - Spreadsheets
 - Attachments

	A1	23								
	Standard Order	Run Order	Block	A:hollow shaft thickness	B:rib thickness (mm)	C:depth of spokes (mm)	D:rib fillet (mm)	E:no. of spokes (-)	Torsional stress (MPa)	
1	23	1	1	5	3	10	1	6	119.1	
2	13	2	1	3	3	25	1.25	5	215.5	
3	19	3	1	4	4	10	2	4	88.56	
4	5	4	1	1	5	25	2	6	263.6	
5	24	5	1	5	4	15	1.25	2	109.9	
6	14	6	1	3	4	5	1.5	6	123.8	
7	3	7	1	1	3	15	1.5	4	270.4	
8	2	8	1	1	2	10	1.25	3	293.1	
9	1	9	1	1	1	5	1	2	226.8	
10	22	10	1	5	2	5	2	5	121.2	
11	8	11	1	2	3	20	2	2	206.7	
12	17	12	1	4	2	25	1.5	2	135.3	
13	7	13	1	2	2	15	1.75	6	193.8	
14	25	14	1	5	5	20	1.5	3	92.24	
15	11	15	1	3	1	15	2	3	158.5	
16	16	16	1	4	1	20	1.25	6	186	
17	18	17	1	4	3	5	1.75	3	132.1	
18	21	18	1	5	1	25	1.75	4	129	
19	12	19	1	3	2	20	1	4	149.7	
20	10	20	1	2	5	5	1.25	4	194.8	
21	6	21	1	2	1	10	1.5	5	186.5	
22	15	22	1	3	5	10	1.75	2	147.3	
23	4	23	1	1	4	20	1.75	5	229.7	
24	20	24	1	4	5	15	1	5	126.9	
25	9	25	1	2	4	25	1	3	179.4	

ReliaSoft DOE++

File Edit View Project Sheet Data Tools Window Help

optimization shaft

- Standard Folios
 - Folio1
 - Additional Plots
 - Other Tools
 - Spreadsheets
 - Attachments

Folio: Folio1 (Analysis)

ANOVA Table						
Source of Variation	Degrees of Freedom	Sum of Squares [Sequential]	Mean Squares [Sequential]	F Ratio	P Value	
Model	20	7.56E+04	3780.4376	15.2389	0.0085	
A:hollow shaft thickness	4	6.27E+04	1.57E+04	63.2162	0.0007	
B:rib thickness	4	5307.9926	1326.9982	5.3491	0.0666	
C:depth of spokes	4	1657.4014	414.3504	1.6702	0.3157	
D:rib fillet	4	5325.5358	1331.384	5.3668	0.0663	
E:no. of spokes	4	587.819	146.9548	0.5924	0.6878	
Residual	4	992.3096	248.0774			
Lack of Fit	4	992.3096	248.0774			
Total	24	7.66E+04				

S = 15.7505
R-sq = 98.70%
R-sq(adj) = 92.23%

Regression Information						
Term	Coefficient	Standard Error	Low CI	High CI	T Value	P Value
Intercept	171.196	3.1501	164.4805	177.9115	54.3463	6.86E-07
A[1]	85.524	6.3002	72.093	98.955	13.5748	0.0002
A[2]	21.044	6.3002	7.613	34.475	3.3402	0.0288
A[3]	-12.236	6.3002	-25.667	1.195	-1.9422	0.1241
A[4]	-37.424	6.3002	-50.855	-23.993	-5.9401	0.004
B[1]	6.164	6.3002	-7.267	19.595	0.9784	0.3833
B[2]	7.424	6.3002	-6.007	20.855	1.1784	0.304
B[3]	17.564	6.3002	4.133	30.995	2.7879	0.0494
B[4]	-24.924	6.3002	-38.355	-11.493	-3.9561	0.0167
C[1]	-11.456	6.3002	-24.887	1.975	-1.8184	0.1431
C[2]	-4.284	6.3002	-17.715	9.147	-0.68	0.5338
C[3]	0.794	6.3002	-12.727	14.135	0.1117	0.9164
C[4]	1.672	6.3002	-11.759	15.103	0.2654	0.8038
D[1]	-10.816	6.3002	-24.247	2.615	-1.7168	0.1612
D[2]	28.664	6.3002	15.733	42.095	4.5497	0.0104

Response: Torsional stress

Transformation: Y = Y

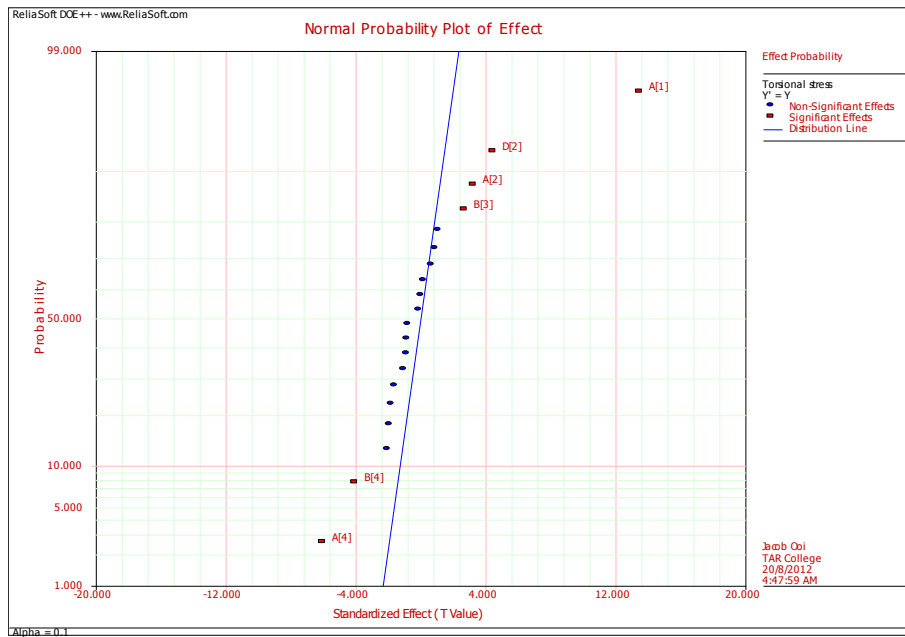
Risk Level (Alpha): 0.1

Analysis Settings: Calculated, Observations = 25

Analysis Summary: P()=...

Loaded folios: 1 | Active Folio "Folio1" | Project: C:\Users\user\Desktop\Master Work\Paper 2\optimization shaft.rso7

	Run Order	Standard Order	Actual Value (Y)	Fitted Value (YF)	Residual	Standardized Residual	Studentized Residual	External Studentized Residual	Leverage	Cook's Distance
1	1	23	119.1	122.816	-3.716	-0.2359	-0.5898	-0.5346	0.84	0.087
2	2	13	215.5	223.316	-7.816	-0.4962	-1.2406	-1.3698	0.84	0.3848
3	3	19	88.56	96.376	-7.816	-0.4962	-1.2406	-1.3698	0.84	0.3848
4	4	5	263.6	266.436	-2.836	-0.1801	-0.4501	-0.4001	0.84	0.0507
5	5	24	109.9	112.736	-2.836	-0.1801	-0.4501	-0.4001	0.84	0.0507
6	6	14	123.8	119.096	4.704	0.2987	0.7466	0.697	0.84	0.1394
7	7	3	270.4	260.736	9.664	0.6136	1.5339	2.0702	0.84	0.5882
8	8	2	293.1	288.396	4.704	0.2987	0.7466	0.697	0.84	0.1394
9	9	1	226.8	234.616	-7.816	-0.4962	-1.2406	-1.3698	0.84	0.3848
10	10	22	121.2	111.536	9.664	0.6136	1.5339	2.0702	0.84	0.5882
11	11	8	206.7	201.996	4.704	0.2987	0.7466	0.697	0.84	0.1394
12	12	17	135.3	139.016	-3.716	-0.2359	-0.5898	-0.5346	0.84	0.087
13	13	7	193.8	201.616	-7.816	-0.4962	-1.2406	-1.3698	0.84	0.3848
14	14	25	92.24	100.056	-7.816	-0.4962	-1.2406	-1.3698	0.84	0.3848
15	15	11	158.5	162.216	-3.716	-0.2359	-0.5898	-0.5346	0.84	0.087
16	16	16	186	176.336	9.664	0.6136	1.5339	2.0702	0.84	0.5882
17	17	18	132.1	134.936	-2.836	-0.1801	-0.4501	-0.4001	0.84	0.0507
18	18	21	129	124.296	4.704	0.2987	0.7466	0.697	0.84	0.1394
19	19	12	149.7	152.536	-2.836	-0.1801	-0.4501	-0.4001	0.84	0.0507
20	20	10	194.8	198.516	-3.716	-0.2359	-0.5898	-0.5346	0.84	0.087
21	21	6	186.5	189.336	-2.836	-0.1801	-0.4501	-0.4001	0.84	0.0507
22	22	15	147.3	137.636	9.664	0.6136	1.5339	2.0702	0.84	0.5882
23	23	4	229.7	233.416	-3.716	-0.2359	-0.5898	-0.5346	0.84	0.087
24	24	20	126.9	122.196	4.704	0.2987	0.7466	0.697	0.84	0.1394
25	25	9	179.4	169.736	9.664	0.6136	1.5339	2.0702	0.84	0.5882



APPENDIX C

SAMPLE OF ANALYTICAL GEAR STRESS CALCULATIONS

Lewis bending stress

$$W_t = 576 \text{ Nm}$$

$$p_d = \frac{1}{m_t} = \frac{1}{0.4233 \text{ mm}}$$

$$b_w = 25.4 \text{ mm}$$

$$Y = 0.35$$

$$\sigma_t = \frac{W_t p_d}{b_w Y} = \frac{576}{(25.4)(0.35)(0.4233)(10^{-6})} = 153.06 \text{ MPa}$$

AGMA bending stress

All AGMA coefficients are assumed to be 1.0. Hence,

$$W_t = 576 \text{ Nm}$$

$$Y_j = 0.37$$

$$m_t = 0.4233 \text{ mm}$$

$$\begin{aligned} \sigma_t &= W_t K_o K_v K_s \frac{K_H K_B}{b_w m_t Y_j} = (576)(1)(1)(1) \frac{(1)(1)}{(25.4)(0.4233)(0.37)(10^{-6})} \\ &= 144.79 \text{ MPa} \end{aligned}$$

Hertz contact stress

$$W = 576 \text{ Nm}$$

$$b_w = 25.4 \text{ mm}$$

$$r_{b1} = 72 \text{ mm}$$

$$r_{b2} = 63.5 \text{ mm}$$

$$E_1 = E_2 = 210 \text{ GPa}$$

$$\nu_1 = \nu_2 = 0.3$$

$$\phi = 20^\circ$$

$$\begin{aligned} \sigma_c &= \sqrt{\frac{W(1 + r_{b1}/r_{b2})}{r_{b1}b_w\pi[(1 - \nu_1^2)/E_1 + (1 - \nu_2^2)/E_2] \sin \phi}} \\ &= \sqrt{\frac{576(1 + 72/63.5)}{(72)(25.4)(\times 10^{-6})\pi[(1 - 0.3^2)/210 \times 10^9 + (1 - 0.3^2)/210 \times 10^9] \sin 20^\circ}} \\ &= 268.65 \text{ MPa} \end{aligned}$$

AGMA contact stress

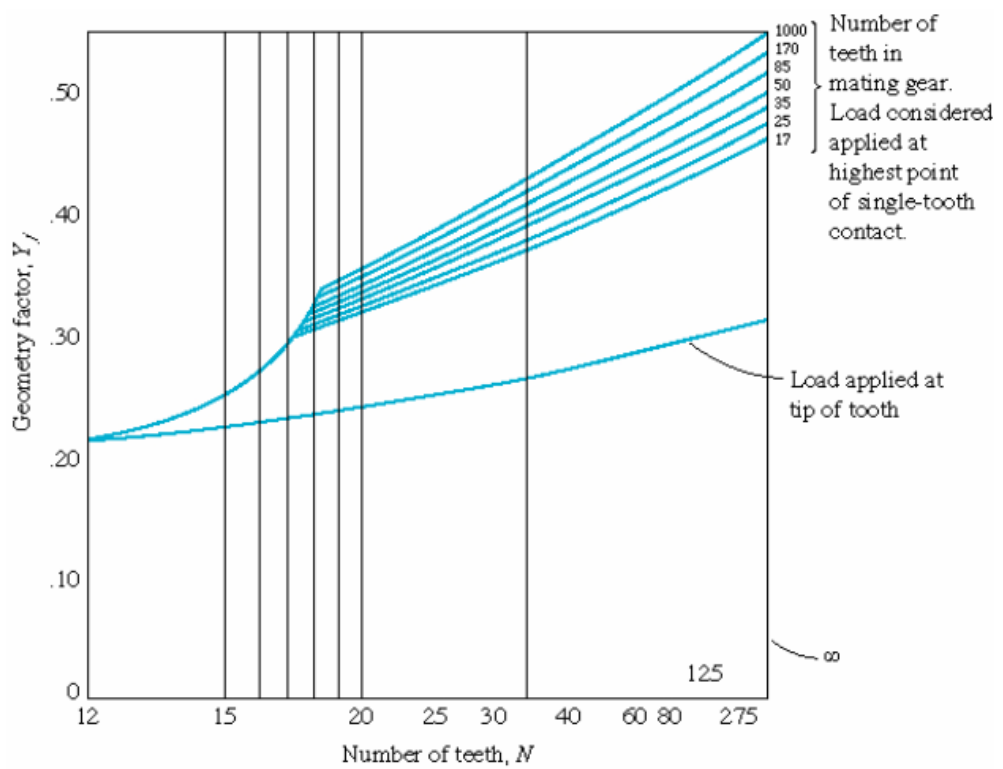
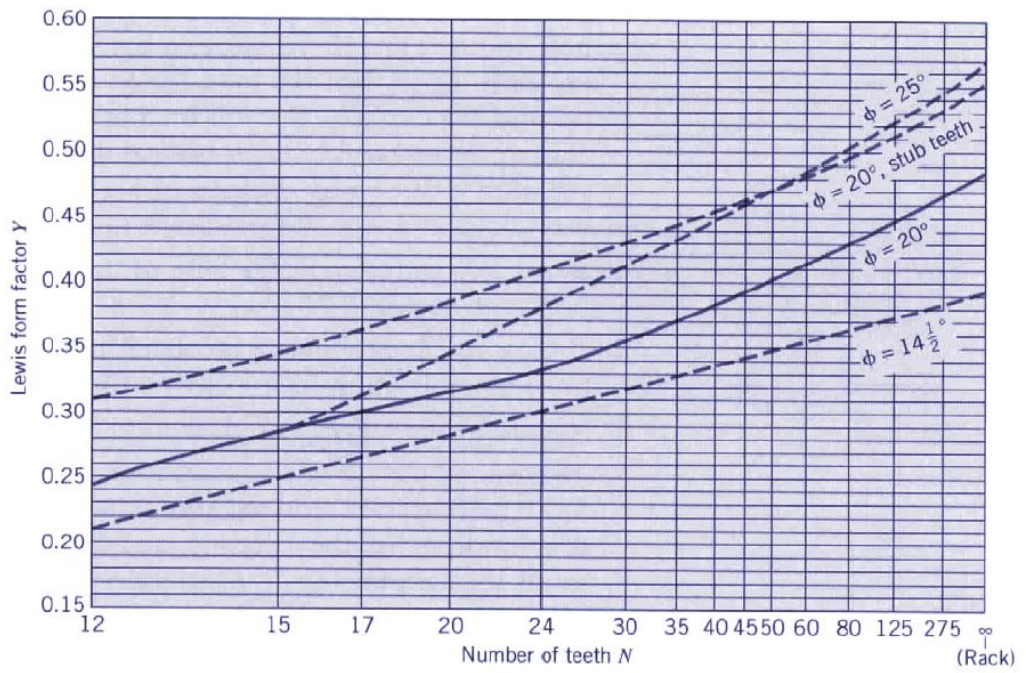
All AGMA coefficients are assumed to be 1.0. Hence,

$$Y_j = 0.37$$

$$d_p = 131.75 \text{ mm}$$

$$\begin{aligned} C_p &= \sqrt{\frac{1}{\pi \left(\frac{1 - \nu_1^2}{E_1} + \frac{1 - \nu_2^2}{E_2} \right)}} = \sqrt{\frac{1}{\pi \left(\frac{1 - 0.3^2}{210 \times 10^9} + \frac{1 - 0.3^2}{210 \times 10^9} \right)}} \\ &= 191645.6725 \end{aligned}$$

$$\begin{aligned} \sigma_c &= C_p \sqrt{W_t K_o K_v K_s \frac{K_m C_f}{d_p b_w Y_j}} \\ &= 191645.6725 \sqrt{(576)(1)(1)(1) \frac{(1)(1)}{(131.75)(25.4)(\times 10^{-6})(0.37)}} \\ &= 130.71 \text{ MPa} \end{aligned}$$



APPENDIX D

SAMPLE OF ANALYTICAL SHAFT TORSIONAL STRESS

CALCULATIONS

$$T = 100 \text{ Nm}$$

$$D = 37 \text{ mm}$$

$$d = 31 \text{ mm}$$

Since only torque is applied, there is no transverse load in the x and y direction.

So, the bending moment M is zero. Hence,

$$\sigma_x = \frac{32MD}{\pi(D^4 - d^4)} = 0$$

$$\sigma_y = 0$$

$$\tau_{xy} = \frac{16TD}{\pi(D^4 - d^4)} = \frac{16(100)(0.037)}{\pi(0.037^4 - 0.031^4)} = 19.82 \text{ MPa}$$

$$\sigma_{1,2} = \frac{\sigma_x + \sigma_y}{2} \pm \sqrt{\left(\frac{\sigma_x + \sigma_y}{2}\right)^2 + \tau_{xy}^2} = \pm \tau_{xy} = \pm 19.82 \text{ MPa}$$

$$\sigma_e = (\sigma_1^2 - \sigma_1\sigma_2 + \sigma_2^2)^{\frac{1}{2}} = 34.33 \text{ MPa}$$

APPENDIX E

LIST OF PUBLICATIONS

- International Journals
 - J. B. Ooi, X. Wang, C.S. Tan, J. H. Ho, K. C. Wong and Y. P. Lim, “Parametric optimization of the output shaft of the portal axle using finite element analysis,” *Journal of Mechanical Engineering Science*. [Journal Impact factor: 0.473. Submitted 11 August 2012]
 - J. B. Ooi, X. Wang, C.S. Tan, J. H. Ho, and Y. P. Lim, “Modal and stress analysis of gear train design in portal axle using finite element modeling and simulation,” *Journal of Mechanical Science and Technology*, vol. 26, no. 2, pp. 575–589, 2012. [Journal Impact factor: 0.448]
 - H. C. Qua, C. C. Khaw, C. S. Tan, X. Wang, J. B. Ooi, "Fast identification of O₂ corrosion in economiser tubes,” *Journal of Engineering Failure Analysis*, vol. 18, no.8, pp.2201-2210, Sept 2011. [Journal Impact factor: 1.086]

- Y.P. Lim, J.B. Ooi, and X. Wang, “Microstructural and mechanical properties of gravity-die-cast A356 alloy inoculated with yttrium and Al-Ti-B grain refiner simultaneously,” *Archives of Foundry Engineering*, vol. 11, pp. 77-82, 2011.

- International Conferences

- J. B. Ooi, X. Wang and Y. P. Lim, “Design optimization of the hollow output shaft used in portal axle unit using finite element method,” *50th Annual Conference of the British Institute for Non-Destructive Testing*, 2011.

- X. Wang, K. W. Ng, J. B. Ooi, Y. P. Lim, J. H. Ho, C. S. Tan and N. Q. Guo, “Finite element simulation of thermography non-destructive testing for gear inspection,” *49th Annual Conference of the British Institute for Non-Destructive Testing*, 2010.

- B. S. Wong, Y. G. Low, X. Wang, J. H. Ho, C. S. Tan and J. B. Ooi, 2010. “3D Finite element simulation of magnetic particle inspection,” *IEEE Conference on Sustainable Utilization and Development in Engineering and Technology*, pp. 50-55, 2010.

Modal and stress analysis of gear train design in portal axle using finite element modeling and simulation[†]

JongBoon Ooi¹, Xin Wang^{1,*}, ChingSeong Tan², Jee-Hou Ho³ and Ying Pio Lim¹

¹Faculty of Engineering & Science, Universiti Tunku Abdul Rahman, 53300 Kuala Lumpur, Malaysia

²Faculty of Engineering, Multimedia University, Jalan Multimedia, 63100, Cyberjaya, Selangor, Malaysia

³Faculty of Engineering, University of Nottingham Malaysia Campus, 43500 Semenyih, Malaysia

(Manuscript Received May 26, 2011; Revised September 2, 2011; Accepted October 24, 2011)

Abstract

The portal axle is a gearbox that is specially designed for off-road driving conditions. It is installed between the wheel and the axle shaft to give higher ground clearance to the vehicle. The modeling and simulation of spur gears in portal axle is important to predict the actual motion behavior. However, gear train design in portal axle is difficult to study comprehensively due to their relatively low cost and short product life cycle. In this study, modal analysis of portal axle is simulated using finite element method (FEM). Modal analysis is simulated on three different combinations of gear train system commonly designed for portal axle. The three gear trains being analyzed are gear train without idler gear, one idler gear and two idler gears. FEM static stress analysis is also simulated on three different gear trains to study the gear teeth bending stress and contact stress behavior of the gear trains in different angular positions from 0° to 18°. The single and double pair gear teeth contact are also considered. This methodology serves as a novel approach for gear train design evaluation, and the study of gear stress behavior in gear train which is needed in the small workshop scale industries.

Keywords: Portal axle, Spur gears, Stress analysis, Modal analysis, Angular position, Gear train

1. Introduction

The portal axle is a gearbox unit with at least two gears (input and output gear) combined to give greater off-set between the input gear and output gear. Portal axles are commonly installed on four wheel-drive (4WD) vehicles for driving on off-road conditions and to gain additional ground clearance to protect underneath components from damage. Fig. 1 shows the comparison between a normal vehicle and a vehicle with a portal axle.

The modeling and simulation of such all-terrain vehicles are important to predict the actual motion behavior [1]. When designing gears for portal axle, consideration of the gear train dynamic response is critical. Modal response is a dynamic response from the portal axle in the form of periodic or quasi-periodic excitations such as in noise analysis, and structural response to vibration. Modal analysis can predict the resonance of the structure excited by the dynamic input. In this situation, the structural stress level may become very high and generate structural deficiencies [2]. Sinisca [3] investigated the model of double-stage helical gear reduction using finite

[†] This paper was recommended for publication in revised form by Associate Editor Heung Soo Kim

*Corresponding author. Tel.: +60341079802, Fax.: +60341079803

E-mail address: wangx@utar.edu.my

© KSME & Springer 2012

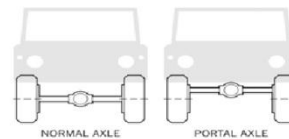


Fig. 1. Difference between normal and portal axle unit.

element simulation. The author analyzed modal analysis of the model using free and forced response. The dimensional effects such as the shaft length, output shaft angle effect, and bearing stiffness effects were also considered in modal analysis and compared to the benchmark model.

In this paper, Sec. 2.0 outlines the modeling of the portal axle gears and the three different gear combinations in the interest of FEM for analysis. The FEM modeling and simulation is computed using the Autodesk Inventor 2010 Student Edition. In Sec. 3.0, the mode shapes and critical natural frequencies of the three different gear trains are analyzed. In Sec. 3.1 to 3.3, the theory and formulation of the modal analysis using FEM is expressed clearly. Subsequently, Sec. 3.4 covers the technique applied in the mesh settings on the gear trains, and Sec. 3.5 covers the boundary conditions and assumptions made for modal analysis using FEM. In Sec. 3.6, the critical

natural frequencies or called the resonance frequencies are calculated on the different gear trains using FEM modeling and simulations. The first eight critical frequencies are then calculated and will be compared to the operating frequencies of the portal axle unit. Each gear train model represents different gear combinations of a portal axle to study the relationship between the numbers of idler gear and its natural frequencies. Modal analysis is performed on the gear trains under free stress and pre-stressed condition.

The analysis of gear stress in transmission application is very important and often requires the analysis of gear teeth bending stress and contact stress. FEM has often been applied in stress and strain analysis of a complicated structure including gears [4-6]. Meanwhile, the understanding of stress distribution between the interacting gear pairs would help in predicting the bending fatigue life of the gear. Kramberger et. al. [7] performed numerical studies to examine the bending fatigue life of thin-rim spur gears of truck gearboxes. FEM modeling and simulation have been considered a common practice in gear stress analysis subjected to static and dynamic loading conditions [8-12].

Wei [13] and Zu [14] have developed a two-dimensional and three-dimensional gear meshing model using FEM to study the effect of gear tooth bending stress and surface contact stress. The authors validated the FEM gear model and simulation by comparing the FEM stress with theoretical Lewis bending stress equation and Hertz contact stress equation. The behavior of gears in operation is important to understanding how stresses are being distributed from one meshing gear to another.

Chen and Tsay [15] conducted stress analysis on a helical gear set by studying the influences of the gear design parameters and the contact positions on the gear stress distribution. Hassan [16] studied the contact stress of spur gear in two-dimensional model based on different angular position. Abdullah [17] investigated the root stress of the gear used in powertrain transmission by FEM analysis. The root stress was analyzed based on the effect of mesh refinement, number of teeth reduction, and rim thickness reduction.

In Sec. 4.8 and 4.9, the gear tooth bending stress and gear tooth contact stress are calculated using FEM software to study the behavior of the gear train under different angular position. In Sec. 4.1 and 4.4, the Lewis theory and the Hertz theory are explained with their assumptions to be compared to the FEM gear train models, respectively. Similarly, Sec. 4.2 and 4.5 explain the details of the FEM setup for obtaining the gear bending stress and gear contact stress. Secs. 4.3 and 4.6 cover the validation of the gear train FEM models by comparing with the theoretical Lewis and Hertz stress results with increasing torque load.

In Sec. 4.7, both gear teeth bending stress and contact stress are analyzed on three different gear trains with varying angular position (0° to 18°). The analysis also includes single and double pair gear teeth contact. Positioning of each gear in a gear train to the desired position for FEM simulation requires

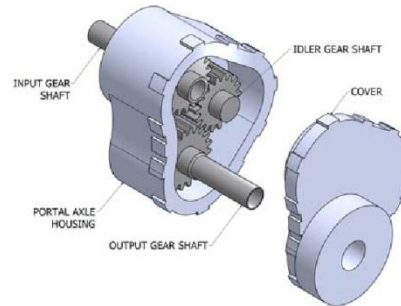


Fig. 2. Gear shafts assembly of the portal axle unit.

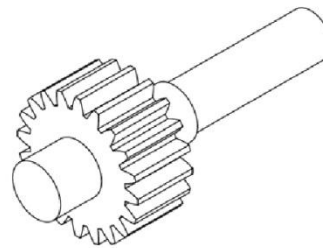


Fig. 3. Model of the gear input shaft and gear output shaft.

accurate contact settings, constraints and positioning technique. The critical stress calculated using FEM is recorded at the input gear shaft and output gear shaft and simulated for three different gear trains. The critical stress results at the gear root fillet and the gear teeth surface of the input and output gear shaft are recorded with gear angular position incremented every 2 interval from 0° to 18° . Finally, discussions and conclusions are pointed out from the analysis of this work.

2. Model of gear shaft and idler gear

Fig. 2 shows the assembly model of the three-gear system of the portal axle unit. In this analysis, the model of the input gear shaft, output gear shaft, and idler gear is only considered in FEM analysis to save computing time. This ignores the interaction of the housing fitting and the bearings fitting of the portal axle.

The output shaft and input shaft of the portal axle are modeled as the same gear shaft which shares the same design parameters. The gear shaft is modeled using the Autodesk Inventor 2010 Student Edition as shown in Fig. 3. The length of the shaft is 200 mm and the diameter is 30 mm. The idler gear, which is meshed between the input gear and output gear, is model with the same shaft diameter and having a shorter length of 100 mm. The idler gear is positioned between the input gear and output gear to offset the vertical distance and

Table 1. Gear shaft parameters and material properties.

Gear type	Standard involute, full depth teeth
Number of teeth (N)	20
Pitch diameter (d)	80 mm
Module (M)	4.00 mm
Diametral pitch (p_d)	250 mm^{-1}
Pressure angle (ϕ)	20°
Addendum (mm)	1.0 M
Dedendum (mm)	1.25 M
Face width (b_w)	40 mm
Tooth root fillet (r_f)	1 mm
Material	Structural steel
Modulus of elasticity (E)	200 GPa
Ultimate tensile strength (UTS)	460 MPa
Tensile yield strength (Y_s)	250 MPa
Poisson's ratio (ν)	0.3

allow only one directional rotation.

All gears (gear shaft and idler gear) are modeled following the same gear design parameters and material properties as shown in Table 1. The effects of gear case hardening, gear tempering and other gear heat treatment process are not considered in this study. Therefore, only the material of the gear is taken account into the analysis in FEM.

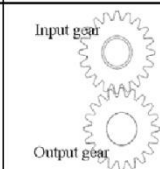
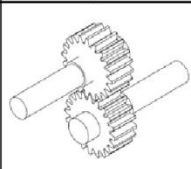
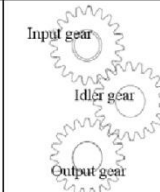
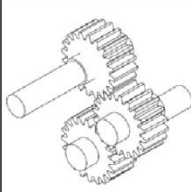
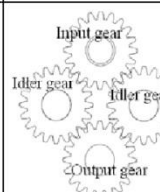
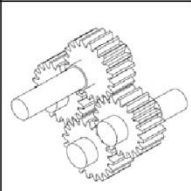
2.1 Model of the three different gear trains

There are three different gear train designs considered in the interest of this research, and three different gear trains are assembled as shown in Table 2 so that FEM simulation can be carried out separately. A gear train with no idler gear which is made up of two identical gear shafts is constrained to mesh with one and another. The gear shafts are set at center distance 80 mm and are aligned vertically with reference to both the gear shaft axis.

A gear train with one idler gear is built up of two gear shafts and one idler gear. The idler gear is the intermediate gear which connects between the two gear shafts. The center distance between the input gear and idler gear is 80 mm and the input gear is aligned to 45° from horizontal to mesh with the idler gear. Similarly, the center distance between the output gear and idler gear is 80 mm and the output gear is aligned $120\ 45^\circ$ from horizontal downwards. Fig. 4 illustrates the side view of the gear alignment of the gear train with one idler gear.

A gear train with two idler gears is arranged in the same position compared to the gear train with one idler gear but with one more idler gear attached on the other side between the input gear and output gear. All gear components in gear trains are constrained to rotate based on a gear ratio of 1:1 for FE analysis in the later sections.

Table 2. Gear train with different combinations (no idler gear, one idler gear and two idler gears).

Gear train	2-D view	Isotropic view
No idler gear		
One idler gear		
Two idler gears		

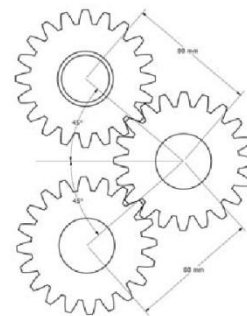


Fig. 4. Side view of the gear train with one idler gear.

3. Modal analysis of three different gear trains

Modal analysis, which means the study of the structure mode shape under excitation to its natural frequency, is important in the design stage. The modal analysis of the gear train with different combinations (no idler, one idler and two idler gears) was analyzed under free stress condition and pre-stress condition. Single pair tooth contact and double pair tooth contact between gears were also considered in the analysis.

3.1 Modal response

The mass M and stiffness K are the main properties that affect the overall modal response of a system. In general, the dynamic equilibrium is given by the differential matrix system:

$$[M]\ddot{\bar{u}} + [K]\bar{u} = \bar{f}(t) \quad (1)$$

where \bar{u} is the nodal displacement vector, $\ddot{\bar{u}}$ is the nodal acceleration vector, and $\bar{f}(t)$ the nodal applied force vector. For a homogeneous system, the solution of the second order linear differential equation is:

$$[M]\ddot{\bar{u}} + [K]\bar{u} = 0. \quad (2)$$

The matrix $[K]$ is not singular if the boundary conditions are considered. Thus the non-zero solutions exist if and only if:

$$\det[-M\omega^2 + K] = 0. \quad (3)$$

The roots in Eq. (3) are the eigenvalues of the matrix system. The number is generally equal to the number n of equations unless multiple roots are present, which happens when the structure has much symmetry. The roots are noted φ_j , $j = 1$, and the corresponding frequencies are $f_j = \Omega_j/2\pi$. A function solution is associated with each φ_j noted $\bar{\varphi}_j$, φ_j which the resonance mode, is defined by:

$$[K]\bar{\varphi}_j = [M]\Omega_j^2\bar{\varphi}_j. \quad (4)$$

$\bar{\varphi}_j$ are the eigenvectors of Eq. (3). The following properties of eigenmodes are:

$$\bar{\varphi}_k^T [K] \bar{\varphi}_j = 0 \quad \bar{\varphi}_k^T [M] \bar{\varphi}_j = 0 \quad (5)$$

for $j \neq k$.

These two qualities define the orthogonality of the eigenmodes with respect to the matrices $[K]$ and/or $[M]$. The quantities $\bar{\varphi}_k^T [K] \bar{\varphi}_j = K_j$ and $\bar{\varphi}_k^T [M] \bar{\varphi}_j = \mu_j$ are, respectively, the j^{th} modal stiffness and modal mass.

3.2 Harmonic excitation

If $f(t)$ is equal to $f_0 \sin \omega t$, $r(t)$ which is a linear combination of the $f(t)$ components has also the same form. The solution for harmonic excitation is given as:

$$\bar{q}_j(t) = \frac{\bar{r}_j \sin \omega t}{\mu_j (-\omega^2 + \Omega_j^2)}. \quad (6)$$

$\bar{q}_j(t)$ is the displacement, Ω_j is the components of modal basis. When ω varies, its value closer to one φ_j , and the corresponding $\bar{q}_j(t)$ is increasingly predominant in the re-

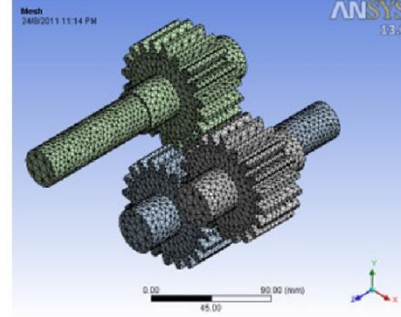


Fig. 5. Mesh model of the gear train with one idler gear for modal analysis.

sponse which is called the resonance phenomenon. Theoretically, when $\omega = \Omega_j$, $\bar{q}_j(t)$ is infinite. In practice, damping ensures finite values of $\bar{q}_j(t)$ but because the damping may be small the vibration level may remain high enough to cause a collapse of the structure. Theoretically, a continuous structure has an infinite number of resonances.

3.3 Mode shapes

The mode shapes of the gear in FEM were calculated independently of the excitation, which means that the structure is only mass and stiffness distribution dependent. According to Berlioz and Trompette [2], low resonance modes (first few modes) correspond to higher global modal response (higher amplitude of excitation) compared to higher resonance modes. The authors also verified that higher modes are more sensitive to structural modifications. Local modifications of the geometry generally have very limited impact on the strain energy distribution. Hence, structural changes may be inefficient if they do not correspond to a significant modification of the masses, as the resonance frequencies depend on ratio of K/M [2, 3].

3.4 Mesh settings of the gear train

In ANSYS Workbench, the three gear train designs are imported. In modal analysis using FEM, each gear train model was meshed with purely tetrahedron elements with average element size of 5 mm. Fig. 5 shows the mesh model of the gear train with one idler gear. The model consists of 18277 nodes and 9803 elements.

3.5 Boundary condition settings of gear train

ANSYS Workbench program was used to apply the motion constraints and contact conditions. There are two different conditions being analyzed in conducting modal analysis of the gear trains. The first six natural frequencies and their mode shapes were analyzed on the gear train without pre-stress state

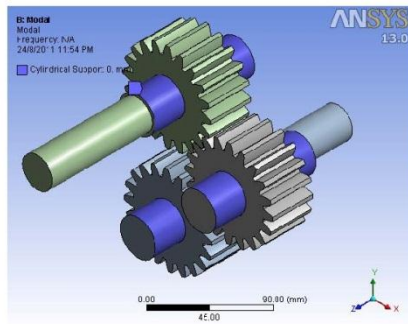


Fig. 6. Free stress state of the gear train with one idler gear.

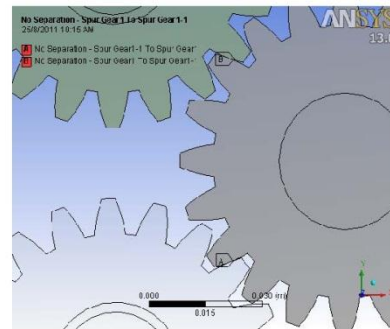


Fig. 8. Detailed side view of the single pair tooth contact between two gears.

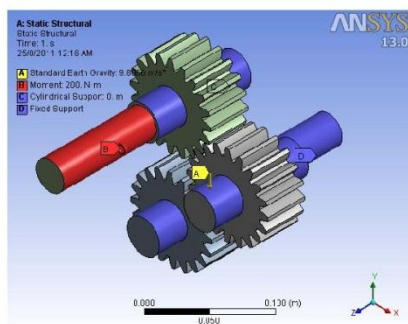


Fig. 7. Pre-stress state of the gear train with one idler gear.

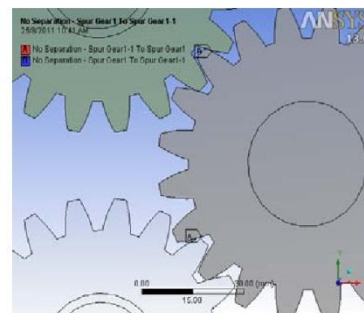


Fig. 9. Detailed side view of the double pair tooth contact between two gears.

involving constraints only and pre-stress state which is inclusive of loads and constraints. Fig. 6 shows the constraints applied for the gear train with one idler gear under free stress state.

In the free stress state, cylindrical supports were assumed as the bearing supports for the gear components, which allows rotational motion along the shaft axis but restricts axial motion and radial motion. Fig. 7 shows the gear train with one idler gear under pre-stress state. In the pre-stressed state of the gear train, the cylindrical supports are set the same as the one in the free stress state. The gravitational load due to the component's weight was applied and a torque load of 200 Nm was applied at the input gear shaft. The cylindrical surface of the output gear shaft was fully constrained to create static loading condition. In pre-stress state, the stress due to moment and gravity was calculated first before modal analysis was applied.

In modal analysis of the gear trains, a single pair tooth contact between gears and double pair tooth contact between gears were also analyzed. Fig. 8 illustrates in detail how the single pair tooth contact is set between the two meshing gears for the gear train with one idler gear.

Before importing the model to the ANSYS Workbench, the

gear tooth surface of two different gears was aligned to surface contact by using 'Tangential constraint' in Autodesk Inventor 2011 modeling program. To set the single pair tooth contact in FEM, the contact surface and target surface were defined and the contact type was set to 'No Separation' contact. In ANSYS Workbench, 'No Separation' contact is a linear contact in which the surface contact is a rigid surface and allows very small sliding in the tangential direction from the contact surface. Similarly, the gear train is rotated so that each gear has two teeth contact in with another gear. Later, the model is imported to ANSYS Workbench and the contact surfaces are defined. Fig. 9 shows the side view of the double pair tooth contact between gears.

3.6 Modal analysis of gear trains in free stress state

Fig. 10 shows the first six mode shapes of the gear train with one idler gear under free stress state and subjected to single pair tooth contact. The first mode shape and sixth mode shape of the gear train corresponded to twisting and radial expansion around the gear teeth. Bending vibrations occur at

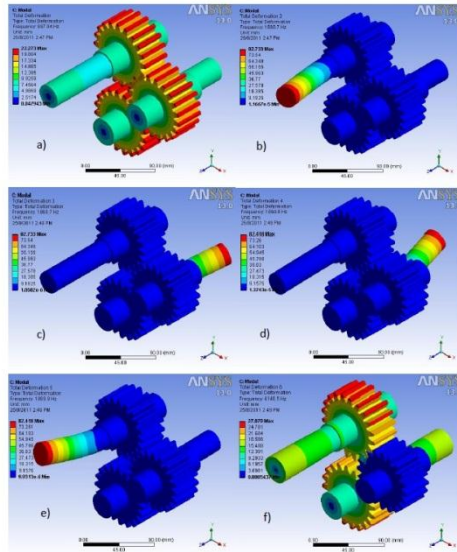


Fig. 10. First six mode shapes of the gear train with one idler gear in free stress state and subjected to double pair tooth contact.

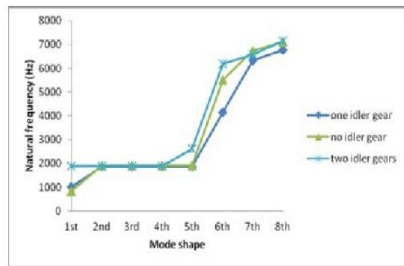


Fig. 11. First eight natural frequencies of the three different gear trains in free stress state subjected to single pair tooth contact.

the shaft of the input gear for the second and fourth mode shape, whereas the third and fifth mode shape show bending and twisting vibrations occurring at the shaft of the output gear.

Fig. 11 shows the first eight natural frequencies of the three different gear trains subjected to single pair tooth contact obtained from FE simulations. In comparison, the second to fourth mode shape of all three gear trains have very close or identical natural frequencies, but they are excited to different kinds of mode shapes such as bending and twisting vibrations. All three gear trains show quite similar natural frequency characteristics as presented from the graph, however, the mode shapes are not the same. The natural frequencies of the gear trains become higher starting at the sixth mode shape and

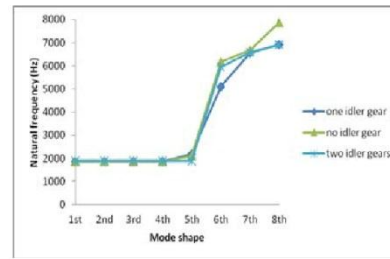


Fig. 12. First eight natural frequencies of the three different gear trains in free stress state subjected to double pair teeth contact.

so on.

Fig. 12 shows the first eight natural frequencies of the three different gear trains subjected to double pair tooth contact. The first to fifth mode shapes of the three gear trains are of similar natural frequencies but correspond to different mode shapes. This shows that there are possibilities of more than one mode shape occurring for the same natural frequencies. For the first to fifth of mode shapes occurred a close natural frequency of 1800 Hz. All the gear trains also show similar natural frequencies behavior with respect to the number of modes.

Table 3 briefly describes the first eight critical mode shapes (highest amplitude of deformations) of the three gear trains in free stress state obtained from FEM. It is found that input gear is more vulnerable to vibrational deformations in all types of gear trains. This is followed by output gear and idler gear. Shaft bending, gear rotation and radial expansion are vibrational deformations that frequently occur in gear trains.

3.7 Modal analysis of gear trains in pre-stressed state

Fig. 13 shows the first six mode shapes of the gear train with one idler gear with each gear meshed with another gear in a double pair tooth contact. The wireframe indicates the undeformed model of the gear train. From the first six mode shapes, the shaft of the input gear is more prone to high deformations in gear radial expansion, shaft bending, slender at the shaft and gear twisting.

Fig. 14 shows a comparison of the eight lowest natural frequencies of the three gear trains in pre-stressed state subjected to single pair tooth contact. The first to third mode shapes are excited by similar natural frequencies close to 1800 Hz. However, all gear train natural frequencies increase drastically with the following mode shape starting from the fourth mode shape.

Fig. 15 shows a comparison of the eight lowest natural frequencies of the three gear trains in pre-stressed state subjected to double pair tooth contact. The first and second mode shapes are excited by similar natural frequencies around 1900 Hz. The gear train natural frequencies increase drastically with the following mode shape starting from the third mode shape.

In dynamic analysis or vibrational analysis, the natural

Table 3. Mode shapes of the gear trains in free stress state.

Mode shape	Gear train with no idler		Gear train with one idler		Gear train with two idlers	
	Single pair tooth contact	Double pair tooth contact	Single pair tooth contact	Double pair tooth contact	Single pair tooth contact	Double pair tooth contact
1st	Gear rotation (input gear)	Shaft bending (input gear)	Gear rotation (output gear)	Shaft bending (input gear)	Shaft bending (output gear)	Shaft bending (output gear)
2nd	Shaft bending (input gear)	Shaft bending (input gear)	Shaft bending (input gear)	Shaft bending (output gear)	Shaft bending (input gear)	Shaft bending (input gear)
3rd	Shaft bending (input gear)	Shaft bending (input gear)	Shaft bending (input gear)	Shaft bending (input gear)	Shaft bending (output gear)	Shaft bending (output gear)
4th	Shaft bending (input gear)	Shaft bending (input gear)	Shaft bending (output gear)	Shaft bending (input gear)	Shaft bending (input gear)	Shaft bending (output gear)
5th	Shaft bending (input gear)	Gear rotation (input gear)	Shaft bending (input gear)	Gear rotation (output gear)	Gear rotation (idler gear)	Shaft bending (input gear)
6th	Shaft radial expansion (input gear)	Shaft radial expansion (input gear)	Gear rotation (input gear)	Gear rotation (output gear)	Shaft radial expansion (output gear)	Shaft radial expansion (output gear)
7th	Shaft radial expansion (input gear)	Shaft radial expansion (input gear)	Shaft radial expansion (output gear)	Shaft radial expansion (output gear)	Shaft radial expansion (input gear)	Shaft radial expansion (input gear)
8th	Shaft radial expansion (input gear)	Radial expansion and rotation (input gear)	Shaft radial expansion (output gear)	Shaft radial expansion (input gear)	Shaft radial expansion (output gear)	Shaft radial expansion (output gear)

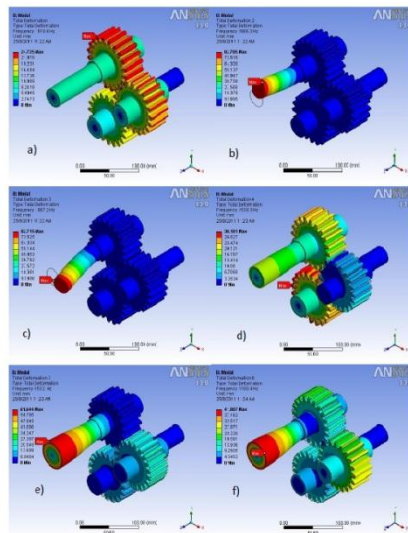


Fig. 13. First six mode shapes of the gear train with one idler gear under pre-stress state.

frequency of the gear train design cannot meet the operating frequency range of the portal axle unit or else resonance causing very high amplitude of excitation will occur. To study the resonance frequency behavior of the gear train, the range of operating frequencies of the portal axle unit is compared with the first eight natural frequencies calculated from FEM. The range of operating speed of the portal axle is obtained from the specification sheets provided by the manufacturer, which is between 500 rpm to 4000 rpm. Therefore, the range of operating frequencies of the portal axle unit calculated is be-

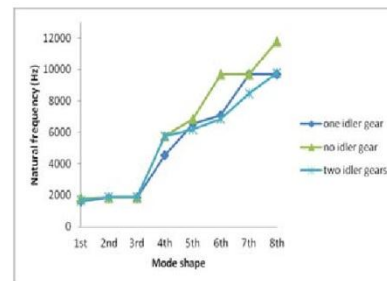


Fig. 14. First eight natural frequencies of the three different gear trains in pre-stressed state subjected to single pair tooth contact.

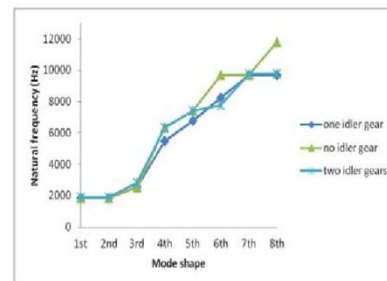


Fig. 15. First eight natural frequencies of the three different gear trains in pre-stressed state subjected to double pair teeth contact.

tween 8 Hz to 66 Hz. The range of operating frequency is very small that it is safe to operate since the lowest natural frequency of any three gear train design is as low as 2000 Hz. FEM predicts that resonance will not occur on any of the gear train designs and it is safe to operate.

Table 4. First eight vibrational mode shapes of gear trains in pre-stressed state.

Mode shape	Gear train with no idler		Gear train with one idler		Gear train with two idlers	
	Single pair tooth contact	Double pair tooth contact	Single pair tooth contact	Double pair tooth contact	Single pair tooth contact	Double pair tooth contact
1 st	Gear rotation (input gear)	Shaft bending (input gear)	Gear rotation (input gear)	Shaft bending (input gear)	Gear rotation (input gear)	Shaft bending (input gear)
2 nd	Shaft bending (input gear)	Shaft bending (input gear)	Shaft bending (input gear)	Shaft bending (input gear)	Shaft bending (input gear)	Shaft bending (input gear)
3 rd	Shaft bending (input gear)	Gear rotation (input gear)	Shaft bending (input gear)	Gear rotation (input gear)	Shaft bending (input gear)	Gear rotation (input gear)
4 th	Shaft radial expansion (input gear)	Shaft radial expansion (input gear)	Gear rotation (output gear)	Shaft radial expansion (input gear)	Shaft radial expansion (input gear)	Shaft radial expansion (input gear)
5 th	Shaft radial expansion (input gear)	Shaft radial expansion (input gear)	Shaft radial expansion (input gear)	Shaft radial expansion (input gear)	Gear rotation (idler gear)	Gear rotation (idler gear)
6 th	Shaft slender (input gear)	Shaft slender (input gear)	Shaft radial expansion (input gear)	Gear rotation (idler gear)	Shaft radial expansion (input gear)	Shaft radial expansion (input gear)
7 th	Shaft slender (input gear)	Shaft slender (input gear)	Shaft slender (input gear)	Shaft slender (input gear)	Gear rotation (input gear)	Shaft slender (input gear)
8 th	Shaft axial compression (input gear)	Shaft axial compression (input gear)	Shaft slender (input gear)	Shaft slender (input gear)	Shaft slender (input gear)	Shaft slender (input gear)

Table 4 briefly describes the first eight critical mode shapes (highest amplitude of deformations) of the three gear trains in pre-stressed state. For gear trains in pre-stressed state, the input gear is also the most vulnerable to vibrational deformations compared to the idler gear and output gear. Shaft bending, gear rotation and radial expansion are vibrational deformations that frequently occur in gear trains. From the mode shapes analysis, the order or sequence of the vibrational deformations for the first eight mode shapes of the gear train in free stress state is normally unique and will not be the same as the one found in the pre-stressed state. This also applies for gear train subjected to single pair tooth contact and double pair tooth contact.

4. Static stress analysis of three different gear trains

Static stress analysis using FEM was performed on the three types of gear train, focusing mainly on the gear tooth bending stress and contact stress caused by two contacting gear teeth. FEM stress analysis was simulated on gear trains with different combinations (without idler, one idler and two idler gears). The three types of gear train bending stress and contact stress behavior are analyzed separately with respect to the variation in angular position of the gears from 0° to 18°.

4.1 Gear tooth bending stress using Lewis equation

Bending stress evaluation in modern gear design is generally based on the Lewis equation. This equation, applied with the stress concentration factor K_f , defines the bending stress geometry factor J for traditionally designed standard or close-to-standard gears [18]. The first equation used to determine the bending stress at the root of the gear tooth was derived by Wilfred Lewis (1893). In this equation the gear tooth is considered as a simple cantilever beam as shown in Fig. 16.

The Lewis equation is stated as below:

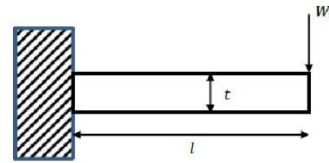


Fig. 16. Loads and length dimensions used in cantilevered beam by Lewis.

$$\sigma_r = \frac{W_t P_d}{b_s Y} \quad (7)$$

where P_d = diametral pitch, b_s = face width, and the Lewis form factor, Y is

$$Y = \frac{2xP_d}{3} \quad (8)$$

and x dimension can be determined from

$$l = \frac{t^2}{4x} \quad (9)$$

To analyze the worst load condition on gear teeth, the tip-load condition as proposed originally by Lewis is not the most critical. In nearly all gear designs, the contact ratio is high enough to put a second pair of teeth in contact when one pair has reached the tip-load condition on one member [19]. Hence, considering worst load condition in this work, the Y Lewis factor for a gear with 20 teeth, full depth profile, and 20 degree pressure angle is 0.33 [20]. Fig. 17 shows the tooth gear with applied load approximately near to the pitch diameter of the tooth surface and their dimensions used in determining bending tooth stress.

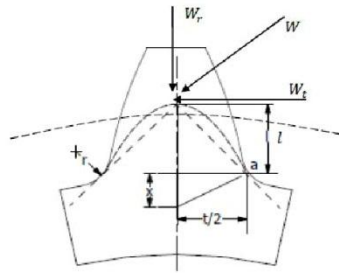


Fig. 17. Loads and length dimensions used in determining tooth bending stress.

The Lewis equation is based on following assumptions:

- (1) The effect of radial load is ignored.
- (2) The effect of stress concentration at the root fillet is ignored.
- (3) It is assumed that at any time only one pair of teeth is in contact.
- (4) It considers static loading and does not take the dynamics of meshing teeth into account.
- (5) The Lewis form factors with various numbers of teeth only assume a pressure angle of 20 and a full-depth involute.

4.2 Gear teeth bending stress using FEM

A three-dimensional (3D) model of the gear train with no idler gear was modelled. A single pair tooth contact between gears was carefully aligned using the Autodesk Inventor program. Tetrahedron element was selected to construct the FE mesh model of the gear train with coarse element size between 10 mm to 15 mm. Mesh refinement was focused on the root fillet of the gear to determine the critical bending stress. The mesh refinement of 1mm element size was carried out by setting a sphere influence radius of 3 mm at every vertex of the gear root fillet as shown in Fig. 18. Fig. 19 shows the mesh model after the customized meshing setup.

The two meshing gears were identical and the single pair tooth contact was aligned touching each other tangentially at one point. In bending stress, the contact surface between gears was set to be rigid contact by selecting 'No Separation' contact, which is also known as linear contact. Frictional or non-linear contact was ignored in this analysis to reduce computing time. The main scope of this analysis is to obtain bending stress rather than contact stress. Cylindrical support was treated as the ideal bearing support, which only allows rotational motion and is applied on the gears as shown in Fig. 20.

A moment of 500 Nm was applied on the shaft of the input gear and the shaft of the output gear was fully constrained to create reaction force between the gear teeth. Fig. 21 shows the maximum bending stress of 291.82 MPa occurring at one side of the root fillet of the input gear. FE simulations predict that the root fillet is more prone to compressive stress rather than tensional stress.

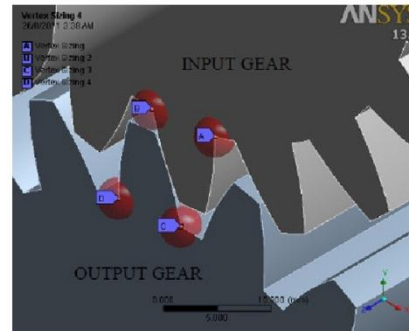


Fig. 18. Highlighted vertex for mesh refinement using 3mm radius of sphere influence.

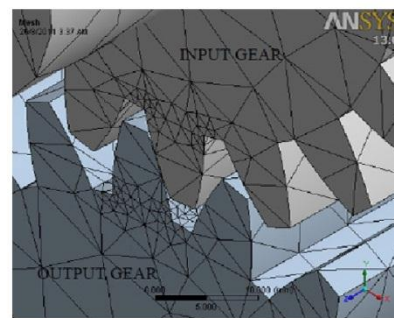


Fig. 19. Mesh model of the gear train for FE simulation.

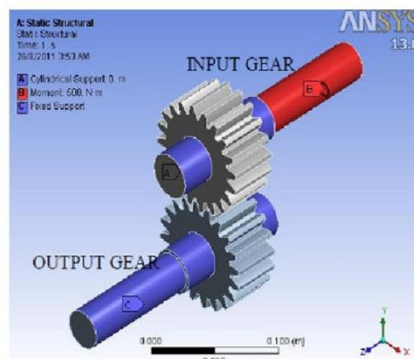


Fig. 20. Boundary condition settings of the gear train for FE bending stress analysis.

4.3 Results comparison between the theoretical Lewis bending stress and the calculated FEM bending stress

The gear tooth bending stress results calculated from the 3D FE model of the gear train without idler gear were compared

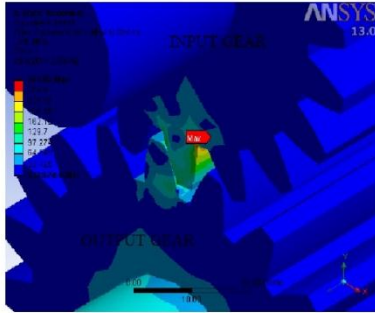


Fig. 21. FE simulation results shows the maximum bending stress at the root fillet of the input gear.

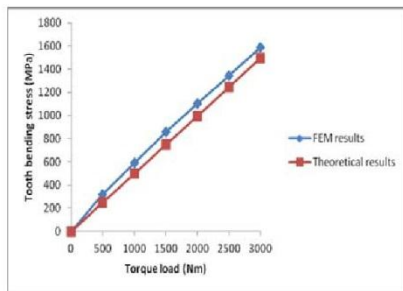


Fig. 22. Lewis theoretical stress results and the FEM simulation stress results.

to gear tooth bending stress results calculated using the Lewis equation. The gear tooth bending stress was calculated using both methods with respect to the increased torque load. Fig. 22 shows the comparison between the FEM simulation results and theoretical calculation results for gear tooth bending stress. Both methods show a linear relationship in bending stress when plotted against increasing torque load. However, the FEM stress results are slightly higher than the one calculated from the results calculated using the Lewis formula. This is because FEM takes into account the radial load component of the resultant force exerted from the torque load, which causes higher stress results.

The FEM results agree well with the theoretical results for both cases. The percentage difference between the theoretical and FEM stress results is of average 6%, which is still acceptable. Therefore, this validates the calculated FE stress results and also the FE model of the gear train.

4.4 Gear tooth contact stress using Hertzian equation

In addition to considering the critical bending stress in gears, analysis of gear tooth contact stress is equally important because excessive contact stress may cause failure such as pitting, scoring, and scuffing of surfaces [19, 20].

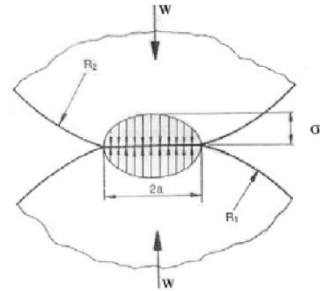


Fig. 23. Hertzian model of the two cylinders in contact under normal load [16].

The contact stress was calculated by using a Hertzian contact stress analysis. The Hertzian contact stress of gear teeth is based on the analysis of two cylinders under a radial load. It is assumed in the gear model that the radii of cylinders are the radii of curvature of the involute tooth forms of the mating teeth at the band of contact as shown in Fig. 23. The band of contact between the two cylinders can be calculated as $2a$ where the deformed distance, a is equal to

$$a = 2 \sqrt{\frac{W(1-\nu_1^2) + \frac{1-\nu_2^2}{E_2}}{E_1} \frac{1}{b \pi \left(\frac{1}{R_1} + \frac{1}{R_2} \right)}} \tag{10}$$

The Hertzian theory assumes an elliptic stress distribution, as seen in the Fig. 1, the maximum stress is in the middle and equals

$$\sigma_o = \sqrt{\frac{W \left(\frac{1}{R_1} + \frac{1}{R_2} \right)}{b \pi \left[\frac{1-\nu_1^2}{E_1} + \frac{1-\nu_2^2}{E_2} \right]}} \tag{11}$$

where W is the normal load, E_1 and E_2 are the modulus of elasticity of the pinion and gear, respectively, ν_1 and ν_2 are Poisson's ratios of the pinion and gear, respectively, and b_s is the face width of pinion. R_1 and R_2 are the respective radii of the involute curve at the contact point, as shown in Fig. 24.

However, the pitch radius of the pinion and gear denoted as r_{p1} and r_{g2} , respectively, can be related to the gear involute radii as $R_1 = r_{p1} \sin \phi$ and $R_2 = r_{g2} \sin \phi$. Hence, the Hertzian equation for contact stresses in the teeth becomes

$$\sigma_o = \sqrt{\frac{W \left(1 + \frac{r_{g1}}{r_{p2}} \right)}{r_{p1} b_s \pi \left[\frac{1-\nu_1^2}{E_1} + \frac{1-\nu_2^2}{E_2} \right] \sin \phi}} \tag{12}$$

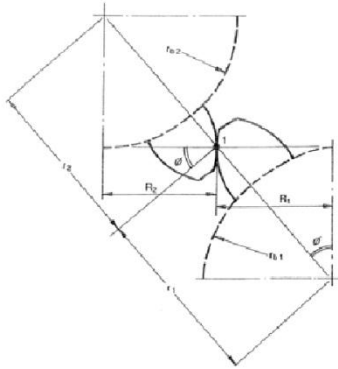


Fig. 24. Two involute teeth in contact [16].

In the Hertz contact stress equation, a few assumptions are made, such as pure bending of short beam, elliptic distribution of stresses at tooth contact, and friction between the gear contacting surfaces is not accounted in the stress equation. A question therefore arises concerning their accuracy [22]. The elastic compression of two-dimensional bodies in contact cannot be calculated solely from the contact stresses given by the Hertzian theory. Some account must be taken for the shape and size of the bodies themselves and the way in which they are supported. In most practical circumstances such calculations are difficult to perform, which has resulted in a variety of approximate formulae for calculating the elastic compression of bodies in line contact such as gear teeth and roller bearings in line contact [23].

4.5 Gear tooth contact stress using FEM

The 3D FE gear train with no idler gear is imported into the ANSYS Workbench. FEM settings of gear train without idler gear FE model are described in this section for close comparison with the Hertzian contact model, which describes on two identical and symmetrical cylindrical contacts [19, 20]. Single pair tooth contact between gears was carefully aligned using the Autodesk Inventor program. For contact stress analysis between two interacting gear teeth, non-linear contact or also known as frictional contact was assigned. The coefficient of friction of the contacting gear tooth surface was set to 0.2.

In the ANSYS contact settings, Augmented Lagrange was selected as the solver for the contact non-linearity problem. Since the input gear was being applied load, the input gear contact surface was defined as the 'Contact' and the contact surface of the output gear was the 'Target' of the contact. Fig. 25 shows the side view of the gear tooth contact settings for the gear train with one idler gear. To further enhance the accuracy of the contact physically and avoid errors, the interface treatment was set to 'Adjust to Touch' and the pinball region was set to 'Auto Detection Value'.

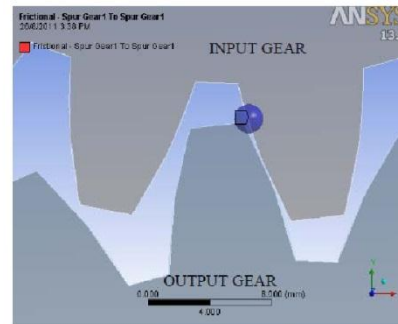


Fig. 25. Contact settings of the contacting gear in side view.

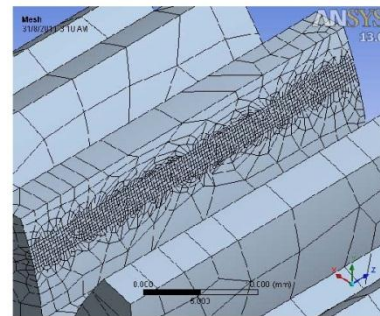


Fig. 26. Finer mesh elements at the contacting gear tooth surface of the output gear.

In contact stress analysis, a hexahedron element was selected to construct the FE mesh model of the gear train with coarse element size set to 10 mm. The percentage of the hexahedron is 90% and the other 10% are tetrahedron elements. Hexahedron element was selected for FE meshing because of a higher degree of freedom of the element that may yield higher accuracy and also smoother node distribution over the surface in solving contact problems.

To obtain more accurate contact stress results using FEM, a surface mesh refinement of 0.3 mm element size was assigned to the area of teeth surface contact of both the input gear and output gear as shown in Fig. 26. The area of contact at the gear tooth surface representing the finer mesh is approximately 2 mm by 40 mm. The resulting number of nodes is 126463 nodes, and the number of elements formed for the gear train model is 41409 elements. The input gear was hidden to show the finer mesh elements on the gear tooth contacting surface.

The load and constraints were set similar to the one set for FEM bending analysis as shown in Fig. 27. The cylindrical support, which only allows free rotation, represents the virtual bearings to support the gear. Moment of 500 Nm was applied at the shaft of the input gear and the shaft of the output gear is

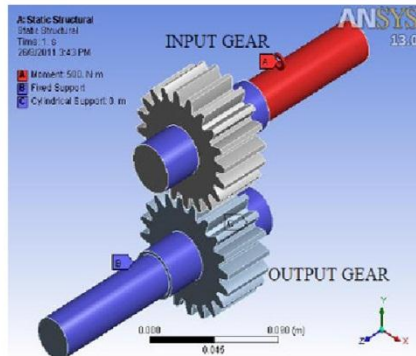


Fig. 27. Boundary condition settings on gear train with one idler gear.

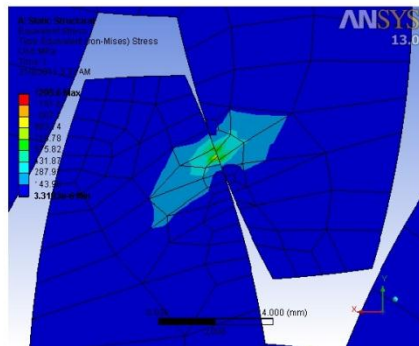


Fig. 28. FEM stress distribution of the two contacting gear teeth in side view.

fully constrained.

Fig. 28 shows the stress distribution of the two contacting gears in side view when subjected to 500 Nm torque. The maximum stress of 1295.6 MPa occurs at the gear teeth surface of the input gear. From the side view, the contact stress distribution between the two gears is not precise because the contacting nodes are not arranged in a similar pattern. The nodes built from the element of both gear teeth must coincide to form a much precise solution to contact stress.

A more detailed contact stress distribution on the gear tooth surface of the input gear can be seen in Fig. 29 after putting input gear model to hidden. It is expected that a long stretch of high stress band contact should be formed along the gear tooth surface. However, this is not the case due to uneven node formation along the gear tooth surface.

4.6 Results comparison between the theoretical Hertz contact stress and the calculated FEM contact stress

The contact stress results calculated from the 3D FE model of the gear train without idler gear were compared to the con-

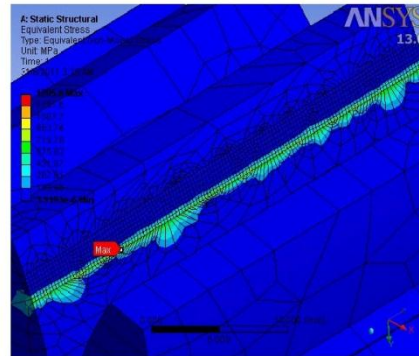


Fig. 29. Detailed view of FEM contact stress distribution of the input gear together with mesh elements.

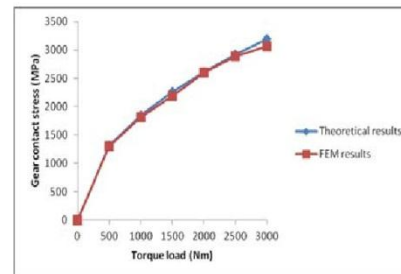


Fig. 30. Hertzian theoretical contact stress results and the FEM simulation contact stress results.

tact stress results calculated from the Hertzian equation. The contact stress results calculated using both methods were compared to the increased torque load. Fig. 30 shows the gear tooth surface stress contact comparison between the FEM simulation results and theoretical calculation results. Both methods show the contact stress results vary exponentially when plotted against increasing torque is loaded.

The percentage difference between the theoretical and FEM stress results is on average 4%. There is a difference in the results calculated between both methods because the Hertz equation does not consider the tangential force, which contributes to frictional force on the gear tooth surface. FEM results agree well with the theoretical results for both cases. The slight difference between the two methods is acceptable, which validates the calculated FE contact stress results and the FE model of the gear train.

4.7 Angular position settings for the three gear trains

Prior to conducting bending stress analysis and contact stress analysis using FEM, the angular position of the gears in gear train must first be defined clearly. In the Autodesk Inventor program, the gears are assembled to rotate and contact with

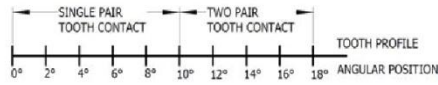


Fig. 31. Angular intervals of the gear pair contact of the gear train.

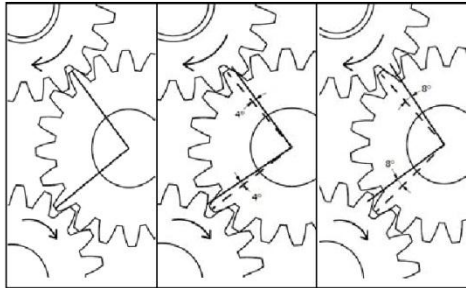


Fig. 32. Gear train with one idler gear in 0°, 4° and 8° angular positions where single pair tooth contact takes place between meshing gears.

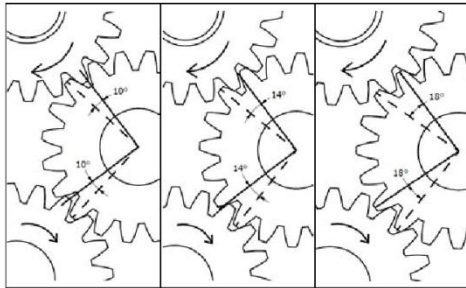


Fig. 33. Gear train with one idler gear in 10°, 14° and 18° angular positions where double pair tooth contact takes place between meshing gears.

the other gear teeth in a contact ratio of 1.5. This means that during the rotational operation of the mating gears, single pair tooth contact and double pair tooth contact the contact ratio is the most important parameter which plays in this situation [16]. Fig. 31 shows the angular intervals during the contact operation of a single gear tooth and it also shows the load distribution within these contact locations along with the angle of contact.

Figs. 32 and 33 illustrate the technique of positioning the gear train with one idler gear before simulating stress analysis on the model. When rotating the input gear of the gear train model, single tooth pair contact takes place when the angular position of the gears is between 0° to 10°.

Subsequently, double pair tooth contact takes place when the angular position of the gears is between 10° to 20°. The same technique was applied to the other two gear trains to obtain the FE stress results.

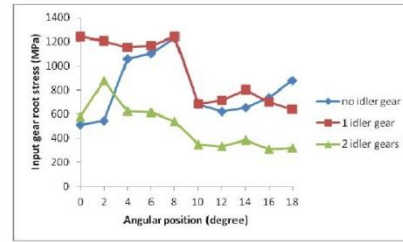


Fig. 34. Input gear root stress comparison of gear train with (a) no idler gear, (b) 1 idler gear, (c) 2 idler gears.

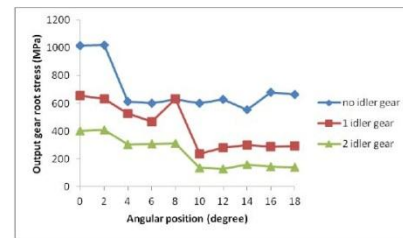


Fig. 35. Output gear root stress comparison of gear train with (a) no idler gear, (b) 1 idler gear, (c) 2 idler gears.

4.8 Gear tooth bending stress analysis of the three types of gear train in different angular positions

The maximum gear teeth bending stress at the input gear and output gear was calculated using FEM for the three types of gear train. In this analysis, a torque load of 2000 Nm was applied to the input gear of the three different gear trains. Figs. 34 and 35 show the gear root stress behavior of the input gear and output gear for three different gear trains positioning from 0° to 18°, respectively. The three types of gear trains show similar behavior with respect to angular position. Generally, the gear root stress at the input and output gear shaft is found to be higher from 0° to 10° and lower between 10° to 18° due to the difference in the number of pair tooth contact.

The gear tooth bending stress at the input gear is higher for the gear train with one idler gear compared to the gear train without an idler gear. However, the root stress at the output gear shows that the gear train without an idler gear has the highest stress for all angular positions. FEM simulation shows that the input gear on the gear train with two idler gears has the lowest bending stress with respect to its angular positions. The input gear has overall higher root bending stress compared to the root bending stress at the output gear.

4.9 Contact stress analysis of the three types of gear train subjected to angular position 0° to 18°

The gear tooth contact stress behavior of the input gear and output gear of the gear trains was studied with respect to dif-

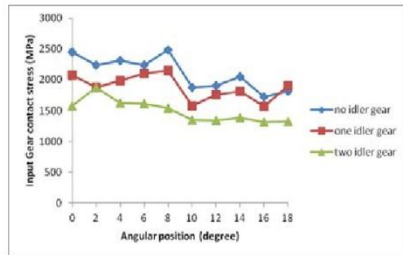


Fig. 36. Input gear root stress comparison of gear train with (a) no idler gear, (b) 1 idler gear, (c) 2 idler gears.

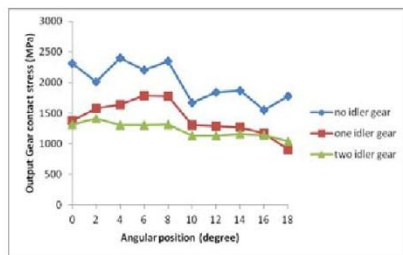


Fig. 37. Output gear root stress comparison of gear train with (a) no idler gear, (b) one idler gear, (c) two idler gears.

ferent angular position. Fig. 36 shows the gear tooth surface stress of the three gear trains when the gear is rotated to different angular positions. The gear train with no idler gear has an average higher gear tooth contact stress and the gear train with two idler gears has the lowest average gear teeth contact stress. This can be explained by the energy loss due to friction and multiple contacts of the gear teeth for gear train with more gear meshing.

Fig. 37 shows the results of the gear tooth surface stress calculated from the three different gear trains when the gear is rotated to different angular positions. In comparison, the gear tooth contact stress is higher on input gear rather than for output gear. Theoretically, the contact stresses should be the same on both contacting gear teeth surface. However, FEM calculated the results to be of slight difference due to inconsistency and non-smooth surface formation of the gear geometry meshing. In both gear analyses, the gear tooth contact stress of all the gear trains shows similar contact stress characteristics. The difference between gear tooth contact stress when subjected to single pair tooth contact and double pair tooth contact is quite significant. However, FEM results show that the gear train with two idler gears has slight difference in single pair and double pair tooth contact.

5. Conclusions

Modal analysis on three different gear trains of the portal axle unit was studied using FEM simulation under free-stress state

and pre-stressed state. The gear tooth maximum bending stress and contact stress were calculated using FEM for the three different gear trains with respect to the varying angular position involving single and double pair tooth contact. In FEM modal analysis of the gear trains under free and pre-stressed state, the first three mode shapes were excited at average low frequencies of 2000 Hz. All gear trains have similar resonance frequency behavior when plotted against the first eight mode shapes. The resonance frequency of the gear trains increases significantly when subjected to pre-stressed state. Vibrational bending of the shaft, gear rotation, and shaft radial occurred quite often at the input gear rather than output gear regardless of the type of gear train. There was a big difference between the natural frequencies of the gear trains compared to the operating frequency of the portal axle unit in which it is a normal case. Therefore, resonance will not occur when the portal axle unit is operating at its speed range. However, modal analysis must be performed as a safety precaution in portal axle design.

The gear tooth bending stress and contact stress were validated by comparing the FEM stress results with the results calculated from Lewis theory and Hertz theory. Both Lewis stress and contact stress have good agreement with difference of 4% to 6% on average. In bending stress analysis, the gear train without an idler gear has the highest stress among the other two. Besides, the input gear has overall higher root bending stress compared to the root bending stress at the output gear. In analyzing the gear train under varying angular positions, the bending stress and contact stress results were not consistent when plotted against the angular position. This was due to irregularities and low surface smoothness in the geometrical mesh model. The precision of setting the angular position contact between gears also critically affects the bending stress and contact stress results. However, in a real case, the bending and contact stress behavior of the gear is not constant throughout the rotation but rather in a 'zig-zag' stress behavior.

Acknowledgments

The authors would like to thank the Centre for Vehicular Technology, Universiti Tunku Abdul Rahman for the facilities and system support.

References

- [1] T. Bruns and E. Schafer, Modelling and identification of an all-terrain vehicle, *International Journal of Vehicle Systems Modeling and Testing*, 2 (3) (2007) 276-295.
- [2] A. Berlioz and P. Trompette, *Solid mechanics using the finite element method*, ISTE Ltd and John Wiley & Sons, Inc, 2010.
- [3] S. Draca, *Finite element model of a double-stage helical gear reduction*, Master's thesis, University of Windsor, (2006).
- [4] J. Lu, F. L. Litvin and J. S. Chen, Load share and finite element stress analysis for double circular-arc helical gears, *Math. Comput. Model.*, 21 (1995) 13-30.

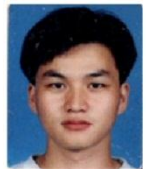
- [5] G. D. Bibel, A. Kumar, S. Reddy and R. Handschuh, Contact stress analysis of spiral bevel gears using finite element analysis, *Trans. ASME, J. Mech. Des.*, 117 (1995) 235-240.
- [6] F. L. Litvin, J. S. Chen, J. Lu and R. F. Handschuh, Application of finite element method for determination of load share, real contact ratio, precision of motion, and stress analysis, *Trans. ASME, J. Mech. Des.*, 118 (1996) 561-567.
- [7] F. L. Litvin, Q. Lian and A. L. Kapelovich, Asymmetric modified spur gear drives: reduction of noise, localization of contact, simulation of meshing and stress analysis, *Comp. Meth. App. Mech. Eng.*, 188 (2000) 363-390.
- [8] J. Kramberger, M. Šraml, I. Potrč and J. Flašker, Numerical calculation of bending fatigue life of thin-rim spur gears, *Engineering Fracture Mechanics*, 71 (4-6) (2004) 647-656.
- [9] S. Mohamed Nabi and N. Ganesan, Static stress analysis of composite spur gears using 3D-finite element and cyclic symmetric approach, *Composite Structure*, 25 (1-4) (1993) 541-546.
- [10] V. Simon, FEM stress analysis in hypoid gears, *Mechanism and Machine Theory*, 35 (9) (2000) 1197-1220.
- [11] T. Lin, H. Ou and R. Li, A finite element method for 3D static and dynamic contact/impact analysis of gear drives, *Computer Methods in Applied Mechanics and Engineering*, 196 (9-12) (2007) 1716-1728.
- [12] S. Park, J. Lee, U. Moon and D. Kim, Failure analysis of a planetary gear carrier of 1200 HP transmission, *Engineering Failure Analysis*, 17 (2) (2010) 521-529.
- [13] Z. Wei, *Stresses and deformations in involute spur gears by Finite Element Method*, Master's thesis, University of Saskatchewan, 2004.
- [14] R. Zu, *Finite element modeling and simulation on quenching effect for spur gear design optimization*, Master's thesis, University of Akron, 2008.
- [15] Y. Chen and C. Tsay, Stress analysis of a helical gear set with localized bearing contact, *Finite Elements in Analysis and Design*, 38 (2002) 707-723.
- [16] A. R. Hassan, Contact stress analysis of spur gear pair teeth, *World Academy of Science, Engineering and Technology*, 58 (2009) 611-616.
- [17] A. Abdullah, *Powertrain engine timing gear contact analysis – Noise analysis using FEM*, Master's thesis, Brunel University (2005).
- [18] A. L. Kapalevich and Y. V. Shekhtman, Direct gear design: Bending stress minimization, *Gear Technology* (2002) 29-35.
- [19] D. W. Dudley, *Handbook of Practical Gear Design*, CRC Press LLC, 2002.
- [20] B. J. Hamrock, S. R. Schmid and B. Jacobson, *Fundamentals of machine elements* 2nd Edition, McGraw Hill, New York, 2005.
- [21] J. A. Collins, *Failure of materials in mechanical design*, Wiley, New York, 1981.
- [22] E. Zahavi, *The finite element method in machine design*, Prentice-Hall, New Jersey (1991).
- [23] R. J. Roark, *Formula for Stress and Strain*, 4th edition, McGraw-Hill, New York, 1965.



Jong Boon Ooi received his B.Eng (Hons) in Mechanical Engineering in 2009 from Universiti Tunku Abdul Rahman (UTAR), Malaysia. He is currently a Lecturer in School of Technology at Tunku Abdul Rahman College and also pursuing his Master of Engineering Science in UTAR. His research interests are in the area of finite element analysis, failure analysis, and parametric optimization in machine elements.



Xin Wang received her PhD degree in 2007 from Nanyang Technological University (NTU), Singapore. She was research fellow at the Robotics Research Center, NTU from 2007 to 2009. She is currently an Assistant Professor at Faculty of Engineering & Science, Universiti Tunku Abdul Rahman, Malaysia. Her research interests include finite element analysis, non-destructive testing and measurement, and machine vision.



ChingSeong Tan received his PhD degree from Nanyang Technological University, Singapore. He was also drilling services engineer in Schlumberger Ltd, Research Engineer ASTAR, Senior Lecturer Multimedia University, Assistant Professor UTAR. In 2011, he joined Multimedia University where he is currently an associate professor in the Faculty of Engineering. His research interests include machine vision, optical measurement and failure analysis.



Jee-Hou Ho received his B.Eng (Hons) and M.Eng in 2000 and 2004 from Nanyang Technological University (NTU), Singapore and Ph.D in 2010 from The University of Nottingham Malaysia Campus. He was researcher at the Robotics Research Center, NTU from 2000 to 2005, primarily involved in simulation platform development for underwater robotic vehicles and ground mobile robots. He is currently an Assistant Professor at University of Nottingham Malaysia Campus and his research interests are in the area of robotics, vibro-impact dynamics and vibration energy harvesting.



Ying Pao Lim received his B.Eng (Hons) in 1993 from Universiti Teknologi Malaysia, Msc in Manufacturing System Engineering in 1995 from University of Warwick and Ph.D in 2006 from Universiti Putra Malaysia. He is currently an Assistant Professor at Universiti Tunku Abdul Rahman Malaysia. His research interests are in the area of finite element analysis, mold and die design, aluminum casting and rare earth effects on casting properties.

**Proceedings of the Institution of Mechanical Engineers, Part C, Journal of
Mechanical Engineering Science**

**Parametric optimization of the output shaft of the portal axle using finite element
analysis**

--Manuscript Draft--

Manuscript Number:	JMES4194R1
Full Title:	Parametric optimization of the output shaft of the portal axle using finite element analysis
Article Type:	Original Article
Section/Category:	Design and Manufacture
Corresponding Author:	Xin Wang Monash University Sunway Campus Bandar Sunway, Selangor MALAYSIA
Corresponding Author Secondary Information:	
Corresponding Author's Institution:	Monash University Sunway Campus
Corresponding Author's Secondary Institution:	
First Author:	Jong Boon Ooi
First Author Secondary Information:	
Order of Authors:	Jong Boon Ooi Xin Wang Ying Pio Lim ChingSeong Tan Jee-Hou Ho Kok-Cheong Wong
Order of Authors Secondary Information:	
Abstract:	Portal axle unit is a gearbox unit installed on vehicle for higher ground clearance and driving in off-road conditions. Shafts must be exceptionally tough and lightweight to improve the overall performance of the portal axle unit. In this paper, a hollow shaft with rib at both ends was proposed. The three-dimensional model of the shaft torsional stress was determined using finite element analysis (FEA) and validated by experimental test. The hollow shaft thickness, rib thickness, depth of spokes, rib fillet radius, and number of spokes are the 5 type of parameters considered in the torsional strength analysis of the rib. Taguchi orthogonal array L25 was applied to determine the optimum set of parameters for the proposed shaft. The strength and weight of the optimised model were calculated and compared to the solid shaft, hollow shaft, and proposed model. The optimized model showed improvement in torsional strength with slight increase in weight compared to the benchmark model.

Parametric optimization of the output shaft of the portal axle using finite element analysis

Jong Boon Ooi¹, Xin Wang^{2*}, Ying Pio Lim¹, ChingSeong Tan³, Jee-Hou Ho⁴ and Kok-Cheong Wong⁴

¹Universiti Tunku Abdul Rahman, Malaysia

²Monash University Sunway Campus

³Multimedia university, Malaysia

⁴University of Nottingham Malaysia Campus

* Corresponding author

E-mail address: wang.xin@monash.edu

Abstract: Portal axle unit is a gearbox unit installed on vehicle for higher ground clearance and driving in off-road conditions. Shafts must be exceptionally tough and lightweight to improve the overall performance of the portal axle unit. In this paper, a hollow shaft with rib at both ends was proposed. The three-dimensional model of the shaft torsional stress was determined using finite element analysis (FEA) and validated by experimental test. The hollow shaft thickness, rib thickness, depth of spokes, rib fillet radius, and number of spokes are the 5 type of parameters considered in the torsional strength analysis of the rib. Taguchi orthogonal array L25 was applied to determine the optimum set of parameters for the proposed shaft. The strength and weight of the optimised model were calculated and compared to the solid shaft, hollow shaft, and proposed model. The optimized model showed improvement in torsional strength with slight increase in weight compared to the benchmark model.

Keywords: parametric optimization, finite element analysis, shaft design, portal axle.

1 INTRODUCTION

In the motorsports industry, portal axle plays an important role in giving higher ground clearance to four wheel drive (4WD) vehicle so it can be driven off-road. Fig. 1 shows the comparison between normal vehicle and vehicle with portal axle. In the event of driving into off-roads, the operating portal axles are frequently subjected to shock and overloading may eventually lead to failure shafts. Therefore, shafts in the portal axle must be designed with exceptionally high strength and lightweight for improved reliability and performance.

For most portal axle gearboxes, hollow gear shafts with acceptable thickness are normally assembled to it to achieve higher strength to weight ratio. However, extremely high torsion and cyclic loading resulting from driving off-road may cause higher fatigue failure or complete shaft breakage [1]. Torsional, bending and normal forces occur during the working of the shaft [2]. There is evidence of failure in shaft due to many factors. Heyes [3] studied the common failure types in automobiles and revealed that the failure in the transmission system elements cover quarter of all the automobile failures. Vogwell [4] has carried out a study on a failed axle and obtained the stresses on the axle by numerical analysis technique. Several researchers also studied on the failures of the elements of power transmission system as there are many cases of the failures [5–11].

Shaft designers and engineers are constantly finding solutions to redesign shaft based on parameters to achieve improved strength to weight ratio. However, they often investigate the effect of a single factor to the shaft strength and obtain the relationship. This type of analysis can be less effective when investigating one factor at a time because other parameters that are considered may be dependent with one and another and affect the overall shaft strength. Even though there are shaft design standards [8, 12-14] that can be used as a guide for engineers, they are often too general to be applied for specific applications. These design standards are

also limited to certain design criteria and design parameters for designing shaft. In the case of designing shafts for portal axle gearbox, it is necessary to propose a customized shaft design for extreme operating condition. In this paper, a hollow shaft with rib at both ends is proposed. The hollow shaft thickness, rib thickness, rib fillet radius, depth of spokes and number of spokes of the rib structure are the quantitative parameters being considered for the proposed hollow shaft. Fig. 2 shows the schematic flow diagram of the steps for optimizing the proposed shaft model through parametric analysis.

ANSYS v12 software was used to investigate the torsional stress behaviour of the shaft. FEA is a widely accepted numerical method in evaluating and verifying shaft design [15]. Recently, the gear bending stress and contact stress of the gears of the portal axle gearbox has been analysed using FEA [16]. H. Göksenli and Eryürek used FEA program to simulate stress analysis on the keyway shaft of an elevator to verify their mathematical calculations for determining the maximum stress [15]. Bayrakceken et al. [17] determined the stress conditions of the failed section at the universal joint yoke of the shaft using FEA program. In order to investigate the 5 type of parameters that may affect the shaft strength, the Taguchi orthogonal array L25 was applied. This method was also applied to investigate the sensitivity of the 5 parameters to the torsional strength of the hollow shaft with rib and also to determine the possible set of optimum parameters. The strength and weight of the optimised model were obtained and compared with the solid shaft, hollow shaft, and proposed shaft.

2 VALIDATION OF THE FEA SHAFT MODEL

2.1 Finite element analysis

ANSYS v12.0 software is used to determine the maximum torsional stress of the shaft. Firstly, a three-dimensional hollow shaft of 3mm in thickness, length of 210 mm and 37 mm in diameter is modelled using Autodesk Inventor Professional 2010 software. The surface

boundary conditions are applied to the shaft model as shown in Fig. 3. Fixed support is applied at one end shaft and 100 Nm of torsion is applied on the other end of the shaft.

In the mesh settings, tetrahedron element is selected to mesh the shaft model. The average element size was set to 5 mm in the mesh settings. Table 1 shows the details of the mesh settings generated in ANSYS software. Refined mesh size surface of 2 mm is set to the critical area of the applied torsion and the normal angle curvature element is set to 15°.

Table 1 Mesh settings of the benchmark model

Mesh type	
Object Name	Patch Conforming Method
State	Fully Defined
Scope	
Scoping Method	Geometry Selection
Geometry	1 Body
Definition	
Method	Tetrahedron
Algorithm	Patch Conforming
Element Midside Nodes	Use Global Setting
Sizing	
Element Size	5 mm
Initial Size Seed	Active Assembly
Smoothing	Medium
Transition	Fast
Normal angle curvature	15°
Minimum Edge Length	3.29310 mm
Statistics	
Nodes	11212
Elements	5678

The FEA solver for the model was set to solve for each sub-step of the ten sub-steps set in duration of 1 second. Thus, the stress results are incremented every 0.1 seconds until it reaches 1 seconds. With the linear increment of the torque, the solver will calculate the torsional stress at an instant sub-step time before obtaining the final result. Fig. 4 shows the maximum stress occurred at the discontinuity surface close to one of the splined joints. The

maximum von Mises stress (torsional stress) of the hollow shaft model calculated in ANSYS is 141.76 MPa.

2.2 Analytical method

Distortion energy theory (DET) is applied to determine the von Mises stress of the hollow shaft. DET also known as the von Mises criterion, postulates that failure is caused by the elastic energy associated with shear deformation. The hollow shaft is assumed to be ductile material thus DET is valid and can be applied. DET considers the maximum axial stress σ_x in transverse direction (perpendicular to the shaft axis) caused by bending moment and the maximum shear stress τ_{xy} caused by torque. For a hollow shaft, the maximum axial stress is:

$$\sigma_x = \frac{32MD}{\pi(D^4-d^4)} \quad (1)$$

Similarly, the maximum shear stress is:

$$\tau_{xy} = \frac{16TD}{\pi(D^4-d^4)} \quad (2)$$

Where M is the bending moment, T is the applied torque, D is the external diameter of the hollow shaft, and d is the internal diameter of the hollow shaft. The principal stresses can be determined with the known value of σ_x and τ_{xy} as in the following:

$$\sigma_{1,2} = \frac{\sigma_x + \sigma_y}{2} \pm \sqrt{\left(\frac{\sigma_x + \sigma_y}{2}\right)^2 + \tau_{xy}^2} \quad (3)$$

For the plane stress state, the principal normal stresses when $\sigma_y = 0$, are:

$$\sigma_1, \sigma_2 = \frac{16}{\pi d^3} (M \pm \sqrt{M^2 + T^2}) \quad (4)$$

Finally, the general equation for calculating the von Mises stress of the shaft is:

$$\sigma_e = (\sigma_1^2 - \sigma_1\sigma_2 + \sigma_2^2)^{\frac{1}{2}} \quad (5)$$

In using the DET for determining the shaft torsional stress, there are few assumptions considered as in the followings:

1. It is based on two-dimensional schematic diagram.
2. The effect of gravity and mass of the shaft are neglected.
3. DET is only valid for ductile material.

2.3 Experiment test

In the experiment test, the Tinius Olsen torsion tester is used to apply torsion to the hollow shaft. Firstly, the long rod of normalized AISI 4340 alloy steel with one and a half inch in outer diameter and 3 mm hollow shaft thickness is cut to a length of 210 mm. The cylindrical surface of the hollow shaft is slightly machined to approximately 37 mm in outer diameter and also for smoother surface finish by using the CNC lathe machine. The hollow shaft is then pre-assembled with a strain gage rosettes that provide shear strain data. When torsion is applied to the shaft causing it to twist, shear stresses are induced. The stresses are measured by bonding the strain gauges at 45° to the horizontal torque axis. Fig. 5 shows the bonding of the strain gauge on the hollow shaft.

Fig. 6 shows the mounting of the hollow shaft on the Tinius Olsen torsion tester. Both ends of the shaft are gripped and tightened using the jaw and chuck. This machine comes with a built-in data acquisition system where a notebook retrieves all the measured data required. The LabView program read all data and writes to a text file that is readable into Microsoft Excel format sheet.

Fig. 7 shows the schematic diagram of the process flow in obtaining the shaft torsional stress. In the LabView software, the initial torque load was set at 100 Nm with an increment of 20 Nm. All of the data files were recorded in LabView and the experimental results of the

measured shear stress of the shaft are collected and plotted. The results are directly imported into 'Microsoft Excel' sheet file for analysis of the results.

2.4 Comparison of the FEA model with the experimental and analytical model

The FEA model is compared with the experimental and analytical model. With the same size and dimension of the solid shaft, the torsional stresses of the models were plot against the increasing torque as shown in Fig. 8. All models show linear relationship when torsional stress is plotted against the linear increment of torque.

The experimental model has higher torsional stress compared to the FEA and analytical model. However, the torsional stress calculated for FEA model is quite close to the torsional stress measured from the experimental model. The average percentage of difference between them is only 9.83%. This shows the FEA model agree well with the experimental model. The huge difference between the analytical model with the FEA and experimental models is due to the consideration of the shaft analysis of the shaft in one dimension and many assumptions are made to perform the calculations. From the comparisons between the FEA model and analytical model, it was obvious that FEA model is valid and more accurate method for evaluation of the shaft torsional stress.

3 PARAMETRIC OPTIMIZATION OF THE HOLLOW SHAFT WITH RIB

3.1 Modelling of the hollow shaft with rib

A hollow shaft with rib at both ends is proposed for the output shaft of the portal axle. The proposed shaft with 5 types of parameter is modelled as shown in Fig. 9. Table 2 shows the material properties and the dimensions used for modelling the shaft.

Table 2 Dimensions and material properties of the proposed shaft model

Length	210 mm
Outer diameter	37 mm
Material	AISI 4340 alloy steel (normalized at 870°C)
Ultimate tensile stress (UTS)	1279.0 MPa
Tensile yield strength	861.8 MPa
Young's Modulus	210 GPa
Poisson's Ratio	0.30
Density	7850 kg/m ³

3.2 Parametric Optimization

Taguchi Orthogonal Array (OA) L25 is applied to determine the optimum combination of the 5 types of parameters (the hollow shaft thickness, rib thickness, depth of spokes, rib fillet radius, and the number of spokes) that will result in the lowest torsional stress. Minitab 16 statistical software is applied to run the Taguchi Orthogonal Array (OA) L25. Firstly, the factorial design is set by selecting 5 factors (5 parameters) with 5 levels (5 variables) as shown in Table 3. Table 4 shows 25 unique sets of parametric combination that are randomly generated for L25 Taguchi OA when 5 factors with 5 different variables are selected. This means there are 25 test runs in the L25 Taguchi OA.

Table 3 Factorial design of the shaft model using 5 factors with 5 levels

	Factor	Unit	Type	Level 1	Level 2	Level 3	Level 4	Level 5
A	hollow shaft thickness	mm	Qualitative	1	2	3	4	5
B	rib thickness	mm	Qualitative	1	2	3	4	5
C	depth of spokes	mm	Qualitative	5	10	15	20	25
D	rib fillet radius	mm	Qualitative	1	1.25	1.5	1.75	2
E	no. of spokes	nil	Qualitative	2	3	4	5	6

Table 4 Taguchi Orthogonal Array L25 design factors

Standard order	Run order	Hollow shaft thickness (mm)	Rib thickness (mm)	Depth of spokes (mm)	Rib fillet radius	No. of spokes	von Mises stress (Mpa)
23	1	5	3	10	1	6	119.1
13	2	3	3	25	1.25	5	215.5
19	3	4	4	10	2	4	88.56
5	4	1	5	25	2	6	263.6
24	5	5	4	15	1.25	2	109.9
14	6	3	4	5	1.5	6	123.8
3	7	1	3	15	1.5	4	270.4
2	8	1	2	10	1.25	3	293.1
1	9	1	1	5	1	2	226.8
22	10	5	2	5	2	5	121.2
8	11	2	3	20	2	2	206.7
17	12	4	2	25	1.5	2	135.3
7	13	2	2	15	1.75	6	193.8
25	14	5	5	20	1.5	3	92.24
11	15	3	1	15	2	3	158.5
16	16	4	1	20	1.25	6	186
18	17	4	3	5	1.75	3	132.1
21	18	5	1	25	1.75	4	129
12	19	3	2	20	1	4	149.7
10	20	2	5	5	1.25	4	194.8
6	21	2	1	10	1.5	5	186.5
15	22	3	5	10	1.75	2	147.3
4	23	1	4	20	1.75	5	229.7
20	24	4	5	15	1	5	126.9
9	25	2	4	25	1	3	179.4

In the next step, Analysis of Variance (ANOVA) is generated to determine the ‘F Ratio’ and ‘P value’ so that the level of significance of the parameters to the output (objective) can be distinguished. Table 5 shows the ANOVA of the 5 factors. The lowest P value indicates that the highest level of significance to the output response. From the ANOVA table, the level of significance in the ascending order is the number of spokes, depth of spokes, rib

thickness, rib fillet radius, and hollow shaft thickness. This means that the hollow shaft thickness affect the torsional stress of the shaft the most compared to the other 3 factors.

Table 5 Analysis of Variance (ANOVA) of the 5 parameters

Source of Variation	Degrees of Freedom	Sum of Squares [Partial]	Mean Squares [Partial]	F Ratio	P Value
Model	20	7.56E+04	3780.4376	15.2389	0.0085
A: hollow shaft thickness	4	6.27E+04	1.57E+04	63.2162	0.0007
B: rib thickness	4	5307.9926	1326.9982	5.3491	0.0666
C: depth of spokes	4	1657.4014	414.3504	1.6702	0.3157
D: rib fillet radius	4	5325.5358	1331.384	5.3668	0.0663
E: no. of spokes	4	587.819	146.9548	0.5924	0.6878
Residual	4	992.3096	248.0774	-	-
Lack of Fit	4	992.3096	248.0774	-	-
Total	24	7.66E+04	-	-	-

Lastly, diagnostic analysis is carried out as shown in Table 6 to determine the actual value based on the results obtained earlier in Table 5. The one highlighted in green is the optimum design parameters where the actual value corresponds to the lowest torsional stress whereas the highlighted red corresponds to the highest actual value of the torsional stress. Therefore, the standard order 25 is the optimum set of parameter for the hollow shaft with rib in which the hollow shaft thickness is 4 mm, rib thickness is 4 mm, depth of spokes is 10 mm, rib fillet is 2 mm, and the number of spokes is 4.

Table 6 Diagnostic analysis of the L25 design factors

Run Order	Standard Order	Actual Value (Y)	Fitted Value (YF)
1	23	119.1	122.816
2	13	215.5	223.316

3	19	88.56	96.376
4	5	263.6	266.436
5	24	109.9	112.736
6	14	123.8	119.096
7	3	270.4	260.736
8	2	293.1	288.396
9	1	226.8	234.616
10	22	121.2	111.536
11	8	206.7	201.996
12	17	135.3	139.016
13	7	193.8	201.616
14	25	92.24	100.056
15	11	158.5	162.216
16	16	186	176.336
17	18	132.1	134.936
18	21	129	124.296
19	12	149.7	152.536
20	10	194.8	198.516
21	6	186.5	189.336
22	15	147.3	137.636
23	4	229.7	233.416
24	20	126.9	122.196
25	9	179.4	169.736

3.4 Strength and weight comparison of the optimized shaft model

The optimized shaft is compared with the benchmark shaft, hollow shaft, and solid shaft by comparison to the torsional stress and weight reduction. The torsional stress and weight of the 4 shafts were obtained using ANSYS software. Table 7 shows the torsional stress and weight reduction comparisons between the 4 different shafts. The weight reduction is calculated by comparing with the mass of the solid shaft which is the heaviest.

Table 7 Shaft models comparison in strength and weight reduction

	Optimized shaft	Benchmark shaft	Hollow shaft	Solid shaft
Length (mm)			210	
Diameter (mm)			37	
Material		AISI 4340 alloy steel (normalized at 870°C)		
Torque (Nm)			100	
Hollow shaft	4	3	3	-

thickness (mm)				
Rib thickness	4	3		
Depth of spokes (mm)	10	15	-	-
Rib fillet radius (mm)	2	1.5	-	-
Number of spokes	4	4	-	-
Torsional stress (MPa)	88.56	102.70	141.76	81.28
Weight (kg)	0.744	0.595	0.552	1.796
Weight reduction (kg) compared to solid shaft	1.052	1.201	1.244	-
Stress to weight reduction ratio	84.18	85.51	113.96	-

From the shaft comparisons, the optimized shaft has lower torsional stress compared to the benchmark shaft and the hollow shaft. The weight of the shaft is measured using ANSYS software to determine the percentage of weight reduction. The hollow shaft is the lightest among the four shafts, thus having the highest weight reduction. In order to evaluate the shaft with overall most improved strength and amount of weight reduction, the stress to weight reduction ratio is calculated for each shaft. The optimized shaft has the lowest stress to weight reduction compared to the benchmark shaft and hollow shaft which indicates it has most significant improvement in both torsional strength and weight reduction. The optimized shaft has an improved strength by 13.77% but an increase of 20% in weight compared to the benchmark model.

4 CONCLUSION

The shaft models were modelled using FEA and validated through comparisons with the experimental results. The optimum set of parameters was determined where hollow shaft thickness is 4 mm, rib thickness is 4mm, depth of spokes is 10 mm, rib fillet radius is 2 mm, and the number of spokes is 4. It was found that the hollow shaft thickness affects the torsional strength of the hollow shaft with rib the most compared to the other 4 parameters.

The optimized shaft has an improvement in strength of 13.77% but an increase in 20% in weight compared to the benchmark shaft. The presented methodology for determining the shaft torsional stress and the optimum set of parameters for shaft can be served as a guide for engineers.

ACKNOWLEDGEMENT

The authors would like to thanks the Centre for Vehicular Technology, Universiti Tunku Abdul Rahman and the Department of Mechanical Engineering, Tunku Abdul Rahman College for the facilities and system supports.

REFERENCES

- 1 **Xu, X. L., Yu, Z. W. and Ding H.X.** Failure analysis of a diesel engine gear-shaft. Eng Fail Anal., 2006, 13(8):1351–7.
- 2 **Heisler, H.** Vehicle and engine technology. 2nd ed. London: SAE International, 1999.
- 3 **Heyes, A. M.** Automotive component failures. Eng Fail Anal., 1998, 5(2):129–41.
- 4 **Vogwell, J.** Analysis of a vehicle wheel shaft failure. Eng Fail Anal., 1998, (4):271–7.
- 5 **Tasgetiren, S, Aslantas, K, and Uzun, I.** Effect of press fitting pressure on the fatigue failure of spur gear tooth root. Technol Res: EJMT, 2004:21–9.
- 6 **Ozmen, Y.** Tribological failures of machine elements and selection of suitable materials. Technol Res: EJMT, 2004(1):31–7.
- 7 **Yuksel, C. and Kahraman, A.** Dynamic tooth loads of planetary gear sets having tooth Pro.Le wear. Mech Mach Theory, 2004, 39:695–715.

- 8 **Ranganath, VR, Das, G, Tarafder, S, and Das, S. K.** Failure of a swing pinion shaft of a dragline. *Eng Fail Anal*, 2004, (11):599–604.
- 9 **Tasgetiren, S, Aslantas, K, and Uzun I.** Effect of press fitting pressure on the fatigue failure of spur gear tooth root. *Technol Res: EJMT*, 2004, 21–9.
- 10 **Yu "ksel, C. and Kahraman, A.** Dynamic tooth loads of planetary gear sets having tooth Pro.Le wear. *Mech Mach Theory*, 2004, 39:695–715.
- 11 **Design of Transmission Shafting.** American Society of Mechanical Engineers, New York, ANSI/ASME Standard B106.1M-1985
- 12 **Shigley, J.E. and Mischke, C.R.** *Mechanical Engineering Design*, McGraw Hill Publication, 5th Edition. 1989.
- 13 **Spotts, M.F.** *Design of Machine Elements*, Prentice Hall India Pvt. Limited, 6th Edition, 1991.
- 14 **Khurmi, R.S. and Gupta, J.K.** *Text book on Machine Design*, Eurasia Publishing House, New Delhi.
- 15 **Göksenli, A. and Eryürek, I.B.** Failure analysis of an elevator drive shaft, *Engineering Failure Analysis* 16, 2009, 1011–1019.
- 16 **Ooi, J. B., Wang, X., Tan, C.S., Ho, J.H. and Lim, Y.P.** Modal and stress analysis of gear train design in portal axle using finite element modeling and simulation, *Journal of Mechanical Science and Technology*, 2012, 26 (2) 575~589.
- 17 **Bayrakceken, H., Tasgetiren, H., and Yavuz, I.** Two cases of failure in the power transmission system on vehicles: A universal joint yoke and a drive shaft, *Engineering Failure Analysis* 14, 2007, 716–724.

Figure

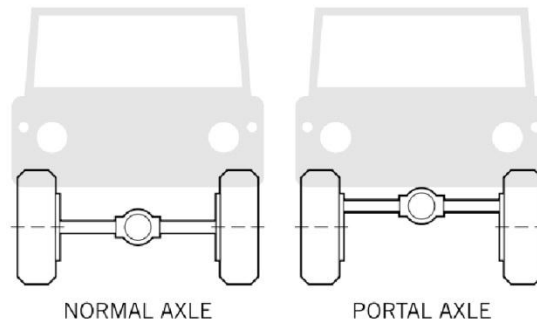


Fig. 1 Difference between normal axle and portal axle

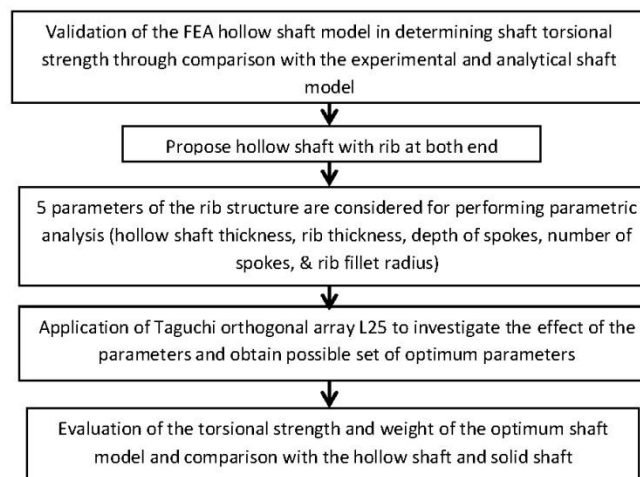


Fig. 2 Schematic flow diagram for obtaining the optimum set of parameters of the hollow shaft with rib

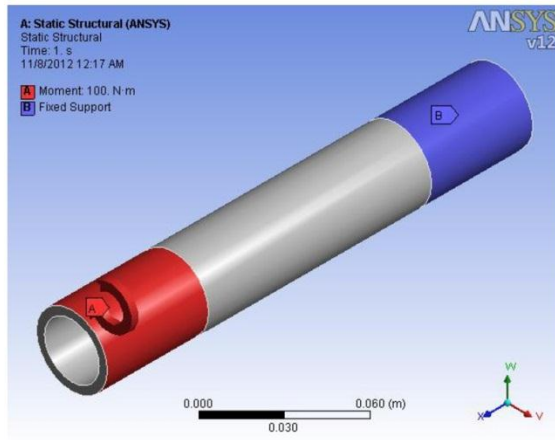


Fig. 3 Boundary condition settings of the hollow shaft model

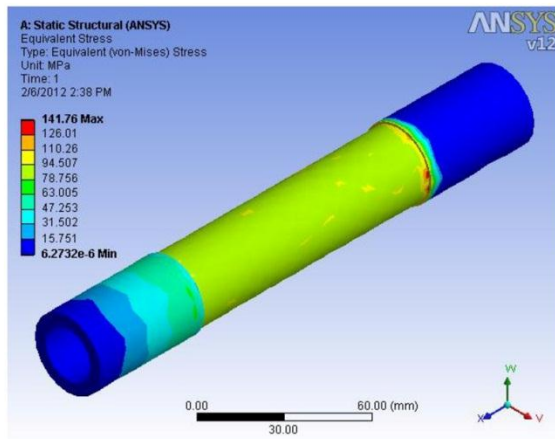


Fig. 4 FEA simulation of maximum stress on the shaft model

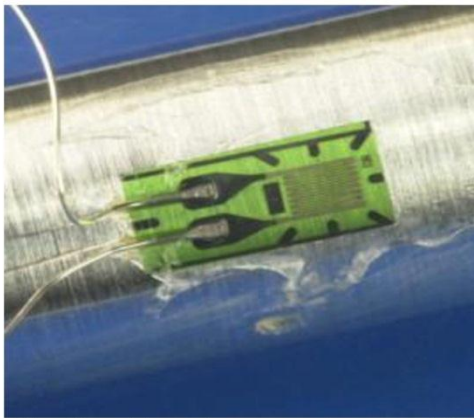


Fig. 5 Bonding of the strain gauge at the center of the shaft



Fig. 6 Mounting of the shaft to the Tinius Olsen torsion testing machine

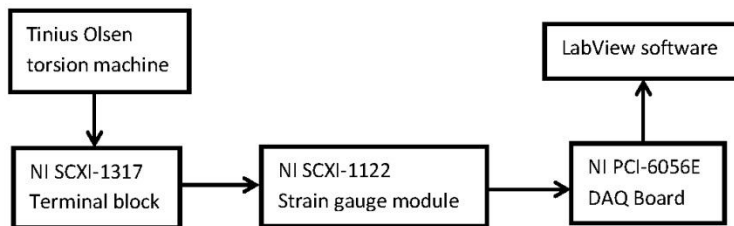


Fig. 7 Strain measurement system of the torsion tester machine

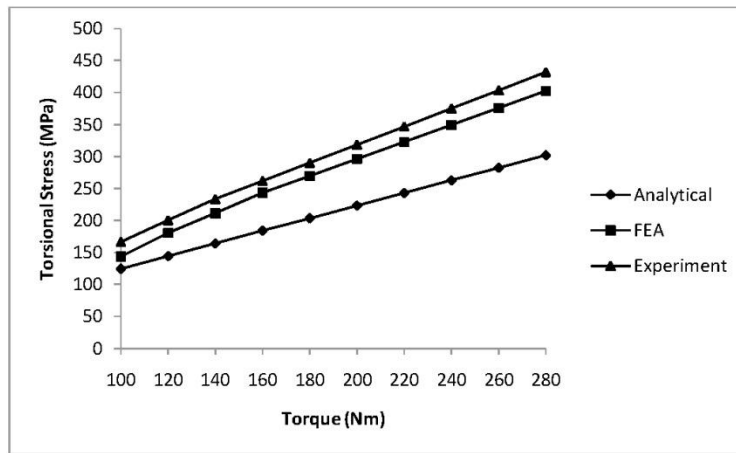


Fig. 8 Comparison between the FEA model, experimental model, and the analytical model by plot of the torsional stress against increasing torque

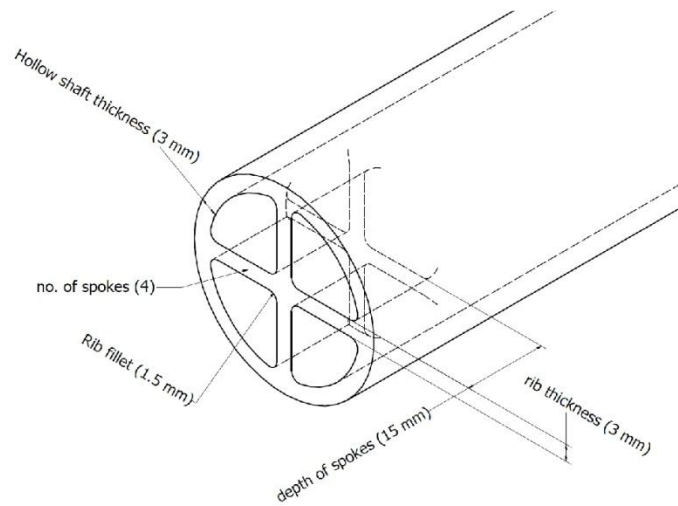


Fig. 9 Model of the hollow shaft with rib and the 5 types of parameter